Thesis:
The Algebra and Geometry of using Continued Fractions for approximating real and complex numbers

by

Carminda Margaretha Mennen

A thesis submitted to the School of Mathematics
in fulfilment of the requirements for the degree of
Doctor of Philosophy

Under the supervision of
Professor E. Mphako-Banda

Faculty of Science
University of the Witwatersrand
October 2022

Johannesburg, South Africa

I declare that this thesis is an original report of my research, and that my debts (for words, images and definitions) have been appropriately acknowledged. It is being submitted for the degree of Doctor of Philosophy to the Faculty of Science in the University of the Witwatersrand, Johannesburg. This thesis has not been submitted in any other university for any previous degree.

Carminda Margaretha Mennen

Signed on the 14th day of October 2022

Abstract

Through geometric analysis we forge a new interpretation of the link between nearest integer continued fractions and the Farey tessellation of hyperbolic space. Instead of just truncating the continued fraction to generate approximations, we focus on

- how to parse the product of maps derived from the nearest integer continued fraction into a product of parabolic and elliptic Möbius maps and
- on the collection of points on which these maps act.

It turns out that we need to set apart the elliptic maps that permute a collection of six vertices, three values in $\mathbb{R}$, namely ∞, 0 and 1, and three values in $\mathbb{C}$, namely i, $1 + i$ and $\frac{1+i}{2}$. The action of the remaining parabolic maps on the same six vertices results in the creation of a sequence of nested Farey quadrilaterals, containing the target, whose boundaries are based in the Schmidt arrangement formed by the Farey sets and dual Farey sets of Schmidt.

— University of the Witwatersrand

Acknowledgements

Thank you, first and foremost, to my supervisor Professor Eunice Mphako Banda for sharing this journey with me from the very first steps. Your guidance, insights, encouragement and humour have made this endeavour a most remarkable journey.

I also thank my family for their patience and understanding during the writing of this thesis. Your unwavering support and encouragement have meant the world to me.

— Carminda Margaretha Mennen

Contents

List of Tables

List of Figures

Chapter 1

Introduction

"There is another, entirely different face of mathematics, which I like to call its algorithmic face. This is the face of an engineer. The Algorithmic mathematician tells us how to construct the beautiful things of whose existence we are assured by the dialectic mathematician. The rules of the game of algorithmic mathematics, and in particular the significance attached to the results in algorithmic mathematics, depend on the equipment that is available to carry out the required constructions. [Henrici's introduction, page xix, 1980]" [26]

This thesis is about the connections between continued fractions, Farey fractions and the Farey tessellation of hyperbolic space, Möbius maps, discrete groups, complex dynamics and diophantine approximations.

An infinite continued fraction [4] is an expression of the form

$$\mathrm{K}\left(a_n|b_n\right) = \cfrac{a_1}{b_1+\cfrac{a_2}{b_2+\cfrac{a_3}{b_3+\cdots}}} = \frac{a_1}{b_1} + \frac{a_2}{b_2} + \frac{a_3}{b_3} + \cdots, \tag{1.1}$$

where a_i, b_j are infinite sequences of complex numbers, with each $a_i \neq 0$. The continued fraction is said to converge to K if the sequence of truncated continued fractions

$$\frac{A_1}{B_1} = \frac{a_1}{b_1}, \qquad \frac{A_2}{B_2} = \frac{a_1}{b_1} + \frac{a_2}{b_2}, \qquad \frac{A_3}{B_3} = \frac{a_1}{b_1} + \frac{a_2}{b_2} + \frac{a_3}{b_3}, \cdots \tag{1.2}$$

converges to K. These fractions are called the convergents of K. We explore the geometry underlying these convergents in the case where $a_i = 1$ and $b_n \in \mathbb{Z}$ or $b_n \in \mathbb{Z}[i]$ for all $i \in \mathbb{N}$, the set of positive integers $\{1, 2, 3\cdots\}$.

This chapter gives an overview of the thesis. We discuss a brief history of three branches of mathematics that contribute to the development of this thesis. The work of Ford, Series and Schmidt initiate links between the 3 branches, leading Beardon [4, 5, 6] to suggest that we analyse the behaviour of continued fractions in hyperbolic space where Möbius maps act as isometries. We explore a new synthesis of these links that can be extended to higher dimensions.

1.1 Overview of the thesis

In this section we give a brief outline of the thesis and highlight the main results. In Chapter 2, we reinvent the link between regular continued fractions (RCF) and the Farey tessellation $\mathcal{F}$ of hyperbolic space to establish a deeper link between nearest integer continued fractions ($NICF$) and $\mathcal{F}$. In Section 2.2, we use Möbius maps derived from the RCF to show the familiar links between the partial quotients of the RCF and the triangles of the Farey tessellation [41] using a new dynamic approach. We then extend this dynamic approach to the $NICF$, but the result is less pleasing. In Section 2.3, we reinterpret the Möbius maps generated from the $NICF$ to develop a new dynamic involving the use of elliptic Möbius maps. The roles of geometric elements are adjusted to suit the new process and the dynamic that evolves reveals exactly the same kind of links to $\mathcal{F}$ that the RCF has. The outline of the general method for using Möbius maps derived from the $NICF$ is summarised in Section 2.4. Some advantages of using Möbius maps are highlighted in Section 2.6.

In Chapter 3, we develop the geometry required to analyse continued fractions with complex partial quotients from a perspective of using Möbius maps acting in hyperbolic space. We introduce the set of vertices $\nabla = \left\{\infty, 0, 1, i, 1+i, \dfrac{1+i}{2}\right\}$ which forms the basis of our discussion. In the Schmidt arrangement, discussed in Section 3.1, we identify a configuration involving 6 vertices in every intersection between an overlapping Farey set and dual Farey set. These 6 vertices are images of the vertices in ∇ under particular Möbius maps. We recognise the roles that these vertices assume under parabolic and elliptic Möbius maps. Then we describe the role of fixed point and its associated hyperbolic quadrilateral under the parabolic maps, and we become aware of the permutations of the same set of vertices under the elliptic maps.

In Chapter 4, the effects of Möbius maps derived from the $NICF$ are extended to the Hurwitz continued fraction [17] which is derived using the Hurwitz complex continued fraction algorithm using "nearest Gaussian integers". The examples chosen to illustrate each type of continued fraction allow us to build up an overview of the partial quotient patterns that emerge for numbers in $\mathbb{C}$.

In Section 4.2, we show that parabolic Möbius maps have a fixed point at the image of either 0 or ∞. Under successive partial products of Möbius maps, the images of the vertices of the hyperbolic quadrilateral associated with the fixed point are moved toward the fixed point along circular arcs bounding Farey sets and dual Farey sets, resulting in a sequence of nested hyperbolic quadrilaterals that each contain the target. However, we establish that if the product of parabolic maps actually include elliptic Möbius maps, due to negative real or imaginary parts in the partial quotient, then just using parabolic maps yields quadrilaterals that do not contain the target. There are two scenarios that emerge and they are dealt with in Sections 4.3 and 4.4.

In Section 4.3, we introduce a collection of maps that permute the vertices of ∇. They occur in the product of parabolic Möbius maps where the real or imaginary parts of the partial quotients are negative. By isolating the elliptic Möbius maps from among the parabolic maps and adjusting the parabolic maps accordingly, we use the resulting parabolic Möbius maps to find hyperbolic quadrilaterals that contain the target. In the case where successive partial quotients have negative real parts we need to use insertion and deletion techniques, introduced in Section 4.4, to acquire hyperbolic quadrilaterals that contain the target.

In each section we provide examples of how the product of Möbius maps are connected to the geometry. The aim is to be able to factor the Möbius maps derived from the $NICF$ as a result of the understanding of the geometric properties embedded in the maps. The interpretation of partial quotients of more complicated continued fractions becomes an area for further research.

1.2 Historical overview

In Subsections 1.2.1, 1.2.2 and 1.2.3, we discuss the early developments in three branches of mathematics that contribute to this thesis, namely, continued fractions, hyperbolic geometry and Farey numbers. We then illustrate how different aspects of continued fractions are reflected in hyperbolic geometry using Farey numbers. We look at various geometrical representations in Subsection 1.2.4 and the matter of using continued fractions to find rational approximations of irrational numbers in Subsection 1.2.5.

1.2.1 Early examples of continued fractions

The origin of the continued fraction is linked to the development of the Euclidean algorithm for finding the greatest common divisor around 300 BC. While the equations used in the Euclidean algorithm are precisely those that are used to find the continued fraction of a rational, the idea of a continued fraction is not developed further until much later. Finite continued fractions appeared in early Hindu and Greek Mathematics using the natural connection with the iterated application of the Euclidean algorithm. The first known use was by Bombelli in 1572 where $\sqrt{13}$ was approximated with the finite continued fraction $3 + \frac{4}{6} + \frac{4}{6}$, illustrating knowledge of the formula $\sqrt{a^2 + b} = a + \frac{b}{2a} + \frac{b}{2a} \cdots$. Cataldi used the notation

$$\sqrt{18} = 4\& \cfrac{2}{8\& \cfrac{2}{8\& \cfrac{2}{8}}}$$

and discussed the general formula for $\sqrt{a^2+b}$.

The term ‘continued fraction’ was first coined by John Wallis in the book Opera Mathematica in 1695, where it is shown how to calculate convergents and a discussion of the properties of convergents is presented [32]. Wallis also attempted to explore Lord Brouncker's infinite continued fraction for π. Forty years earlier, in the work called Arithmetica Infinitorum, Wallis derived the infinite product

$$\frac{4}{\pi}=\frac{3.3.5.5.7.7.9\cdots}{2.4.4.6.6.8.8\cdots}$$

which Lord Brouncker (1658) converted into the continued fraction

$$\frac{4}{\pi}=1+\cfrac{1^2}{2+\cfrac{3^2}{2+\cfrac{5^2}{2+\cfrac{7^2}{2+\ddots}}}}=1+\frac{1^2}{2}+\frac{3^2}{2}+\frac{5^2}{2}\cdots,$$

without going into detail about the method used. Lord Brouncker was the first to consider infinite continued fractions. More detail of the techniques used for the conversion and other related continued fractions for π are given in [32, 33, 46].

An application of finite RCFs uses convergents as a means of writing fractions involving large numbers in terms of fractions involving smaller numbers. In a work entitled Geometrica Practica (1627), Schwenter found approximations of the rational $\frac{177}{233}$ by finding the greatest common divisor of 177 and 233, and from these calculations he found approximations by calculating the convergents $\frac{79}{104}$, $\frac{19}{25}$, $\frac{3}{4}$, $\frac{1}{1}$ and $\frac{0}{1}$. The Dutch mathematician and astronomer Christiaan Huygens (1629-1695) wrote ’Descriptio Automati Planetarii’ (published posthumously in 1698) explaining how to use the convergents of a continued fraction to find the best rational approximations for gear ratios. These approximations enabled him to pick the gears with the correct number of teeth. His work was motivated in part by his desire to build a mechanical planetarium [26, 32].

According to Brezinski [9] the 17th century saw the beginning of the theory of continued fractions, but the 18th century was really their golden age. The field of continued fractions began to flourish when Leonhard Euler (1707-1783), Johan Heinrich Lambert (1728-1777), and Joseph Louis Lagrange (1736-1813) embraced the topic. Euler laid down much of the modern theory in his work De Fractionlous Continious (1737). He showed that every rational can be expressed as a terminating simple continued fraction. Using the continued fraction expression for e,

$$e - 1 = 1 + \frac{1}{1+}\frac{1}{2+}\frac{1}{1+}\frac{1}{1+}\frac{1}{4+}\frac{1}{1+}\frac{1}{1+}\frac{1}{6+}\frac{1}{1+}\frac{1}{1+}\frac{1}{8+}\frac{1}{1}\cdots,$$

Euler showed that e and e^2 are irrational. He demonstrated how to go from a series to a continued fraction representation of the series, and conversely [47]. The methods used by Euler can be found in [47, 37]. Euler also showed that a periodic continued fraction always represented a quadratic irrational, while La Grange provided the proof of the converse [6, 36]. Continued fractions with complex variables were also introduced by Euler [26]. Through the work of Euler it became clear that continued fractions had uses in both analysis and in number theory.

The initial development of continued fractions seems to have taken a long time, but, once started, the field and its analysis grew rapidly. Even today, the fact that continued fractions are still being used signify that the field is still far from being exhausted. As an example, the work of Corless in [12] links continued fractions to chaotic dynamical systems.

1.2.2 Developments in non Euclidean geometry

The Elements, written by Euclid around 300BC, formed the foundation of geometry for over 2000 years. Euclidean Geometry was based on five axioms or postulates and all further propositions were proved from these axioms.

Euclid's fifth postulate: The fifth postulate of geometry in Euclids elements (300BC) provided mathematicians with a conundrum [30]. The statement of the fifth postulate was different from the first four by being longer with more conditions. It was rewritten by Proclus (410-485) as follows:

"Given a line and a point not on the line, it is possible to draw exactly one line through the point parallel to the given line." [30]

Attempts by Proclus, Saccheri (1697) and Legendre (1794) to prove the fifth postulate from the first four postulates failed. The axiom became known as Playfair's axiom when Playfair introduced the clause 'at most' in the book 'Elements of Geometry' in 1846:

"In a plane, given a line and a point not on it, at most one line parallel to the given line can be drawn through the point. " [30]

In 1817 Gauss, the first person to understand the problem with the fifth postulate, started working on a geometry where the first four postulates remained the same, but the fifth postulate did not hold. This work was never published. Bolyai worked on the same premise and made a breakthrough. Much of this work was already completed by Gauss, but Bolyai proceeded to develop the new geometry further with the fifth postulate not satisfied. Lobachevsky formalised this new geometry in 1840 with a new fifth postulate:

"There exists two lines parallel to a given line through a given point not on the line." [30]

In the new non-euclidean geometry Lobachevsky went on to develop many trigonometric identities which held for triangles in this geometry. It was noted that as triangles got smaller these identities tended to the usual trigonometric identities. Another non-euclidean geometry was formalised in 1868 with independent developments of spherical geometry by Riemann and Beltrami. It was yet another example where the first four postulates of Euclid held, but the fifth did not. Klein completed the ideas of non-euclidean geometry by identifying the three types of geometry - spherical, Euclidean and hyperbolic. The evidence for the consistency of hyperbolic space was demonstrated by Lambert in 1770 by showing the duality between the hyperbolic and the spherical trigonometries.

Development of models for the hyperbolic plane based in the complex plane: Non Euclidean geometry challenges some of the deepest human perceptions about space. Developments in projective geometry in the early 19th century gave a mathematical basis for a true non-euclidean geometry [15]. In 1868 Beltrami developed 3 models whose underlying space is contained in the complex plane [1, 29]. Beltrami constructed a Euclidean model of the hyperbolic plane and, using differential geometry, showed that his model satisfied all the axioms of hyperbolic plane geometry. The geodesics are represented by straight lines but the model is not conformal as angles are not preserved. Klein gave an interpretation of this model in terms of projective geometry. It is now known as Klein's disc model. The generalisation of this model to n-dimensional hyperbolic space is called the Klein ball model. In the same paper Beltrami constructed two other Euclidean models of the hyperbolic plane, one on a disc and the other on a Euclidean half-plane. These are both conformal models as angles are preserved but geodesics are now represented by circular arcs. These models were later generalised to n-dimensions by Poincaré in 1908, and are now associated with his name.

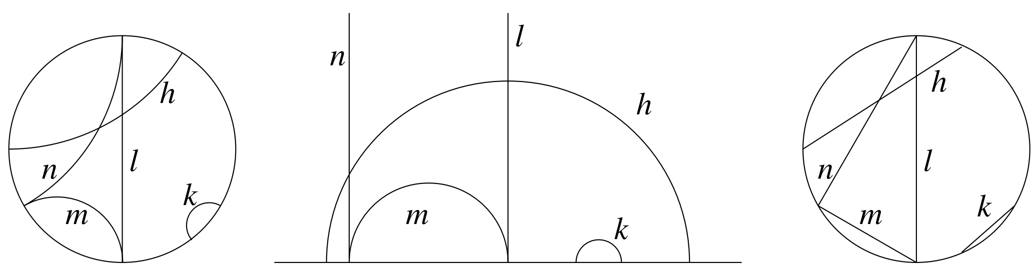

Figure 1.1: The same 5 geodesics displayed in the Poincaré disk model $\mathbb{D}$, the upper half plane model $\mathbb{H}$ and the Klein disk model.

The shortest distance or the geodesic between two points in any of these models is defined by the metric used to define the hyperbolic space, which in turn influences the perceptual aspect or shape of the geodesics. In Figure 1.1 the same five geodesics are shown in three different models of the hyperbolic plane.

Special Relativity and the Hyperboloid model: The high points in the history of the hyperboloid model [34] are Lambert's idea of an "imaginary sphere" in 1766 and Taurinus' calculation of trigonometry on a "sphere of imaginary radius" in 1826. There is no isometric embedding of the hyperbolic plane $\mathbb{H} = \{x + iy | y > 0\}$ in a Euclidean space of the same dimension. The hyperboloid model of the hyperbolic plane is embedded in a euclidean space one dimension higher. The development of the hyperboloid model is linked to Minkowski's interpretation of Einstein's work on special relativity in 1905. The mathematics needed for ideas around relativity required the use of a four dimensional space where the fourth dimension was allocated to time. Minkowski developed a model for space-time geometry with the indefinite norm $x^2 + y^2 + z^2 - t^2$ as the metric.

> *"It has become generally recognised that hyperbolic (i.e. Lobchevskian) space can be represented upon one sheet of a two sheeted cylindrical hyperboloid in Minkowskian space-time. " [2]*

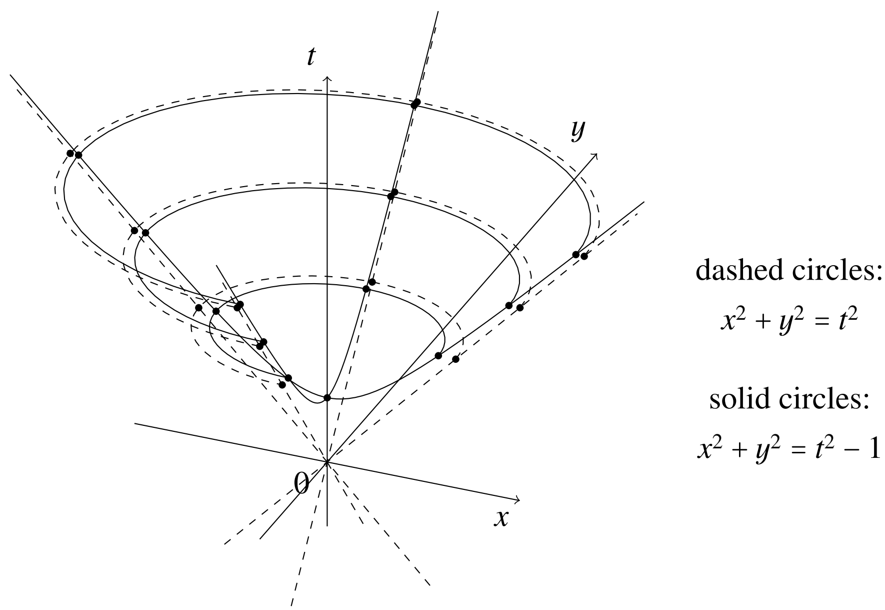

Figure 1.2: The Hyperboloid model of $\mathbb{H}$.

The hyperboloid model, shown in Figure 1.2, is an embedding of hyperbolic 2-space on a surface in Euclidean 3-space, where the metric on the space is given by the indefinite norm $x^2 + y^2 - t^2$ and the points (x, y, t) on this surface satisfies the Minkowski space-time condition $x^2 + y^2 - t^2 = -1$ [25, 34]. The diagram in Figure 1.2 shows two surfaces in Minkowski space:

- The dashed lines and circles lie on the light cone through the origin defined as the set of points of norm zero, that is where $x^2 + y^2 - t^2 = 0$.
- The set of points, with $t > 1$, at constant squared distance from the origin of -1, that is where $x^2 + y^2 - t^2 = -1$, form the hyperboloid of one sheet in the Minkowski space [25] passing through the solid curves and circles. This surface depicts the hyperboloid model of the hyperbolic plane $\mathbb{H}$.

The hyperboloid surface represents a 'sphere' with radius i in Minkowski space. Despite the advantages discussed for the hyperboloid model it is not practical to work with this model, as all real values lie on the circle at ∞.

> *"The main advantages of this model are its naturalness and its symmetry. Being embeddable (distance function and all) in flat space-time, it is close to our picture of physical reality, and all its points are treated alike in this embedding. Once the strangeness of the Minkowski metric is accepted, it has the familiar geometry of a sphere in Euclidean 3-space E^3 as a guide to definitions and arguments. For example, the lines of H^2 are its non-empty intersections with the planes through the origin of the Minkowski space M^3. The length of a line segment of H^2 is defined by analogy with arc length in calculus; this leads naturally to the hyperbolic functions[1]. As in the spherical case, every isometry of H^2 can be extended to a linear transformation of M^3, so that straightforward calculations with matrices can be used to prove theorems and develop the trigonometry of H^2. The circles, horocycles, and equidistant curves have a beautiful interpretation: they are precisely the nontrivial intersections of H^2 with planes of M^3 that do not pass through the origin. An area function for H^2 can be constructed from the volume function on M^3 " [34]*

Möbius maps, the isometries of hyperbolic space: In many of Beardon's works we are urged to use the fact that the Möbius maps that leave $\mathbb{H}$ invariant are the isometries of hyperbolic space and we should incorporate this thinking while analysing continued fractions.

[1] We use the notation $\mathbb{H}$ for H^2 in this thesis

" The remarks on metric spaces and hyperbolic geometry that follow are not necessary for the proofs in the paper, but they do explain the main ideas and motivation that lie behind this work. It is easy to make $\mathbb{C}_\infty$ into a metric space, for we can project it (using stereographic projection) onto the unit sphere $\mathbb{S}$ in $\mathbb{R}^3$ and then transfer the Euclidean metric from $\mathbb{S}$ to a metric χ on $\mathbb{C}_\infty$. Now that $(\mathbb{C}_\infty, \chi)$ is a metric space, we can show that each Möbius map g is a homeomorphism of $\mathbb{C}_\infty$ onto itself. Better still, with an appropriate definition (which we omit here), the group of Möbius maps (under composition) is the group of all conformal mappings of $(\mathbb{C}_\infty, \chi)$ onto itself. With this, we have set up the equipment to deal with continued fractions of the form (1)[2].
Observe that the boundary of $\mathbb{H}$ is $\mathbb{R}_\infty$ and that $\mathbb{H}$, with the metric $\frac{|dz|}{y}$, is one of the standard models of the hyperbolic plane. Moreover, the (conformal) isometries of the hyperbolic plane are precisely the Möbius maps that leave $\mathbb{H}$ invariant. Indeed, the hyperbolic metric on $\mathbb{H}$ is a "natural" metric from the point of view of complex analysis since it is (up to a scalar multiple) the only metric for which the conformal self-maps of $\mathbb{H}$ are isometries. Although we shall not use hyperbolic geometry in this article, we would be remiss if we did not mention the fact that Möbius maps (when suitably defined) exist in Euclidean spaces of all dimensions and form the conformal isometry groups of hyperbolic space of the appropriate dimension. Sadly, the usual introduction of Möbius maps acting on $\mathbb{C}_\infty$ (where they are not isometries) completely misses this point. " [6]

The action of Möbius maps on the Farey tessellation, depicted on the surface $\mathbb{H}$, preserves distances and angles, so Möbius maps embody the complete set of isometries in hyperbolic space.

Definition 1.2.1. An isometry: Let M be some Riemannian 2-manifold. Let $d(p,q)$ denote the distance between two points $p, q \in M$. Then a transformation function $g : M \to M$ which satisfies $d(p,q) = d(g(p), g(q))$ for all $p, q \in M$ is called an isometry of M. The set of all such isometries on M is denoted as $iso(M)$.

[2]Equation for continued fraction $\cfrac{a_1}{b_1 + \cfrac{a_2}{b_2 + \cfrac{a_3}{b_3 + \cdots}}}$

1.2.3 The geometrization of Farey numbers in hyperbolic space.

The Farey tessellation, defined below, has become a useful tool for analysing continued fractions. The structure of the tessellation is governed by the notion of a Farey sum which is defined as follows:

Definition 1.2.2. The mediant (now called the Farey sum) of two (Farey) neighbours $\dfrac{a}{b}$ and $\dfrac{c}{d}$, with $a, b, c, d \in \mathbb{Z}$ and $b, d > 0$, is $\dfrac{a}{b} \oplus \dfrac{c}{d} = \dfrac{a+c}{b+d}$.

Haros' table, published in Journal de l'Ecole Polytechnique in the early 1800's, contained every irreducible fraction with denominators from 2 to 99 and their decimal approximation. Aside from including $\frac{0}{1}$ and $\frac{1}{1}$, Charles Haros had formulated what is now known as the Farey sequence $F99$. To do this he used the mediant property to find the fractions with higher denominators and even provided a sketch proof that it worked [28]. He also noted that if two numbers $\dfrac{a}{b}$ and $\dfrac{c}{d}$ are neighbours in the table then $|ad - bc| = 1$.

Definition 1.2.3. Two reduced rationals $\frac{a}{b}$ and $\frac{c}{d}$, with $a, b, c, d \in \mathbb{Z}$ and $b, d > 0$, are neighbours (now referred to as Farey neighbours), denoted $\frac{a}{b} \sim \frac{c}{d}$, if the condition $|ad - bc| = 1$ is satisfied.

Henry Goodwyn presented a table of fractions and decimal equivalents for every irreducible fraction with denominators between 1 and 1024, published by the Royal Society in April 1816. Within a month John Farey submitted a letter to The Philosophical Magazine and Journal with a note entitled "On a curious Property of the vulgar fractions" where he described the mediant property.

Proposition 1.2.4 (Mediant property)**.** {For two reduced rationals $\frac{a}{b}$ and $\frac{c}{d}$, with $a, b, c, d \in \mathbb{Z}$, $b, d > 0$ and $\gcd(a, b) = \gcd(c, d) = 1$.} If $\frac{a}{b} < \frac{c}{d}$ then their mediant $\frac{a+c}{b+d}$ lies between them, $\frac{a}{b} < \frac{a+c}{b+d} < \frac{c}{d}$.

John Farey's note was then republished in the French magazine "Bulletin de la Société Philomatique". It was from here that Cauchy saw it and provided a proof that the mediant property holds (crediting John Farey) in August 1816 [28].

The usefulness of adjoining $\frac{1}{0}$ to $\mathbb{Q}$ in the context of Farey theory was recognised by Bachman (1910), Lucas (1891) and Denjoy (1938). According to Lagarias and Tresser [28], the relevance of the Farey tessellation in the study of continued fractions was recognised by H. J. S. Smith in 1877, and studied in detail by A. Hurwitz in 1894 and G Humbert in 1916.

Geometrisation of the Farey intervals in hyperbolic 2-space: Ford's geometrisation in [14] of the Farey fractions, in 1938, uses Ford circles where each rational $\frac{p}{q}$ is represented, in the upper half plane of $\mathbb{R}^2$, by a circle with radius $\frac{1}{2q^2}$ tangent to real number line at $\frac{p}{q}$, where $p, q \in \mathbb{Z}$ have no common factors.

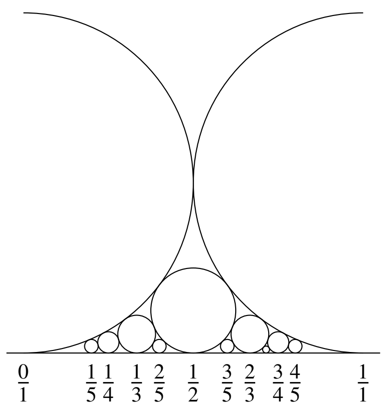

Circles at 0 and 1 have radius $\frac{1}{2}$

Circle at $\frac{1}{2}$ has radius $\frac{1}{8}$

Circles at $\frac{1}{3}$ and $\frac{2}{3}$ have radius $\frac{1}{18}$, etc

Figure 1.3: The Ford circles.

The Ford circles demonstrate the relationships between Farey neighbours and their Farey sums. The Ford circles for rationals with $0 \le \frac{p}{q} \le 1$ and $1 \le q \le 5$ are illustrated in the diagram of Figure 1.3. It is proven that all these circles are tangential to each other at the points of contact. Any two rationals $\frac{p}{q}$ and $\frac{P}{Q}$ are called adjacent if their circles are tangential to each other or, equivalently, if the condition $|Pq - pQ| = 1$ is satisfied. The regions bounded by three pairwise tangent circles are called mesh triangles.

The Farey tessellation $\mathcal{F}$, used by Series [41] in 1985, is a tiling of the upper half plane model of hyperbolic space $\mathbb{H}$ into hyperbolic triangles, where $\mathbb{H} = \{z \in \mathbb{C} : Im(z) > 0\}$ is defined with the Poincare metric $ds^2 = \frac{dx^2+dy^2}{y^2}$. The closure of $\mathbb{H}$ includes the extended real line $\mathbb{R}_\infty$ as the boundary $\partial\mathbb{H}$. Using the Poincare metric, the shortest distance between any two points in $\mathbb{H}$ lies on a geodesic formed by the arc of a semicircle orthogonal to $\partial\mathbb{H}$ or the segment of a vertical ray in $\mathbb{H}$ between the two given points. If both endpoints of a geodesic are in $\partial\mathbb{H}$ then we call the geodesic an ideal geodesic and if the endpoints are rational Farey neighbours $\frac{a}{b}$ and $\frac{c}{d}$ it is called a Farey geodesic denoted $\lambda_{\left(\frac{a}{b},\frac{c}{d}\right)}$. Every triangle in $\mathcal{F}$ is a Farey triangle bounded by three Farey geodesics.

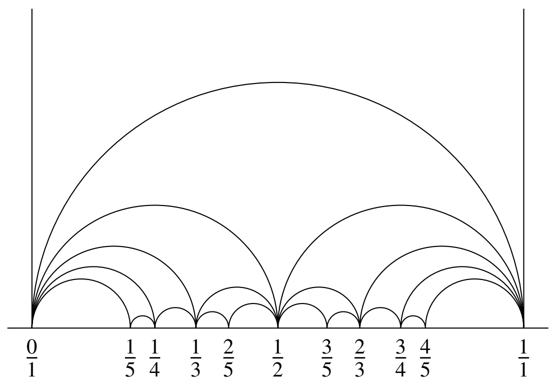

Figure 1.4: The Farey Tessellation of $\mathbb{H}$.

The part of $\mathcal{F}$ shown in the diagram of Figure 1.4 consists of all the geodesics that join Farey neighbours $\frac{a}{b}$ and $\frac{c}{d}$, with $0 \le \frac{a}{b}, \frac{c}{d} \le 1$ and $0 \le b, d \le 5$. The fraction $\frac{1}{0}$ represents ∞ and it lies in $\partial\mathbb{H}$, the boundary of hyperbolic space known as the circle at infinity. The vertical lines at $x = 0$ and $x = 1$ are the Farey geodesics joining the vertex at ∞ to the vertices at 0 and 1 respectively.

Extending the structure of the Farey numbers to the Complex numbers: In 1967, Schmidt [39] noted the development of Farey sections in the complex plane by Cassels, Ledermann and Mahler in [10] as a generalisation of the Farey numbers in the real number system to the complex number system. According to Schmidt the use of Farey fractions should replace the application of RCFs for many purposes. Schmidt extended the Farey interval $\left[\frac{a}{b}, \frac{c}{d}\right]$, $a, b, c, d \in \mathbb{Z}$, $|ad - bc| = 1$ into Farey triangles with vertices in the set of Gaussian rationals [22] given by $\mathbb{Q}[i] = \{r + is | r, s \in \mathbb{Q}, i^2 = -1\}$ using the following two definitions:

Definition 1.2.5. The 2×3 matrix $\left(\begin{smallmatrix} p_1 & p_2 & p_3 \\ q_1 & q_2 & q_3 \end{smallmatrix}\right)$ is a Farey matrix in $\mathbb{Q}[i]$ if $p_j, q_j \in \mathbb{Q}[i], 1 \leq j \leq 3$ and $|p_1q_2 - p_2q_1| = |p_1q_3 - p_3q_1| = |p_2q_3 - p_3q_2| = 1$.

Definition 1.2.6. A Farey triangle $FT\left(\frac{p_1}{q_1}, \frac{p_2}{q_2}, \frac{p_3}{q_3}\right)$ in the complex plane (in the case of $\mathbb{Q}[i]$) is the convex hull of the points $\frac{p_j}{q_j}, q_j \neq 0, 1 \leq j \leq 3$, such that the corresponding matrix $\left(\begin{smallmatrix} p_1 & p_2 & p_3 \\ q_1 & q_2 & q_3 \end{smallmatrix}\right)$ is a Farey matrix in $\mathbb{Q}[i]$.

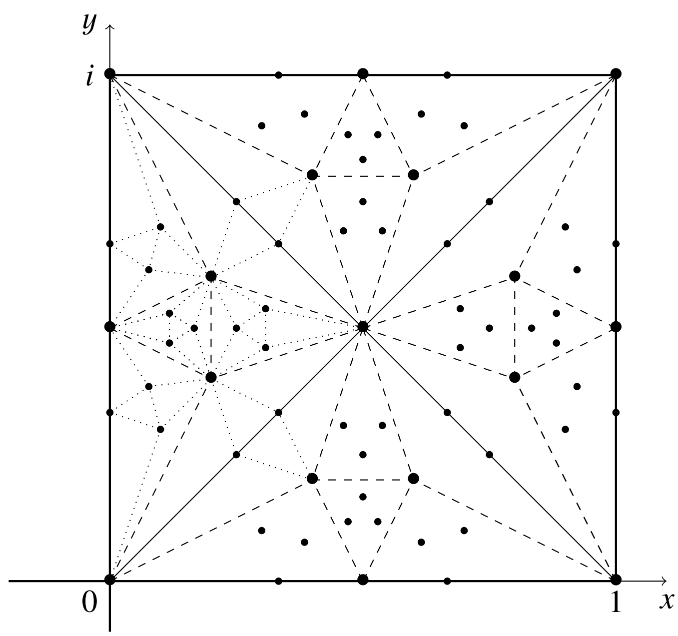

Figure 1.5: The Farey triangles of Schmidt.

All Farey matrices are associated with a matrix of the form $\left(\begin{smallmatrix} a & b \\ c & d \end{smallmatrix}\right)\left(\begin{smallmatrix} 1 & 0 & 1 \\ 0 & 1 & 1 \end{smallmatrix}\right)$ where $\left(\begin{smallmatrix} a & b \\ c & d \end{smallmatrix}\right)$ is a unimodular matrix over $\mathbb{Z}[i]$, $a, b, c, d \in \mathbb{Z}[i]$, $|ad - bc| = 1$. The tessellation of the region with $0 \leq x \leq 1$ and $0 \leq y \leq 1$ by Farey triangles is shown in Figure 1.5. Each triangle is subdivided into 7 triangles. The square with vertices at 0, 1, $1 + i$ and i is divided into 4 triangles by solid lines. These triangles are 4 of the 7 triangles in the subdivision of the triangle with vertices 0, 1 and ∞, known as the fundamental triangle. The other 3 triangles in the subdivision, as well as the fundamental triangle, are degenerate as they have ∞ as a vertex.

Schmidt describes the points $\left(\frac{i}{1}, \frac{1+i}{1}, \frac{1}{1-i}\right)$ as the inner subdivision of the points $\left(\frac{0}{1}, \frac{1}{1}, \frac{1}{0}\right)$ on page 258 of [39] referring to a diagram on page 256 where the same square is drawn but the sides of the square are curved as arcs in 3 dimensions, possibly as a better way to show the link to $\frac{1}{0}$. In Figure 1.5 the subdivision of the first set of triangles is indicated by the dashed lines, and part of the next subdivision is shown by the dotted lines. Each triangle is subdivided into 7 triangles. When the three vertices of a triangle are collinnear the triangle they form is also considered to be degenerate, for example the triangle with vertices $\frac{0}{1}$, $\frac{i}{1}$ and $\frac{i}{2}$.

By 1975, in the paper 'Diophantine approximation of complex numbers' [40], Schmidt developed a new algorithm based on Farey sets and dual Farey sets which are an extension of the circles and mesh triangles of Ford. A Farey set is bounded by a circle passing through the same 3 vertices as the corresponding Farey triangle, or it is the mesh triangle bounded by the three circles that are pairwise tangent at these vertices. The method is based on the notion of homographic maps that map circles to circles, thus allowing us to subdivide the complex plane into regions called Farey sets, which are again subdivided into smaller regions by the same process in an iterative manner.

Each Farey set is determined by three specific complex numbers which are each generated by a matrix $M_n(\xi), n \in \mathbb{N}$, where $M_n = T_1 \dots T_n$ and $T_j \in S$ for all $j = 1, \cdots, n$ with

$$\mathbf{S} = \{V_1, V_2, V_3, E_1, E_2, E_3, C, S, I\},$$

and

$$V_1 = \begin{pmatrix} 1 & i \\ 0 & 1 \end{pmatrix}, \qquad V_2 = \begin{pmatrix} 1 & 0 \\ -i & 1 \end{pmatrix}, \qquad V_3 = \begin{pmatrix} 1-i & i \\ -i & 1+i \end{pmatrix},$$

$$E_1 = \begin{pmatrix} 1 & 0 \\ 1-i & i \end{pmatrix}, \qquad E_2 = \begin{pmatrix} 1 & -1+i \\ 0 & i \end{pmatrix}, \qquad E_3 = \begin{pmatrix} i & 0 \\ 0 & 1 \end{pmatrix},$$

$$C = \begin{pmatrix} 1 & -1+i \\ 1-i & i \end{pmatrix}, \qquad S = \begin{pmatrix} 0 & -1 \\ 1 & -1 \end{pmatrix} \quad \text{and} \quad I = \begin{pmatrix} 1 & 0 \\ 0 & 1 \end{pmatrix}.$$

Schmidt specifies that the E_j matrices for $j = 1,2,3$ may not occur consecutively in the sequence of matrices, in fact they must be separated from each other by a C matrix. The V_j matrices for $j = 1,2,3$ and C matrix may occur in any order without restriction. The aim in Schmidt's work is to generate a sequence of nested regions that contain the target. The use of Farey sets solves one of the issues that emerge from [39]. The Farey triangles are not necessarily nested in earlier triangles in the sequence, but all Farey sets are nested in earlier Farey sets in the sequence.

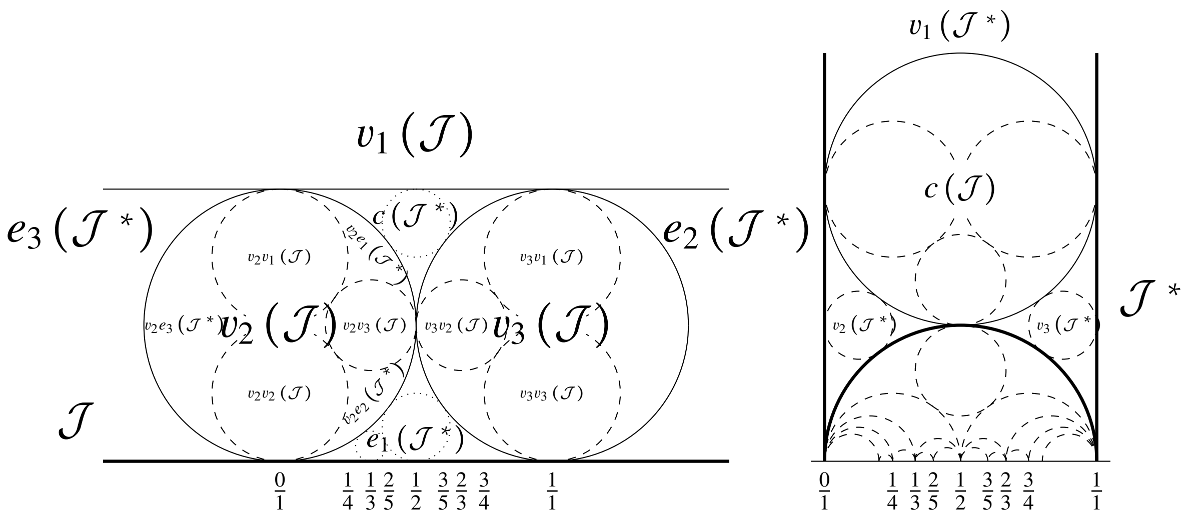

Figure 1.6: a) $\mathcal{J}$ and its subdivision into Farey sets. b) The dual region $\mathcal{J}^*$.

Starting off with one of two closed regions in the complex plane, Schmidt uses the homographic maps associated with the matrices in S to produce two distinct tessellations of the extended complex plane $\mathbb{C}_\infty = \mathbb{C} \cup \{\infty\}$, and they are dual to each other. The upper half plane $\mathcal{J} = \{z = x + iy \mid y \geq 0\}$ is the 'circular' region which is subdivided into 7 regions and $\mathcal{J}^* = \left\{z = x + iy \mid 0 \leq x \leq 1, y \geq (x - x^2)^{\frac{1}{2}}\right\}$ is the triangular region which is subdivided into 4 regions as shown using solid lines and circles in the diagrams of Figure 1.6. Further subdivisions are indicated using dashed and dotted circles.

Geometrization of the Farey triangles in hyperbolic 3-space: The notion of Farey sums and the Farey tessellation of the hyperbolic plane is extended to the case of complex numbers by Hayward and Hockman in [16, 20] where the 3 vertices of each Farey triangle (of Schmidt) and the 3 vertices of its inner subdivision become the 6 vertices of a Farey octahedron in hyperbolic 3 space. The geodesic edges of one such Farey octahedron is shown in the diagram of Figure 1.7. The faces of the Farey octahedron lie on spheres whose centres lie in $\mathbb{C}$. Each sphere passes through the 3 vertices of a Farey triangle defined by the same 3 vertices. It is proved that the tessellation of hyperbolic 3-space by Farey octahedrons is invariant under Möbius maps.

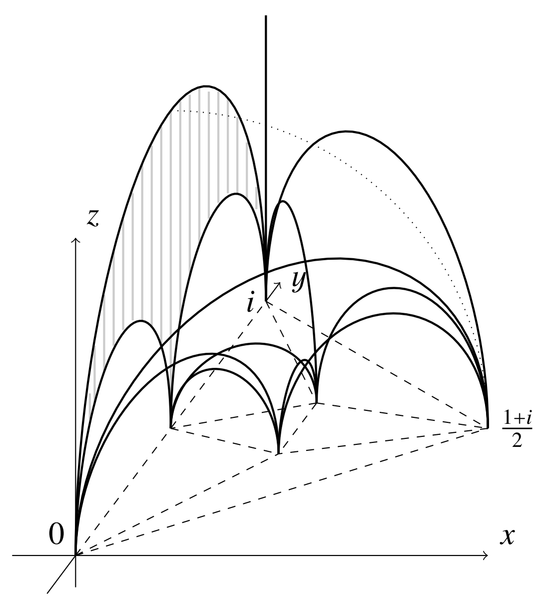

Figure 1.7: An ideal Farey octahedron in $\mathbb{H}^3$ (with its one vertical triangular face shaded) and its projection, in $\mathbb{C}$, to a Farey triangle with its inner subdivision.

Hayward and Hockman explore the properties of Farey neighbours, Farey geodesics and Farey triangles that arise from the Farey tessellation. They treat the Farey addition of two rationals in $\mathbb{R}$ as a subdivision of a Farey interval and hence are able to generalise this notion to a subdivision of a Farey triangle with Gaussian Farey neighbour vertices. They revisit the Farey triangle subdivision given by Schmidt [39] and interpret it as a theorem about adjacent octahedra in the Farey tessellation of $\mathbb{H}^3$. Hockman continues to explore these links in [20, 21].

The vertices of $\infty, 0, 1, i, 1+i, \dfrac{1+i}{2}$ are a feature common to the Farey triangles developed by Schmidt [39], the Farey sets of Schmidt [40], the Farey octahedron found in the work of Hayward [16] and Hockman [19] and in the Schmidt arrangement discussed by Stange in [45].

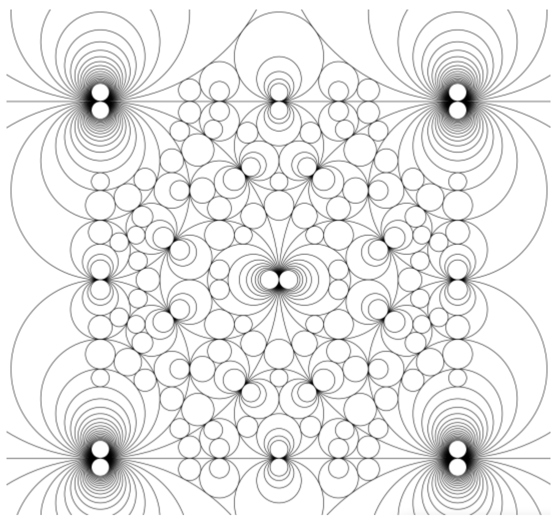

Figure 1.8: The Schmidt arrangement $S_{\mathbb{Q}(\sqrt{-1})}$

According to Stange, the Schmidt arrangement $S_{\mathbb{Q}(\sqrt{-1})}$, in the image[3] in Figure 1.8, was envisioned by Schmidt as a generalization of the theory of Farey fractions and continued fractions to the imaginary quadratic fields [45].

[3]reproduced with kind permission of K. Stange from [45]

The Farey circles shown in Figure 1.8 are the (red) Farey circles of Schmidt arrangement $\hat{S}_{\mathbb{Q}(\sqrt{-1})}$ in Figure 1.9. An identical copy of the Farey circles rotated through 90° about the vertex $\left(\frac{1}{2}, \frac{1}{2}\right)$ give the (blue) dual Farey circles.

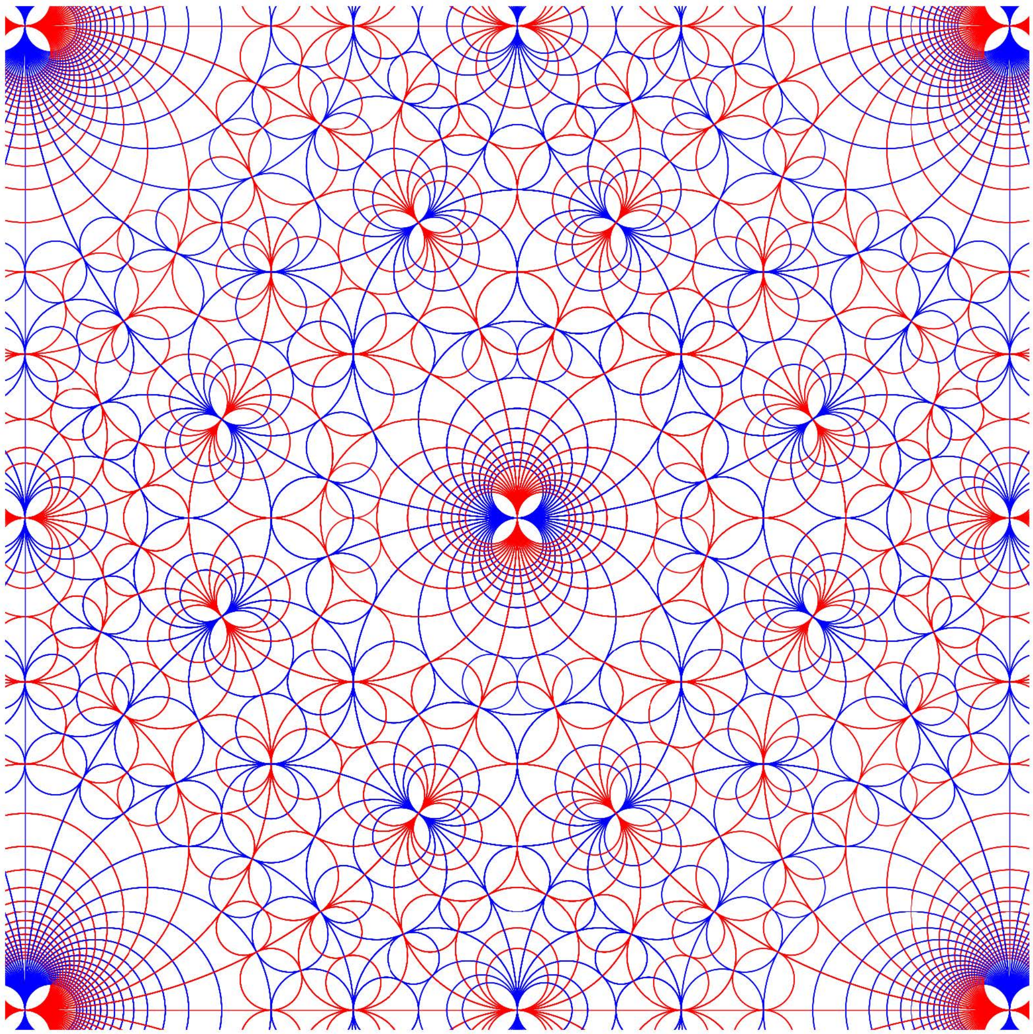

Figure 1.9: The Schmidt arrangement $\hat{S}_{\mathbb{Q}(\sqrt{-1})}$

Stange [45] calls the image[4] in Figure 1.9 the extended Schmidt arrangement $\hat{S}_{\mathbb{Q}(\sqrt{-1})}$. The tessellation consists of red and blue circles in the extended complex plane $\hat{\mathbb{C}} = \mathbb{C} \cup \infty$

[4]reproduced with kind permission of K. Stange from [45]

which are linked directly to the Farey sets and the dual Farey sets of Schmidt respectively. Schmidt works with either the Farey sets or the dual Farey sets at any given time, but never with both simultaneously. Richert [35] proves the structure theorem introduced by Schmidt in [40] which states that each Farey set has a canonical representation in terms of a composition of elements from a special set of seven unimodular maps.

The structure of the arrangement of circles in Figure 1.9 reflects not only the fractal subdivision of $\mathbb{C}$ used in the Gaussian continued fraction algorithm of Schmidt, but also the structure of $S_{\mathbb{Q}(\sqrt{-1})}$ is shown to be an Apollonian super packing. The Farey and dual Farey circles passing through any single complex rational value form a subset of the two orthogonal parabolic pencils of Apollonian circles whose common vertex is located there.

Generalisation of the Farey interval to the Farey simplex and its geometrization in hyperbolic 5-space: The geometry of the analogue of the Farey triangle and the Farey octahedron is, respectively, the Farey simplex and the Farey pentacross described in [31]. The 10 vertices of the pentacross would possibly behave in the same way in the quaternion case as the 3 vertices, 0, 1 and ∞ in the real case, or the six vertices, 0, 1, ∞, i, $1 + i$ and $\frac{1+i}{2}$ in the complex case that are the subject of this thesis. The algebra to be used to explore the case of continued fractions with quaternion 'integer' entries is discussed in [23, 31].

1.2.4 The evolution of thought regarding the geometrical representation of continued fractions.

There are many types of continued fraction. The early continued fractions for π attests to this. The methods used for finding these continued fractions are varied and interesting. We see that the partial quotients of RCFs of square roots of positive integers are periodic and of numbers involving e there are patterns in their partial quotients which manifest an element of periodicity. The geometrical analysis of RCFs was linked to hyperbolic geometry from an early stage.

Finding the regular continued fraction of a real number: The continued fraction with positive b_n for $\xi \in \mathbb{R}$ is generated using the Euclidean algorithm as follows [19, p435]:

- Let $b_0 = \lfloor \xi \rfloor$ the integer part or the floor of ξ.
- Invert the remainder $\xi - \lfloor \xi \rfloor$ to get $\xi_1 = \dfrac{1}{\xi - \lfloor \xi \rfloor}$ and let $b_1 = \lfloor \xi_1 \rfloor$.
- Repeat the last step for $n \geq 2$ by inverting the remainder $\xi_{n-1} - \lfloor \xi_{n-1} \rfloor$ to get

  $$\xi_n = \frac{1}{\xi_{n-1} - \lfloor \xi_{n-1} \rfloor}$$

  and let $b_n = \lfloor \xi_n \rfloor$ until a zero remainder appears or the desired level of accuracy is achieved for the approximant.

For purposes of illustration, we compare the methods of Ford, Series and Schmidt for the periodic RCF of $\sqrt{3} - 1$ found as follows:

- $b_0 = \lfloor \sqrt{3} - 1 \rfloor = 0$.
- $\xi_1 = \dfrac{1}{\sqrt{3} - 1 - 0} = \dfrac{\sqrt{3} + 1}{2} \approx 1,366$, so $b_1 = \lfloor \xi_1 \rfloor = 1$.
- $\xi_2 = \dfrac{1}{\dfrac{\sqrt{3} + 1}{2} - 1} = \sqrt{3} + 1 \approx 2.73$, so $b_2 = \lfloor \xi_1 \rfloor = 2$.
- $\xi_3 = \dfrac{1}{\sqrt{3} + 1 - 2} = \dfrac{\sqrt{3} + 1}{2} = \xi_1$, thus the process repeats.

Hence $\sqrt{3} - 1 = [0, 1, 2, 1, 2, \cdots] = [0, \overline{1, 2}]$, where the integers 1 and 2 recur infinitely. The periodicity of the partial quotients occur as we are using a surd for our example, which is a result discussed in [6]. This periodicity will not affect the generality of the discussion in this thesis.

Ford's method: In the 'Fractions' paper [14], Ford dispenses with the "theory of the elliptic modular group of the complex plane and the scaffolding of group theory" that was used in [13] to work with rational numbers that are represented by circles tangent to the real line in the Euclidean (Cartesian) plane.

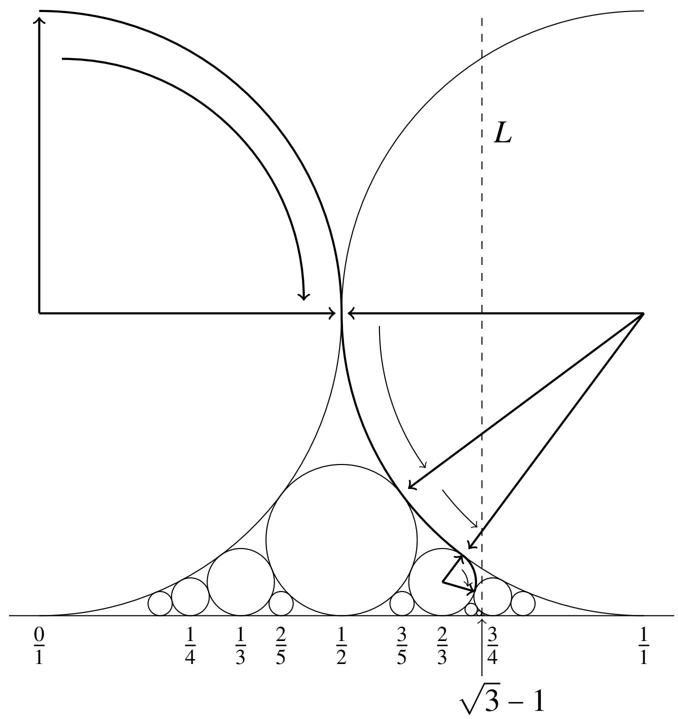

Figure 1.10: The geometric process for using Ford circles to locate $\sqrt{3}-1$.

For the RCF $[0,\overline{1,2}]$ of $\sqrt{3}-1$, we generate convergents C_n by moving through the Ford circles in the diagram of Figure 1.10 as indicated in [14]:

i) Treating each circle as a clock face, start at the circle for $b_0 = 0 = \dfrac{p_0}{q_0}$. Place the hand from the centre of the circle at 0 vertically up. For $b_1 = 1$ we turn the hand clockwise to the first point of tangency. The hand now points to the centre of the circle $\dfrac{p_1}{q_1} = 1$;

ii) For $b_2 = 2$, we now place the hand at the centre of the circle $\dfrac{p_1}{q_1}$ pointing to the centre of circle $\dfrac{p_0}{q_0}$. Turn the hand counter clockwise (which is positive for the second circle) to the second point of tangency on this circle. The hand now points to the centre of circle $\dfrac{p_2}{q_2} = \dfrac{2}{3}$;

iii) This process is continued infinitely to reach the point $\sqrt{3}-1$.

The first three steps illustrated in the diagram of Figure 1.10 gives the first four convergents $\dfrac{0}{1}, \dfrac{1}{1}, \dfrac{2}{3}$ and $\dfrac{3}{4}$.

When considering the problem of approximants that satisfy the condition

$$\left|\frac{p}{q} - \xi\right| < \frac{k}{q^2} \tag{1.3}$$

for some value k, Ford uses the vertical line L that ends at an irrational ξ on the real line. It is clear that L cuts infinitely many circles and is tangent to none when ξ is irrational. If L cuts the circle for $\frac{p}{q}$ then equation (1.3) is satisfied for $k = \frac{1}{2}$. The regions between any 3 circular arcs are called 'mesh triangles'. In the diagram of Figure 1.10 the line L for $\sqrt{3}-1$ is shown and it cuts the circle at $\frac{1}{1}$ and the circle at $\frac{3}{4}$.
Ford proves the following theorem about mesh triangles:

Theorem 1.2.7. Of the 3 fractions whose circles form the boundary of a mesh triangle which L crosses, at least one satisfies the condition $\left|\frac{p}{q} - \xi\right| < \frac{k}{q^2}$ with $k = \frac{1}{\sqrt{5}}$.

Series' method: The approach taken by Series [42], [41] involves the Farey tessellation of the upper half plane model for the hyperbolic space $\mathbb{H}$. The geodesic $\lambda_{(P,\xi)}$ starting at point P on the imaginary axis and ending at the real $\xi > 0$ passes through the triangles of the Farey tessellation. In the following theorem from [42], Series proves that the number of left and right cuts the geodesic creates across the triangles of the Farey tessellation is linked directly to the corresponding partial quotients of the continued fraction.

Theorem 1.2.8. Let $\xi > 1$ have cutting sequence $L^{n_0}R^{n_1}L^{n_2}\cdots$, $n_i \in \mathbb{N}$. Then $\xi = [n_0; n_1, n_2, \cdots]$. Likewise, $0 < \xi < 1$ has cutting sequence $R^{n_1}L^{n_2}R^{n_3}\cdots$, $n_i \in \mathbb{N}$. Then $\xi = [0; n_1, n_2, \cdots]$.

From the work of Series in [42], we describe the connections between the partial quotients of the RCF for $\sqrt{3}-1$ and the Farey tessellation of $\mathbb{H}$, using the diagram of Figure 1.11, as follows:

i) Sketch an oriented geodesic $\lambda_{(P,\sqrt{3}-1)}$ starting at some point P on the imaginary axis and ending at $\sqrt{3}-1$.

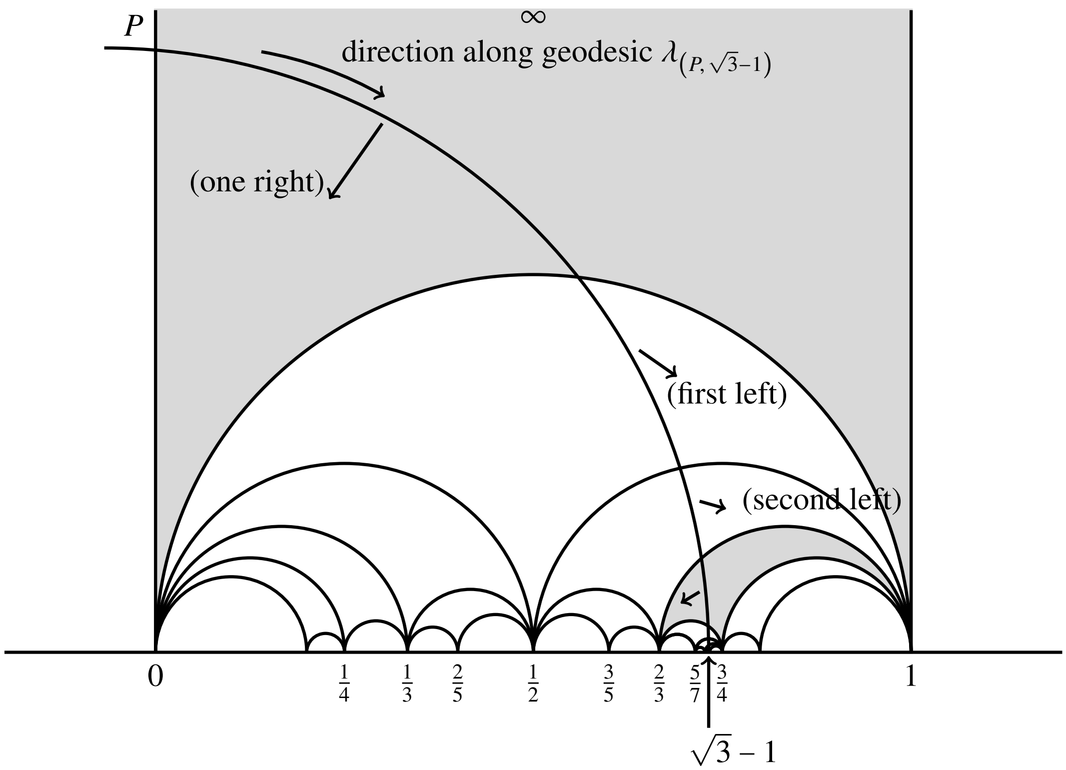

Figure 1.11: The left and right cuts of $\lambda_{(P,\sqrt{3}-1)}$ across the Farey tessellation of $\mathbb{H}^2$.

ii) Mark off the left and right cuts of $\lambda_{(P,\sqrt{3}-1)}$ across the ideal triangles of the Farey tessellation. The shaded triangles have a single vertex to the right of $\lambda_{(P,\sqrt{3}-1)}$ and the white triangles along $\lambda_{(P,\sqrt{3}-1)}$ have a single vertex to the left of the geodesic.

iii) Count the number of consecutive left and right cuts. Along the geodesic $\lambda_{(P,\sqrt{3}-1)}$ there is one shaded triangle followed by two white (unshaded) triangles, and this pattern is repeated as we approach $\sqrt{3}-1$ along the geodesic. This pattern generates the coefficients $0, 1, 2, 1, 2, \cdots$.

The initial 0 of the continued fraction indicates that there are no triangles with one vertex on the left (at ∞) as $\sqrt{3}-1$ lies between 0 and 1.

Schmidt's contribution: In one of the main theorems, Schmidt [40, Thms 2.1 and 2.1*] proves that every complex number ξ is contained in a chain of Farey sets, linked to the vertices of Farey triangles $FT\left(\frac{p_1}{q_1}, \frac{p_2}{q_2}, \frac{p_3}{q_3}\right)$ of Definition 1.2.6, whose vertices satisfy $\lim_{n\to\infty} \frac{p_j^{(n)}}{q_j^{(n)}} = \xi$. A procedure is described for generating chains that are used to generate nested Farey sets that contain ξ. The Möbius transformations used by Schmidt in [40] are drawn from the set $\{v_1, v_2, v_3, e_1, e_2, e_3, c, s, i\}$ associated with the corresponding matrices in S, where the matrix $\begin{pmatrix} a & b \\ c & d \end{pmatrix}$ is associated with the map $m : z \mapsto \dfrac{az+b}{cz+d}$.

These Möbius transformations act on the extended complex plane $\mathbb{C}_\infty$, which can be seen as the boundary of hyperbolic 3-space. Beardon [3, Thm.4.3.4] classifies Möbius transformations of $\widehat{\mathbb{R}^3}$ as follows:

1. g is parabolic if $tr^2(g) = 4$ and g has a unique fixed point in $\mathbb{C}_\infty$
2. g is elliptic if $tr^2(g) \in [0, 4)$ and g has infinitely many fixed points in $\mathbb{R}^3$.
3. g is hyperbolic if $tr^2(g) \in (4, \infty)$ and g has exactly two fixed points in $\mathbb{R}^3$.
4. g is loxodromic if $tr^2(g) \notin [0, \infty)$ and g has exactly two fixed points in $\mathbb{R}^3$. This map combines aspects of hyperbolic and elliptic transformations.

The three relevant maps used by Schmidt for real approximations are illustrated in the diagrams of Figures 1.12, 1.13 and 1.14. We show the complex plane with real x axis and imaginary z axis embedded in $\mathbb{R}^3$. These are Möbius maps acting in $\mathbb{C}$ as they do not preserve $\mathbb{H}$. Schmidt only considers the action of these maps on $\mathbb{C}$, and does not work in hyperbolic space. In fact the role of ∞ is not considered directly. Since Schmidt [40] works with matrices, ∞ is indirectly alluded to in the column with a zero in the bottom row of the matrix $\begin{pmatrix} 1 & 0 & 1 \\ 0 & 1 & 1 \end{pmatrix}$.

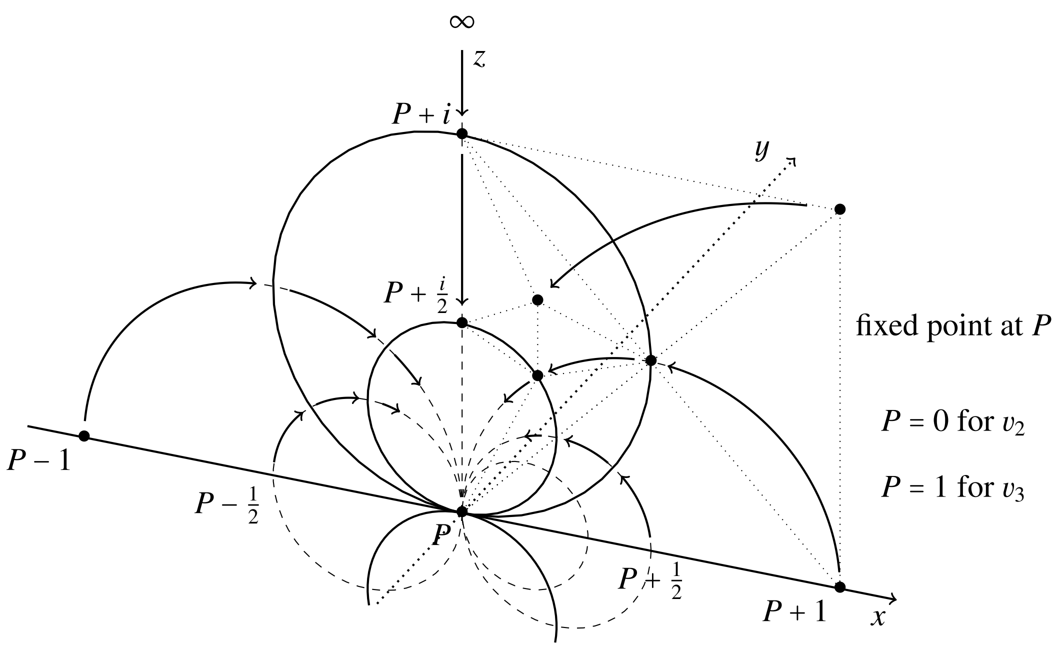

Figure 1.12: The action of the parabolic transformations v_2 (with $P = 0$) and v_3 (with $P = 1$) in $\mathbb{C}$.

Example 1.2.9. The map $v_2(x) = \dfrac{x}{(-i)x + 1}$ is a parabolic map with fixed point at $x = 0$. It maps horocycles tangent to $\mathbb{R}$ at $x = 0$ to each other. This results in the action on $\mathbb{C}_\infty$ shown in the diagram of Figure 1.12 with $P = 0$. In particular:

- ∞ is mapped to i and 1 is mapped to $\dfrac{1+i}{2}$;
- so the real line $\mathbb{R}$ is mapped to the horocycle with diameter from 0 to i;
- which in turn is mapped to the horocycle with diameter from 0 to $\dfrac{i}{2}$.

All points are moved on trajectories which lie on circles that pass through the point 0 and are centred on $\mathbb{R}$.

The action of the map $v_3(x) = \dfrac{(1-i)x + i}{-ix + 1 + i}$ on $\mathbb{C}_\infty$ is the same as the action of the map v_2 illustrated in the diagram of Figure 1.12 but now $P = 1$, so ∞ is mapped to $1 + i$ and 0 is mapped to $\frac{1+i}{2}$.

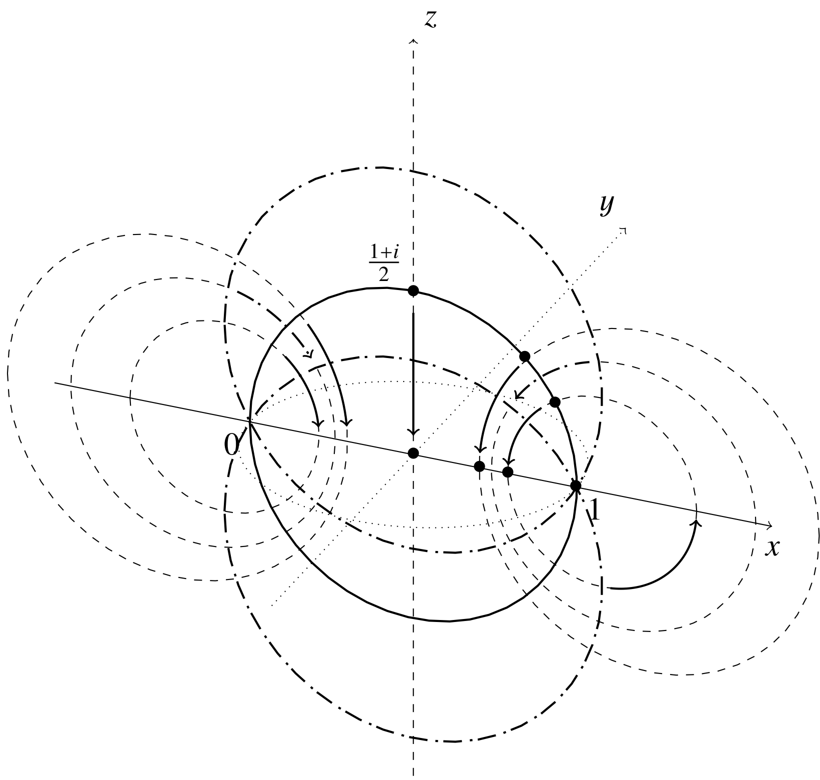

Figure 1.13: The action of the elliptic map e_1 used by Schmidt.

Example 1.2.10. The action of the map $e_1(x) = \dfrac{x}{(1-i)x+i}$ on $\mathbb{C}_\infty$ is illustrated in the diagram of Figure 1.13. The map is elliptic as $tr^2(e_1) = 2$. This map has two fixed points, 0 and 1, in $\mathbb{R}$. Any circle passing through these two points is mapped to another circle through these two points, and individual points are moved along circular trajectories on circles centred on the real axis. In particular the circle with diameter from 0 to 1 is mapped to the extended real line.

Example 1.2.11. The map $f(x) = \dfrac{(3-2i)x+2i}{(2-3i)x+1+2i}$ with $tr^2(f) = 16$ is a hyperbolic map with two fixed points,

$$P_1 = \frac{1+\sqrt{3}-2i}{2-3i} \text{ and } P_2 = \frac{1-\sqrt{3}-2i}{2-3i},$$

which both lie on the circle

$$\left(x-\frac{1}{2}\right)^2 + y^2 = \frac{1}{2}.$$

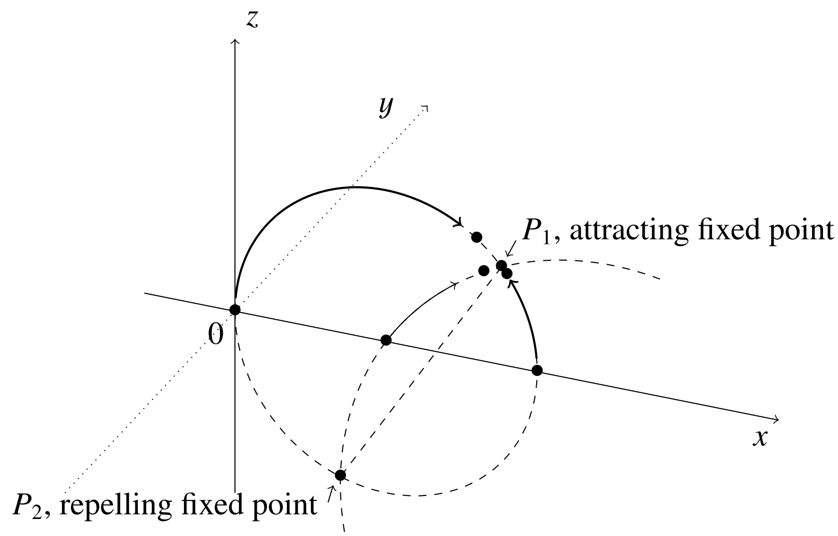

Figure 1.14: The action of the hyperbolic transformation $f(x) = \dfrac{(3-2i)x+2i}{(2-3i)x+1+2i}$ in $\mathbb{C}$.

This is the circle with the diameter from 0 to 1 on the real line and the map f leaves this circle invariant. The action of f on $\mathbb{C}$ is illustrated in the diagram of Figure 1.14

The formulas: For $\xi = \sqrt{3}-1 = [0,\overline{1,2}]$, Schmidts' method yields two sequences of maps [page 18 of [40]]. Firstly, using Farey sets we get the regular chain

$$ch_1\left(\sqrt{3}-1\right) = E_1 V_2^{1-1} V_3^2 V_2 V_3^2 V_2 V_3^2 V_2 \cdots = E_1 \overline{V_3^2 V_2},$$

but, using the dual Farey sets we get the dual regular chain

$$ch_2\left(\sqrt{3}-1\right) = V_1^{-1} C V_3^{1-1} V_2^2 V_3 V_2^2 V_3 V_2^2 V_3 \cdots = V_1^{-1} C \overline{V_2^2 V_3}.$$

The recurring part of the sequence in $ch_1\left(\sqrt{3}-1\right)$ is

$$V_3^2 V_2 = \begin{pmatrix} 3-2i & 2i \\ 2-3i & 1+2i \end{pmatrix}$$

which is the matrix associated with the map f in Example 1.2.11. The Möbius map associated with E_1 is elliptic and it maps the invariant circle to the real line as shown in Example 1.2.10.

The recurring maps $V_2^2V_3$ of the dual chain $ch_2(\sqrt{3}-1)$ have the same invariant circle and fixed points and the Möbius map associated with $V_1^{-1}C$ also maps this circle to the real line. We note that the fixed point $\dfrac{1+\sqrt{3}-2i}{2-3i}$ is the attracting fixed point and it is mapped to $\sqrt{3}-1$ in both cases, while the repelling fixed point $\dfrac{1-\sqrt{3}-2i}{2-3i}$ is mapped to $-\sqrt{3}-1$.

All approximants generated by $ch_1\left(\sqrt{3}-1\right)$ can be read off from the matrices

$$E_1, \quad E_1V_3, \quad E_1V_3^2, \quad E_1V_3^2V_2, \quad E_1V_3^2V_2V_3, \quad E_1V_3^2V_2V_3^2 \ldots.$$

Each product generates three approximations. These three points are the images of 0, 1 and ∞ under the associated Möbius maps acting on $\mathbb{C}_\infty$. One advantage of the Schmidt method is that the best approximant of these points can be determined by noting the next map in the sequence. If V_2 is the next matrix then the image of 0 is the closest of the three to $\sqrt{3}-1$, whereas if V_3 is the next matrix then the image of 1 is the closest to $\sqrt{3}-1$. Associated with this sequence of 'letters', we have a sequence of products $\left\langle M_n\right\rangle$, where $M_n = T_1 \ldots T_n$ and $T_j \in \mathbf{S} = \{V_1, V_2, V_3, E_1, E_2, E_3, C, S, I\}$ for all $j = 1, \cdots, n$. Schmidt specifies that the E_j matrices for $j = 1, 2, 3$ may not occur consecutively in the sequence of matrices, in fact they must be separated from each other by a C matrix. The V_j matrices for $j = 1, 2, 3$ and C matrix may occur in any order without restriction.

1.2.5 The geometry underlying the process of using continued fractions to find rational approximations of irrational numbers.

The calculation of convergents $\frac{A_n}{B_n}$ for continued fractions originally [4] made use of the recurrence relations

$$A_n = b_nA_{n-1} + a_nA_{n-2}$$

$$B_n = b_nB_{n-1} + a_nB_{n-2}$$

to produce successive convergents, with initial conditions

$$A_{-1} = B_0 = 1 \text{ and } B_{-1} = A_0 = 0.$$

However, the sequence of convergents can also be evaluated using the map $s_n(z) = \dfrac{a_n}{b_n + z}$ and $S_n(\infty) = 0$. The truncated continued fractions of Equation (1.2) are

$$s_1(0), s_1 s_2(0), s_1 s_2 s_3(0), \cdots,$$

where fg denotes the maps $z \mapsto f(g(z))$, so the convergence of the continued fraction is equivalent to the convergence of the complex sequence $s_1 \cdots s_n(0)$.

Beardon [4] gives a brief history of the development of the idea of regarding the continued fraction as a sequence of complex Möbius maps, noting that the paper 'The continued fraction as a sequence of linear transformations' by Paydon and Wall (1948) as marking the point from which the continued fraction was consistently viewed as a sequence of Möbius maps.

In [7], Beardon, Hockman and Short discuss the notion of an integer continued fraction expansion (in brevity, an ICF expansion) of a rational number ξ. The sequence of convergents $\langle \infty, \frac{A_1}{B_1}, \frac{A_2}{B_2}, \frac{A_3}{B_3}, \cdots, \xi \rangle$ form a geodesic path generated by the convergents of an ICF expansion. A path that passes through the vertices $v_1, \cdots, v_n$ in this order is denoted by $\langle v_1, \cdots, v_n \rangle$. This path can be realised in the Farey tessellation $\mathcal{F}$ of the upper half plane model of hyperbolic space $\mathbb{H}$ along geodesics joining consecutive vertices v_i and v_{i+1}, if the v_i are reduced rationals with $v_i \sim v_{i+1}$. The shortest such path is called the geodesic expansion of ξ. It is proved that for any rational number x, $C_1, \cdots, C_n$ with $C_n = x$ are the consecutive convergents of some ICF expansion if and only if $\langle \infty, C_1, \cdots, C_n \rangle$ is a path in $\mathcal{F}$ from ∞ to x. There may be more than one shortest path. They construct a shortest path called the ancestral path [see [7], p137], where C_i is a parent of C_{i+1}, $i = 1, \cdots, n$.

1.3 Motivation

In [40], Schmidt states that attempts to generalise the algorithm for the *RCF* to complex numbers (or numbers in higher dimensions) become complicated and loose a lot of the nice features found for the real case. In our endeavour, we are inspired by 2 guiding principles:

- In the various works of Beardon, Hockman and Short ([7, 8, 6, 4, 19, 21]) the approach of interpreting continued fractions by using Möbius maps in the context of hyperbolic space is expounded since these maps act as isometries in this space.

- In "Open problems in geometry of continued fractions" by Karpenkov [27], problem 19 states:

  > *"Find a natural generalization of the Farey tessellation to higher dimensional hyperbolic geometry. " [27]*

  The first requirement in [27] is to generalise Farey summation and its representation as a Farey tessellation.

We start with the examples of Schmidt, bearing these 2 points in mind, in an attempt to mould our approach for interpreting continued fractions.

Developing an approach: Schmidt's work provides the most compelling inspiration. The main focus is to create a sequence of regions that are nested in each other and each of these regions contains the target number. In [39], Schmidt generalises the notion of Farey numbers to the complex plane using Farey triangles. Specific unimodular maps are used to map ∞, 0 and 1, the vertices of the fundamental triangle, to the vertices of any triangle in the tessellation. By choosing the right maps, the fundamental triangle can be mapped to any triangle that contains the target, and these triangles form a sequence of nested regions that contain the target. This approach is problematic as successive triangles in the sequence are not necessarily nested in triangles generated earlier in the sequence.
The second paper [40] proceeds from the first paper, keeping the main ideas of Farey subdivision, unimodular maps and nested regions, but the approach has changed completely. Farey triangles are replaced by Farey sets and nine unimodular maps are introduced that allow us to navigate the Farey sets in a very specific way. The complex plane is tessellated into Farey sets starting with three pairwise tangent circles circumscribed by a fourth circle. Each new circle must be tangential to three pairwise tangential circles in the tessellation.

With $M_n = T_1 \ldots T_n$ and $T_j \in \mathbf{S} = \{V_1, V_2, V_3, E_1, E_2, E_3, C, S, I\}$ for all $j = 1, \cdots, n$, Schmidt's method generates a sequence of nested Farey sets where $\xi \in M_n(R)$ and $M_n(R) \subset M_{n-1}(R)$, where $R = \mathcal{J}$ if $M_n(R)$ is circular and $R = \mathcal{J}^*$ if $M_n(R)$ is a mesh triangle.

Schmidt's method in [40] is linked directly to the partial quotients of the RCF when this method is restricted to the real case, but not at all for the complex case. Another problem is that Schmidt's method introduces a dual situation in the geometry so each number can be represented by one of two separate products of maps - the regular chain and the dual regular chain. We are unclear about the process Schmidt uses to select the maps that appear in these chains.

Using the chain and dual chain of Schmidt we are able to sketch nested Farey sets that contain the target number. These regions provide a visual justification for the choices of maps.

An example: Consider $\sqrt{7+3i}$ which is roughly $2.7033102\cdots + i0.5548752\cdots$. Schmidt generates the chain $ch\sqrt{7+3i} = E_2\overline{V_1CV_1V_3V_1V_1E_2V_1CV_3E_1CE_1V_3V_3V_3SS}$ in [40, Example 3.2]. In the example $ch\sqrt{7+3i}$ is of type (a) with $j = 2$ indicating that when one finishes V_3 at the end of the chain, 2 iterations of S are required before one can proceed with V_1 at the start of the next period. Each iteration of S permutes the values 0, 1 and ∞ before proceeding to the next map. As a matter of interest, there is no dual chain for $\sqrt{7+3i}$ as this number is located outside of the region $\mathcal{J}^*$. From this chain we generate Table 1.1, where the second column consists of the sequence of matrices T_n of $ch\sqrt{7+3i}$. The third column gives the product $M_n = T_1 \ldots T_n$ where $T_j \in \mathbf{S} = \{V_r, E_r, C, S, I\}$, $r = 1, 2, 3$ for all $j = 1, \cdots, n$. The last three columns give the values of v_1, v_2 and v_3 determined directly from the matrix via the calculations shown in the second line of the Table 1.1. Each matrix product has its own vertices v_1, v_2 and v_3. We note from this table which vertices remain fixed as we go from one line to the next. For instance, the map V_1 fixes v_1 (see rows with $i = 4, 6$ and 7) and E_1 fixes v_2 and v_3 (see rows with $i = 12$ and 14).

n	T_n	M_n	v_1	v_2	v_3
		$\begin{pmatrix} a & b & m & n \\ c & d & p & q \end{pmatrix}$	$\frac{a+bi}{c+di}$	$\frac{m+ni}{p+qi}$	$\frac{(a+m)+(b+n)i}{(c+p)+(d+q)i}$
			∞	0	1
1	E_2	$\begin{pmatrix} 1 & 0 & -1 & 1 \\ 0 & 0 & 0 & 1 \end{pmatrix}$	∞	$1+i$	1
2	V_1 start	$\begin{pmatrix} 1 & 0 & -1 & 2 \\ 0 & 0 & 0 & 1 \end{pmatrix}$	∞	$2+i$	2
3	C	$\begin{pmatrix} 2 & 3 & -3 & 0 \\ 1 & 1 & -1 & 0 \end{pmatrix}$	$\frac{5+i}{2}$	3	$3+i$
4	V_1	$\begin{pmatrix} 2 & 3 & -6 & 2 \\ 1 & 1 & -2 & 1 \end{pmatrix}$	$\frac{5+i}{2}$	$\frac{14+2i}{5}$	$\frac{14+3i}{5}$
5	V_3	$\begin{pmatrix} 7 & 7 & -11 & -2 \\ 3 & 2 & -4 & 0 \end{pmatrix}$	$\frac{35+7i}{13}$	$\frac{44+8i}{16}$	$\frac{14+3i}{5}$
6	V_1	$\begin{pmatrix} 7 & 7 & -18 & 5 \\ 3 & 2 & -6 & 3 \end{pmatrix}$	$\frac{35+7i}{13}$	$\frac{123+24i}{45}$	$\frac{93+19i}{34}$
7	V_1	$\begin{pmatrix} 7 & 7 & -25 & 12 \\ 3 & 2 & -8 & 6 \end{pmatrix}$	$\frac{35+7i}{13}$	$\frac{272+54i}{100}$	$\frac{242+49i}{89}$
8	E_2	$\begin{pmatrix} 7 & 7 & -26 & -25 \\ 3 & 2 & -11 & -7 \end{pmatrix}$	$\frac{35+7i}{13}$	$\frac{461+93i}{170}$	$\frac{242+49i}{89}$
9	V_1	$\begin{pmatrix} 7 & 7 & -33 & -18 \\ 3 & 2 & -13 & -4 \end{pmatrix}$	$\frac{35+7i}{13}$	$\frac{501+102i}{185}$	$\frac{282+58i}{107}$
10	C	$\begin{pmatrix} -44 & 22 & 4 & -33 \\ -14 & 11 & -1 & -12 \end{pmatrix}$	$\frac{858+176i}{317}$	$\frac{392+81i}{145}$	$\frac{611+125i}{226}$
11	V_3	$\begin{pmatrix} -55 & 62 & 15 & -73 \\ -15 & 26 & 0 & -27 \end{pmatrix}$	$\frac{2437+500i}{901}$	$\frac{1971+405i}{729}$	$\frac{611+125i}{226}$
12	E_1	$\begin{pmatrix} -113 & -26 & 73 & 15 \\ -42 & -1 & 27 & 0 \end{pmatrix}$	$\frac{4772+979i}{1765}$	$\frac{1971+405i}{729}$	$\frac{611+125i}{226}$
13	C	$\begin{pmatrix} -25 & -84 & 124 & -14 \\ -15 & -28 & 43 & -14 \end{pmatrix}$	$\frac{2727+560i}{1009}$	$\frac{5528+1134i}{2045}$	$\frac{6888+1414i}{2548}$
14	E_1	$\begin{pmatrix} 85 & -222 & 14 & 124 \\ 14 & -85 & 14 & 43 \end{pmatrix}$	$\frac{20060+4117i}{7421}$	$\frac{5528+1134i}{2045}$	$\frac{6888+1414i}{2548}$
15	V_3	$\begin{pmatrix} -13 & -321 & 112 & 223 \\ -28 & -113 & 56 & 71 \end{pmatrix}$	$\frac{36637+7519i}{13553}$	$\frac{22105+4536i}{8177}$	$\frac{6888+1414i}{2548}$
16	V_3	$\begin{pmatrix} -111 & -420 & 210 & 322 \\ -70 & -141 & 98 & 99 \end{pmatrix}$	$\frac{66990+13749i}{24781}$	$\frac{52458+10766i}{19405}$	$\frac{6888+1414i}{2548}$
17	V_3	$\begin{pmatrix} -209 & -519 & 308 & 421 \\ -112 & -169 & 140 & 127 \end{pmatrix}$	$\frac{111119+22807i}{41105}$	$\frac{96587+19824i}{35729}$	$\frac{6888+1414i}{2548}$
18	SS	$\begin{pmatrix} -99 & 98 & -209 & -519 \\ -28 & 42 & -112 & -169 \end{pmatrix}$	$\frac{6888+1414i}{2548}$	$\frac{111119+22807i}{41105}$	$\frac{96587+19824i}{35729}$
19	V_1 repeat	$\begin{pmatrix} -99 & 98 & -307 & -618 \\ -28 & 42 & -154 & -197 \end{pmatrix}$	$\frac{6888+1414i}{2548}$	$\frac{169024+34693i}{62525}$	$\frac{154492+31710i}{57149}$
20	C	$\begin{pmatrix} -1024 & -213 & 619 & -504 \\ -379 & -1 & 183 & -224 \end{pmatrix}$	$\frac{388309+79703i}{143642}$	$\frac{226173+46424i}{83665}$	$\frac{240705+49407i}{89041}$
21	V_1	$\dots$	$\frac{388309+79703i}{143642}$	$\dots$	$\dots$

Table 1.1: v_1, v_2 and v_3 generated by Schmidt's matrices.

The diagrams in Figures 1.15 and 1.16 show the progression of the vertices v_1, v_2 and v_3 read from successive lines in Table 1.1 as well as the Farey set associated with these vertices. The label under each diagram gives the Farey set bound by solid lines and arcs in the diagram above it. Each Farey set bound by solid lines and arcs appears as the shape bound by heavy dashed lines and arcs in the following image. The successive Farey sets contain the value $\sqrt{7+3i}$ which is represented with $*$ in each image.

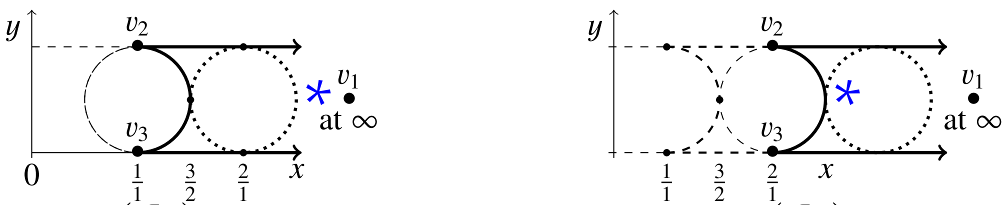

$E_2(\mathcal{J}^*)$ $E_2V_1(\mathcal{J}^*)$

$E_2(\mathcal{J}^*)$ and $E_2V_1(\mathcal{J}^*)$ are triangular as they are images of $\mathcal{J}^*$,

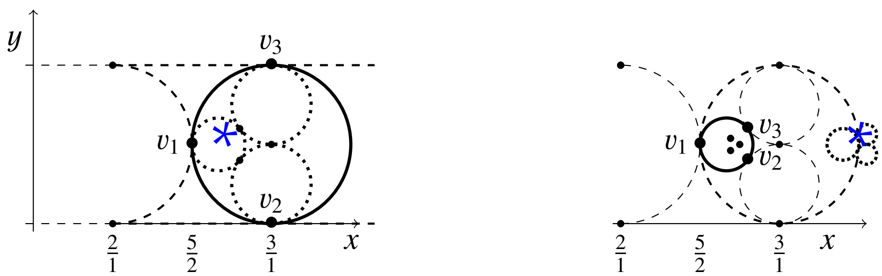

$E_2V_1C(\mathcal{J})$ $E_2V_1CV_1(\mathcal{J})$

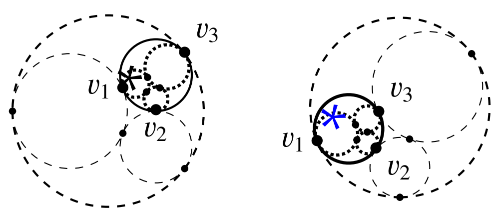

$E_2V_1CV_1V_3(\mathcal{J})$ $E_2V_1CV_1V_3V_1(\mathcal{J})$

$E_2V_1C(\mathcal{J})$, $E_2V_1CV_1(\mathcal{J})$, $E_2V_1CV_1V_3(\mathcal{J})$ and $E_2V_1CV_1V_3V_1(\mathcal{J})$ are all circular as they are images of $\mathcal{J}$,

Figure 1.15: Progression of v_1, v_2 and v_3 under successive Schmidt maps.

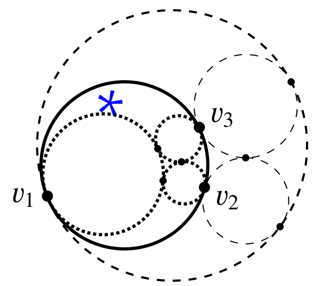

$E_2V_1CV_1V_3V_1V_1\,(\mathcal{J})$

$E_2V_1CV_1V_3V_1V_1\,(\mathcal{J})$ is circular, but the $\ast$ now appears in
a triangular region, so the next Farey set will be an image of $\mathcal{J}^{\,*}$

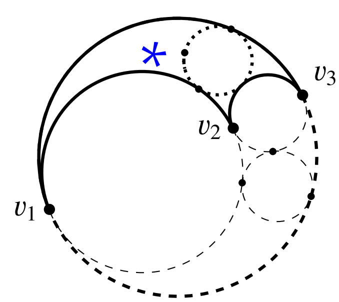

$E_2V_1CV_1V_3V_1V_1E_2\,(\mathcal{J}^{\,*})$

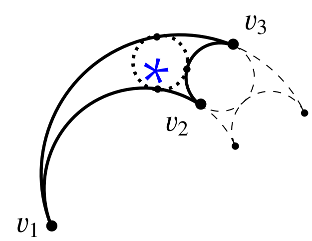

$E_2V_1CV_1V_3V_1V_1E_2V_1\,(\mathcal{J}^{\,*})$

$E_2V_1CV_1V_3V_1V_1E_2\,(\mathcal{J}^{\,*})$ and $E_2V_1CV_1V_3V_1V_1E_2V_1\,(\mathcal{J}^{\,*})$ are both triangular, but now
$\ast$ appears in the circular region given by $E_2V_1CV_1V_3V_1V_1E_2V_1C\,(\mathcal{J})$, and so on...

Figure 1.16: Progression of v_1, v_2 and v_3 under successive Schmidt maps.

The Diophantine approximations to the target ξ are read off from $M_n(\xi)$. We get a sequence of candidate approximations $\dfrac{p_n^{(j)}}{q_n^{(j)}}$, for $j = 1, 2, 3$, given by

$$\begin{pmatrix} p_n^{(1)} & p_n^{(2)} & p_n^{(3)} \\ q_n^{(1)} & q_n^{(2)} & q_n^{(3)} \end{pmatrix} = M_n \begin{pmatrix} 1 & 0 & 1 \\ 0 & 1 & 1 \end{pmatrix}$$

with $v_1 = \frac{p_n^{(1)}}{q_n^{(1)}}$, $v_2 = \frac{p_n^{(2)}}{q_n^{(2)}}$ and $v_3 = \frac{p_n^{(3)}}{q_n^{(3)}}$. We determine a sequence of approximants $\left\langle r_n \right\rangle$, where r_n is whichever of the three fractions $\frac{p_n^{(j)}}{q_n^{(j)}}$, $j = 1, 2, 3$ is nearest ξ [17, 40]. We note that each value of n results in an iteration of the vertices v_1, v_2 and v_3, which, in turn, generate a Farey set containing the target and that each subsequent Farey set is completely contained in all Farey sets earlier in the sequence. The vertices themselves are complex rational approximations of the target.

Bringing back the continued fraction: For $\sqrt{7+3i} = 2.7033102\cdots + i0.5548752\cdots$ we get the $NICF$

$$[3+i, \overline{-1+2i, 2i, -2-3i, -1-3i, 1-i, 5+i}]$$

from which we derive the product of parabolic Möbius maps

$$\tau_{3+i}\overline{(\phi\tau_{-1+2i}\phi)\,\tau_{2i}\,(\phi\tau_{-2-3i}\phi)\,\tau_{-1-3i}\,(\phi\tau_{1-i}\phi)\,\tau_{5+i}}.$$

Our quest: We ask two questions.

- Is it possible to generate the Farey sets and/or dual Farey sets of Schmidt using the Möbius maps derived from the $NICF$?
- Is it possible to trace the orbits of vertices v_1, v_2 and v_3 using the Möbius maps derived from the $NICF$?

We use Schmidts' examples to see if we can achieve his results under these two constraints. All examples of Schmidt, in [40], involve surds, so the $NICF$ are periodic. This is not a problem, as the behaviour of the maps generated by the continued fraction will behave the same whether the products are periodic or not.

Next, Beardon, Hockman and Short [7] present an appealing algorithm for constructing a shortest path through the use of the ancestral path. We wish to explore an alternate algorithm for generating a shortest path using the Möbius maps derived from the $NICF$.

We study the paths generated, both in terms of how the sets of 3 (or 6 in the complex case) vertices emerge in the new algorithm and in terms of which vertex of the 3 (or 6) presented are closest to target.

Method and Tools: We used Microsoft Excel to calculate the images of the vertices ∞, 0 and 1 under Möbius maps by finding the numerators and denominators of $\frac{p_n^{(j)}}{q_n^{(j)}}$ for $j = 1, 2, 3$, where $p_n^{(j)} = a + bi, q_n^{(j)} = c + di \in \mathbb{C}$. Using Microsoft Excel we changed $\frac{p_n^{(j)}}{q_n^{(j)}}$ to a fraction with a real denominator and real and imaginary parts in the numerator using the formula $\frac{ac - bd + i\,(ad + bc)}{c^2 + d^2}$. In Wingeom[5] we represented these points with coordinates $\left(\frac{ac - bd}{c^2 + d^2}, \frac{ad + bc}{c^2 + d^2}\right)$. Wingeom allows one to zoom in to points that have up to 19 decimal places the same, so

$$(0, 0) \text{ and } (0.0000000000000000001\,,\, 0.0000000000000000001)$$

become separate points when you zoom in. One can also circumscribe any 3 points with a circle so it is easy to sketch the Farey sets.

Results and developments: We initially studied the approximations by forming sequences of Farey triangles whose vertices are the images of ∞, 0 and 1 under successive Möbius maps derived from the continued fraction, but the Farey triangles are not necessarily nested in the triangle that appears earlier in the sequence. Then, using the same Möbius maps, we switched to Schmidt's Farey sets which use the same vertices as the Farey triangles but we use circles instead of triangles.

One big difference between Schmidt's maps and our Möbius maps is that Schmidt had a map with a fixed point at 1, and not just at ∞ and 0 as is the case with the Möbius maps.

[5]We used Wingeom[v 1.54] for Windows 95/98/ME/2K/XP/Vista7 version compiled 2010: (Richard Parris) rparis@exeter.edu http://math.exeter.edu/rparris.

One way of dealing with the problem was to use the RCF instead of the $NICF$.

Another way was to find which maps cause a problem and see how we should circumvent the problem. After a bit of experimentation we notice that parsing $\tau_{b_0}\phi\tau_{b_1}\phi\tau_{b_2}\phi\tau_{b_3}\phi\tau_{b_4}\phi\tau_{b_5}\phi\cdots$, the product of maps derived from the $NICF$ $[b_0, b_1, b_2 \ldots]$, as follows:

$$\tau_{b_0}\left(\phi\tau_{b_1}\phi\right)\tau_{b_2}\left(\phi\tau_{b_3}\phi\right)\tau_{b_4}\left(\phi\tau_{b_5}\phi\right)\cdots$$

generates images that are easier to interpret, but sometimes the images go "one Farey set too far".

Why? and How do we fix it?

Essentially, we needed to figure out how to use Möbius maps derived from the continued fraction to generate the same Farey sets that are generated by Schmidt's maps. The recognition that Möbius maps act as the isometries of hyperbolic space introduced a new perspective on using continued fractions to approximate irrationals.

The method evolves: As we were trying to generalize the nice features of the continued fractions from the real case to higher dimensions, we used the examples of Schmidt's paper [40] (1975 - Diophantine approximation of complex numbers) to see which maps derived from the continued fraction would yield the same results. Bearing in mind the vertices of Farey octahedrons in [16], we decided to track the images of the six vertices, namely $0, 1, \infty, i, 1+i$ and $\frac{1+i}{2}$, under successive $T_n = t_1 t_2 t_3 \ldots t_n$ derived from the $NICF$. We started by using parabolic maps only, namely $t_n = \tau_{b_n}$ and $t_{n+1}(x) = \phi\tau_{b_{n+1}}\phi$, where $\tau_{b_n} = x + b_n$ and $\phi = 1/x$, and the t_n factors of T_n alternate between fixing 0 and fixing ∞. The difficulty to overcome is the fact that sometimes the Farey set found using T_n does not contain the target.

Since the approximations are generated by the images of $0, 1, \infty, i, 1+i$ and $\frac{1+i}{2}$, we tracked the progress of the approximations using images under successive T_n which we generated using the partial quotients of the $NICF$. Under the influence of parabolic maps successive images formed a path along trajectories found among the circles of Schmidt's Farey sets and dual Farey sets that lead toward the target ξ.

When the image under T_n yielded a Farey set adjacent to the one that contained the target, we decomposed the final factor of T_n into its constituent parts in an effort to see what this factor should rather be to get the desired Farey set containing the target. We then also had to decide what to do with that part of the factor that caused the problem.

Also, on decomposing the final factor of T_{n+1}, we noticed that the desired Farey set containing the target would be an image again before moving on to further Farey sets containing the target.

An important breakthrough occurred when we realised that the vertices of the "desired Farey set containing the target" were being permuted, as images of $0, 1, \infty, i, 1+i$ and $\frac{1+i}{2}$, when they appeared again. The elliptic maps responsible for permuting the vertices $0, 1, \infty, i, 1+i$ and $\frac{1+i}{2}$ where embedded among the parabolic maps we were using. We had to extract the elliptic maps and treat them as separate factors.

The T_n actually formed products of Möbius maps, in particular of parabolic and elliptic Möbius maps.

1.4 Basic Definitions and techniques

Any irrational number ξ has an infinite continued fraction representation,

$$\xi = b_0 + \cfrac{1}{b_1 + \cfrac{1}{b_2 + \ddots}} = [b_0, b_1, b_2, \cdots],$$

where traditionally the partial quotients $b_j,\ j \in \mathbb{N}_0 = \mathbb{N} \cup \{0\}$ satisfy $b_0 \in \mathbb{Z}, b_j \in \mathbb{N}$. This is the regular continued fraction (RCF) and it is derived using the Euclidean algorithm [19]. One finds rational approximants of ξ by truncating the continued fraction at the nth partial quotient b_n to get convergents $C_n = \dfrac{p_n}{q_n} = [b_0, b_1, \cdots, b_n]$, determined as a rational in reduced form.

For the basis of our geometrical approach to approximate real numbers using reduced rationals, the usual method of bisecting intervals containing the target is replaced by the process of Farey subdivision of the Farey interval containing the target. We start with definition of Farey neighbours and Farey intervals.

Definition 1.4.1. Reduced rationals $\dfrac{a}{b}$ and $\dfrac{c}{d}$, with $a, b, c, d \in \mathbb{Z}$, $b, d > 0$ and $\gcd(a, b) = \gcd(c, d) = 1$, are called Farey neighbours, denoted $\dfrac{a}{b} \sim \dfrac{c}{d}$, if the condition $|ad - bc| = 1$ is satisfied. If $\dfrac{a}{b} < \dfrac{c}{d}$, the interval $\left[\dfrac{a}{b}, \dfrac{c}{d}\right]$ is a Farey interval if $\dfrac{a}{b} \sim \dfrac{c}{d}$.

The method of Farey subdivision requires the Farey sum of two Farey neighbours defined as follows in [19].

Definition 1.4.2. The Farey sums of two Farey neighbours $\dfrac{a}{b}$ and $\dfrac{c}{d}$, with $a, b, c, d \in \mathbb{Z}$, $b, d > 0$ and $\dfrac{a}{b} < \dfrac{c}{d}$, is given by $\dfrac{a}{b} \oplus \dfrac{c}{d} = \dfrac{a+c}{b+d}$.

It is simple to prove that the Farey sum of $\dfrac{a}{b}$ and $\dfrac{c}{d}$ is a Farey neighbour of both $\dfrac{a}{b}$ and $\dfrac{c}{d}$, and it provides the next approximant, as $\dfrac{a}{b} \oplus \dfrac{c}{d} \in \left(\dfrac{a}{b}, \dfrac{c}{d}\right)$.

The use of RCFs to generate approximations shortcuts the process of Farey subdivision. Only a selection of the Farey fractions yielded by Farey subdivision are convergents of the RCF.

While Ford [14] and Series [42, 41] both use processes that involve matching the partial quotients of the RCF to static features of their respective geometric structures, Schmidt [40] develops a much more dynamic approach involving the same structures. Each of the geometrical approaches is linked to the Farey tessellation of the hyperbolic plane $\mathbb{H}$ and the Ford Circles in $\mathbb{R}^2$ by duality.

Schmidt's work on finding Diophantine approximations evolves dramatically from the 'Farey triangles and Farey quadrangles' paper [39] of 1967 to the 'Diophantine approximation of complex numbers' paper [40] of 1975. In [40] the duality between the two representations is recognised and both systems are used in tandem. The latter paper provides diagrams of Farey sets (and their duals) which facilitate the process of finding approximations for complex irrationals. The duality, illustrated in the diagram of Figure 1.17, between the Ford circles and the Farey tessellation is referred to by Beardon, Hockman and Short, in their work on continued fractions in [7, p.135].

Both representations use the Farey fractions as their foundation, thus imposing a new organizational structure on the set of reals. We compare geometric features in Figure 1.17:

- Each endpoint of a geodesic in the Farey tessellation corresponds to a Ford circle, and both represent a reduced rational in their respective contexts.

- All geodesics of the Farey tessellation are Farey geodesics that correspond to the points of contact between Ford circles, and both indicate that the corresponding rationals $\frac{a}{b}$ and $\frac{c}{d}$, $a, b, c, d \in \mathbb{Z}$, are Farey neighbours, denoted $\frac{a}{b} \sim \frac{c}{d}$, satisfying the Farey condition $|ad - bc| = 1$.

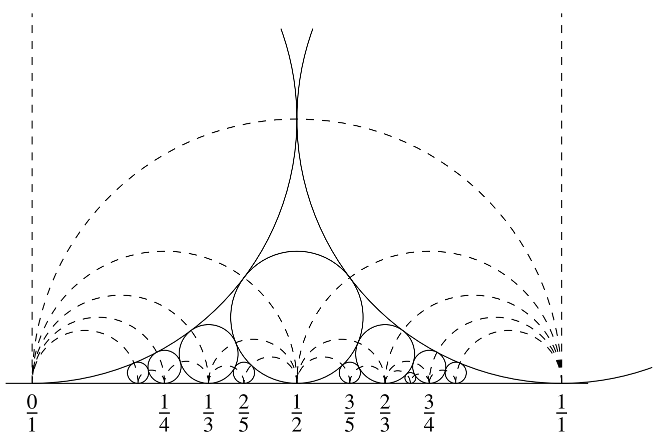

Farey tessellation - dashed

Ford circles - solid

Figure 1.17: Duality between the Ford circles and the Farey tessellation.

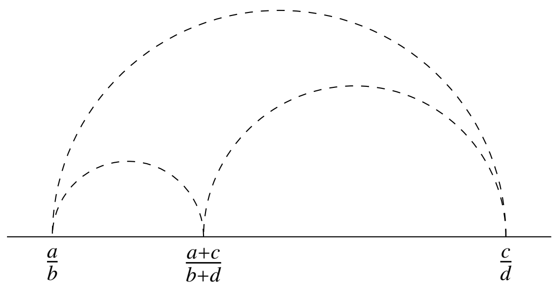

Figure 1.18: Farey subdivision of the Farey interval $\left[\frac{a}{b}, \frac{c}{d}\right]$ represented in the Farey tessellation.

The process of Farey subdivision is illustrated more easily using the Farey tessellation of $\mathbb{H}$, as shown in the diagram of Figure 1.18. Each Farey geodesic $\lambda_{\left(\frac{a}{b}, \frac{c}{d}\right)}$ is one side of a Farey triangle with Farey geodesics $\lambda_{\left(\frac{a}{b}, \frac{a+c}{b+d}\right)}$ and $\lambda_{\left(\frac{a+c}{b+d}, \frac{c}{d}\right)}$ forming the other two sides. Each Farey triangle forms a representation of the process of Farey subdivision of the interval $\left[\frac{a}{b}, \frac{c}{d}\right]$ by the Farey sum $\frac{a}{b} \oplus \frac{c}{d} = \frac{a+c}{b+d}$.

Hensley [17] notes that the algorithm of Schmidt in [40], which is linked to the RCF, generates approximations accurately, but quite slowly, and moves on to discuss the nearest integer algorithm where the partial quotients of the continued fraction are generated using the nearest integer division algorithm. We call this type of continued fraction the nearest integer continued fraction ($NICF$). According to Hensley, we sacrifice accuracy for speed when generating approximants by truncating the $NICF$. For our analysis of the differences between the two types of continued fraction we use Beardon's suggestion [4, 5, 6] that we analyse the behaviour of continued fractions in the context of hyperbolic space where Möbius maps act as isometries.

Definition 1.4.3. Möbius transformations are functions of the form $g(z) = \frac{az+b}{cz+d}$, $a, b, c, d \in \mathbb{C}$ with $ad - bc \neq 0$, which map the extended complex plane $\mathbb{C}_\infty = \mathbb{C} \cup \{\infty\}$ onto itself with $g(\infty) = \frac{a}{c}$ and $g\left(\frac{-d}{c}\right) = \infty$.

The Möbius transformation $f(z) = \dfrac{(b_0b_1+1)\,z+b_0}{b_1z+1}$ expresses the continued fraction $f(z) = b_0 + \dfrac{1}{b_1+\dfrac{1}{z}}$ and it maps Farey geodesics to Farey geodesics, a property we use in our analysis.

There is a strong correlation [6] between quadratic irrationals and continued fractions, so quadratic irrationals play a central role in continued fraction theory. Beardon [6] defines a periodic continued fraction as follows:

Definition 1.4.4. A continued fraction $[b_0, b_1, b_2, \ldots]$ is periodic with period k if $b_n = b_{n+k}$ for all $n \in \mathbb{N}$ and eventually periodic if $b_n = b_{n+k}$ for all n sufficiently large.

The convergents of the RCF form a sequence of vertices $C_0, C_1, C_2, \cdots$ in $\mathcal{F}$. For each pair of vertices C_n and C_{n+1}, $n \in \mathbb{N}_0$ we have that $C_n \sim C_{n+1}$ so there is an infinite geodesic path from ∞ to ξ (as defined in [7]) along a sequence of connected Farey geodesics in $\mathbb{H}$ whose vertices are successive pairs of convergents generated by the RCF. This geodesic path is denoted by $\langle \infty, C_0, C_1, \cdots \rangle$. Beardon, Hockman and Short [7] give an algorithm for constructing shorter geodesic paths using the ancestral path algorithm and the nearest integer division algorithm.

1.5 Conclusion

The links that each author makes between the continued fraction and their respective tessellations of $\mathbb{H}$ are remarkable. By drawing together various elements of each approach we can see that the geometrical shapes provided by the tessellation certainly assist with understanding aspects of continued fractions. However the underlying process may be obscured if we only focus on numbers of triangles that are crossed by geodesics or on the number of points of contact between Ford circles leading to the required irrational.

1.5.1 Choosing a model of hyperbolic space

When analysing geometrically how continued fractions generate rational approximations we immediately need to make a choice. For our analysis, do we use the Ford circles of Ford [14] or $\mathcal{F}$, the Farey tessellation of the upper half plane $\mathbb{H}$ used by Series [41, 42]? These images form the basis of analysis in many papers on continued fractions (see [8, 13, 14, 17, 18, 19, 20, 24, 40, 41, 42, 43, 44]).

The role of ∞ is hard to imagine in the upper half plane model of hyperbolic space. The advantage of using $\mathbb{D}$, the disk model of hyperbolic space, is that ∞ can be treated as any other real number where it is represented by a single point on the boundary. This same point also represents $-\infty$, that is negative infinity. In the diagram of Figure 1.19 we show some of the elements of $\mathbb{R}$ on $\partial\mathbb{D}$, the 'circle at ∞' which forms the boundary of $\mathbb{D}$. The solid circles in this image represent the Ford circles and the dashed arcs are the geodesics of the Farey tessellation in this model.

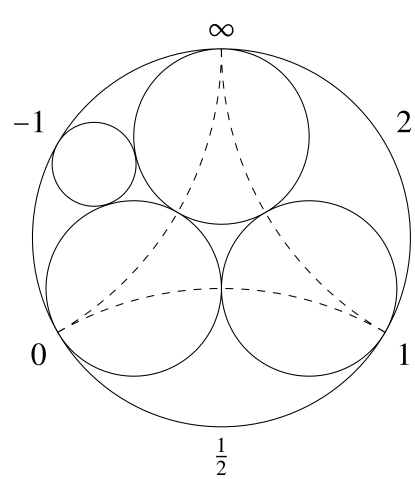

Figure 1.19: The number line on the circle at ∞ - the boundary of $\mathbb{D}$.

The disk model $\mathbb{D}$ is not easy to work in for the purpose of producing diagrams, so we choose to work in the upper-half plane model of hyperbolic space $\mathbb{H}$.

1.5.2 Our approach

In this thesis, we develop an analysis of continued fractions based on visualising dynamic features of images displayed in the upper half plane model of hyperbolic space.

Ultimately the 'process' of the $NICF$ is fully revealed by developing an approach similar to Schmidt's work in [40], but employing different categories of Möbius maps in our analysis. For each type of continued fraction we start with examples of quadratic surds. The fact that their $NICF$s are periodic makes it easier to work with. We follow with examples involving e as their continued fractions also exhibit patterns which are useful. Our approach allows for a dynamic visualisation of the process of finding approximations using continued fractions.

Chapter 2

Geometric structures and the action of Möbius maps in the real case

2.1 Introduction

In this chapter, we compare how the RCF and the $NICF$ generate approximations entirely from the perspective of using Möbius maps that act as isometries of hyperbolic space. We convert the finite continued fraction $C_n = \dfrac{p_n}{q_n} = [b_0, b_1, \cdots, b_n]$ into the function $F_n(x) = [b_0, b_1, \cdots, b_n, x]$ by adding x as one more partial quotient after b_n. It is clear that the truncated continued fraction can now be interpreted as $F_n(\infty)$ or $F_{n+1}(0)$.

Since $F_n(\infty) = F_{n+1}(0)$ for all $n \in \mathbb{N}_0$, geodesics joining $F_n(0)$ and $F_n(\infty)$ have successive end points in common, so there is a continuous geodesic path starting at ∞ with vertices at reduced rationals $F_n(\infty)$, that approach the value ξ. We define a geodesic path as follows:

Definition 2.1.1. The geodesic path of ξ consists of all vertices in $\langle \infty, F_1(\infty), \cdots, F_n(\infty) \cdots \rangle$ and the Farey geodesics that join consecutive pairs of vertices, starting with $\lambda_{(\infty, F_1(\infty))}$ and followed by $\lambda_{(F_k(\infty), F_{k+1}(\infty))}$, for $k \in \mathbb{N}$.

Comparing the paths generated using the RCF and $NICF$, we note that the $NICF$ path is one of the shortest possible, but the geodesics in the RCF path have much nicer properties than those of the $NICF$ path. To reveal the link between the geodesic paths and the partial quotients of the continued fraction, both in the case of the RCF and the $NICF$, we focus on the maps that make up F_n. We set $\tau_{b_n}(x) = b_n + x$ and $\phi(x) = \dfrac{1}{x}$. These are both Möbius maps where τ_{b_n} has $ad - bc = 1$ but ϕ has $ad - bc = -1$. Each F_n is decomposed into the product $\tau_{b_0}\phi\tau_{b_1}\phi\tau_{b_2}\cdots\phi\tau_{b_n}$. Then we parse these maps to get products of parabolic and elliptic Möbius maps that each have $ad - bc = 1$. An analysis of the images of 0, 1 and ∞ under successive F_n results in observable dynamic images of geodesics displayed in $\mathcal{F}$ that are explicitly linked to the partial quotients.

2.2 Convergents, Möbius maps and geodesic paths

In this section, we create a dynamic visualisation that illustrates the process of finding Diophantine approximations of an irrational real using its RCF. For purposes of illustration we use the following example, which was discussed in Chapter 1 for the methods of Ford 1.2.4 and Series 1.2.4.

Example 2.2.1. The value $\xi = \sqrt{3} - 1$ has periodic RCF $[0, 1, 2, 1, 2, \cdots] = [0, \overline{1, 2}]$, where the integers 1 and 2 recur infinitely [6].

The diagram of Figure 2.1, which follows in Example 2.2.3, shows all Farey triangles crossed by the geodesic $\lambda_{(P,\sqrt{3}-1)}$ (from point P on the imaginary axis to $\sqrt{3} - 1$, as shown in Figure 1.11 of Series' method 1.2.4), but the convergents, represented on $\mathbb{R}$ by the ideal end points of Farey geodesics, are now drawn equidistant from each other. This adjustment in the diagram allows us to work with rational values that are very close to $\sqrt{3} - 1$ more easily. Our focus, going forward, changes from the link between the partial quotients and the left and right cuts of Farey triangles along the geodesic $\lambda_{(P,\sqrt{3}-1)}$ of Series in [41, 42], to the movement of geodesics between pairs of successive convergents under the action of the maps generated using the RCF. We use Beardon's definition in [6]:

Definition 2.2.2. The product $S_n = s_0 s_1 \cdots s_n$ with $s_n(x) = b_n + \dfrac{1}{x}$ for $n \in \mathbb{N}_0$ is called the partial product of the RCF.

Clearly, the RCF truncated at the nth partial quotient b_n is represented by the $S_n(\infty)$. In the following example we use successive partial products of the RCF to find a geodesic path from ∞ to $\sqrt{3}-1$

Example 2.2.3. For $\sqrt{3}-1 = [0, \overline{1,2}]$ of example 2.2.1 the geodesic path starting at ∞ and joining successive pairs of convergents is

$$\langle \infty, S_0(\infty), S_1(\infty), S_2(\infty), S_3(\infty), S_4(\infty), \cdots \rangle = \left\langle \infty, 0, 1, \frac{2}{3}, \frac{3}{4}, \frac{8}{11}, \frac{11}{15}, \frac{30}{41} \cdots \right\rangle.$$

The geodesic path, consisting of the solid arcs in the diagram of Figure 2.1, is realised by connecting consecutive pairs $S_n(\infty)$ and $S_{n+1}(\infty)$ with the ideal geodesic $\lambda_{(S_n(\infty), S_{n+1}(\infty))}$ in the upper half plane model of hyperbolic space, $\mathbb{H} = \{z | Im(z) > 0\}$, for each $n \in \mathbb{N}_0$.

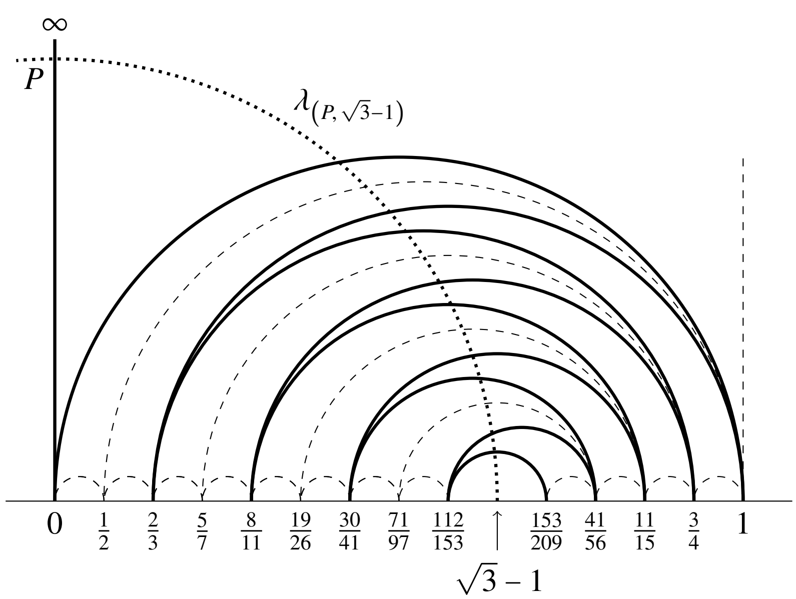

The solid geodesics form a geodesic path from ∞, via each $S_n(\infty)$, to $\sqrt{3}-1$. All geodesics that are crossed by $\lambda_{(P, \sqrt{3}-1)}$ are shown. The dashed geodesics are not part of the geodesic path. All $S_n(\infty)$ are shown as being equidistant in this illustration.

Figure 2.1: The geodesic path from ∞ to $\sqrt{3}-1$ derived from the RCF and the geodesic $\lambda_{(P, \sqrt{3}-1)}$

2.2.1 Using parabolic Möbius maps acting on the fundamental geodesic.

The Farey geodesic from 0 to ∞ is called the fundamental geodesic and we denote it by $\mathbb{I}_0$. Since $S_n(\infty) = S_{n+1}(0)$ for all $n \in \mathbb{N}$, the endpoints of each geodesic in the geodesic path are images of 0 and ∞ for each S_n, but not all the geodesics in diagram of Figure 2.1 are images of $\mathbb{I}_0$ under S_n as the individual s_n maps do not preserve $\mathbb{H}$.

From Beardon [3], parabolic Möbius maps preserve $\mathbb{H}$ and fix a single point on $\partial\mathbb{H}$, the boundary of $\mathbb{H}$. We use $\tau_{b_n}(x) = x + b_n, b_n \in \mathbb{Z}$ and $\phi(x) = \dfrac{1}{x}$ to introduce T, a product of parabolic Möbius maps, whose factors alternate between maps that fix ∞ and 0. We replace the partial products S_n with T_n, the partial product of parabolic Möbius maps.

Definition 2.2.4. Let $[b_0, b_1, b_2, \cdots]$ be the RCF for some irrational number ξ. Then $T = t_0 t_1 \cdots$ is the product of parabolic Möbius maps associated with the RCF of ξ, with $t_n = \tau_{b_n}$ for n even and $t_n = \phi\tau_{b_n}\phi$ for n odd, $b_n \in \mathbb{Z}$, $n \in \mathbb{N}_0$. We call $T_n = t_0 t_1 \cdots t_n$ the partial product of parabolic Möbius maps of the RCF of ξ and it has $n+1$ factors.

In the next example we use successive partial products to track successive convergents on the geodesic path.

Example 2.2.5. For $\sqrt{3} - 1 = [0, \overline{1, 2}]$ of example 2.2.1 the function T_n becomes:

$$T_n(x) = \begin{cases} \tau_0\,(\phi\tau_1\phi)\,\tau_2\,(\phi\tau_1\phi)\cdots(\phi\tau_1\phi)\,\tau_2\,(\phi\tau_1\phi)\,(x), \text{ for } n \text{ odd} \\ \tau_0\,(\phi\tau_1\phi)\,\tau_2\,(\phi\tau_1\phi)\cdots\tau_2\,(\phi\tau_1\phi)\,\tau_2(x), \text{ for } n \text{ even} \end{cases} \tag{2.1}$$

where each product has $n+1$ factors. The values for $T_n(0)$ and $T_n(\infty)$, calculated using equation 2.1, are shown in Table 2.1.

z	$T_0(z)$	$T_1(z)$	$T_2(z)$	$T_3(z)$	$T_4(z)$	$T_5(z)$	$T_6(z)$
0	0	0	2/3	2/3	8/11	8/11	30/41
∞	∞	1	1	3/4	3/4	11/15	11/15

Table 2.1: The images of 0 and ∞ under T_n for $n = 0, \cdots, 6$.

To trace geodesic movements along the geodesic path generated by successive T_n acting on $\mathbb{I}_0$, we track the images of 0 with the left hand and the images of ∞ with the right hand in the diagram of Figure 2.2. For each progression from $T_{n-1}(\mathbb{I}_0)$ to $T_n(\mathbb{I}_0)$ hand movements proceed as follows:

i) For $T_0 = \tau_0$: Start with the geodesic $T_0(\mathbb{I}_0) = \mathbb{I}_0$ by placing the left hand on 0 and the right hand at ∞.

ii) For $T_1 = \tau_0(\phi\tau_1\phi)$: Left hand stays on 0, right hand moves from ∞ to 1.

iii) For $T_2 = \tau_0(\phi\tau_1\phi)\tau_2$: Right hand stays on 1, left hand moves from 0 past $\frac{1}{2}$ to $\frac{2}{3}$.

iv) For $T_3 = \tau_0(\phi\tau_1\phi)\tau_2(\phi\tau_1\phi)$: Left hand stays on $\frac{2}{3}$, right hand moves from 1 to $\frac{3}{4}$ and so on.

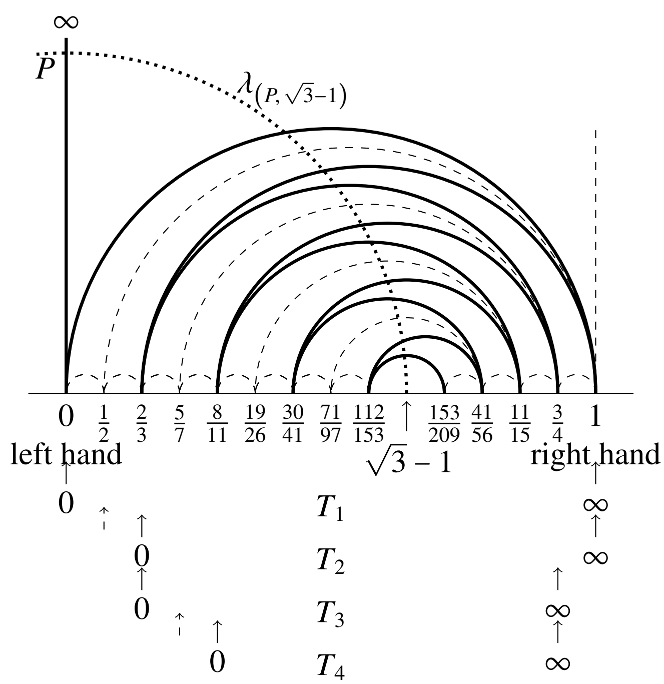

Figure 2.2: Tracking the image of 0 with left hand and the image of ∞ with right hand to trace the movement of geodesics under successive T_n

The hands take turns in moving toward the value $\sqrt{3}-1$. The dynamic progression of the images of $\mathbb{I}_0$ under successive T_n is recorded in the lines below the diagram in Figure 2.2. A dynamic geodesic progression is illustrated by a sequence of geodesics that are images of $\mathbb{I}_0$ under successive T_n derived from the RCF. The process is guided by the convergents as each C_n is the point that connects $T_n(\mathbb{I}_0)$ to $T_{n+1}(\mathbb{I}_0)$.

The process developed in Example 2.2.5 allow us to state the following theorem:

Theorem 2.2.6. Each Farey geodesic in the geodesic path is an image of $\mathbb{I}_0$ under a partial product $T_n = t_0 t_1 \cdots t_n$ for some value of $n \in \mathbb{N}_0$.

Proof. As the maps $t_n = \tau_{b_n}$ (for n even) and $t_n = \phi\tau_{b_n}\phi$ (for n odd) alternate in the partial product of parabolic Möbius maps T_n, we ensure that successive geodesics $T_n(\mathbb{I}_0)$ and $T_{n+1}(\mathbb{I}_0)$ share a common endpoint for all $n \in \mathbb{N}_0$. The maps τ_{b_n} and $\phi\tau_{b_n}\phi$ are both parabolic Möbius maps that preserve $\mathbb{H}$. □

The images shown in Figure 2.2 result in the creation of a new way of visualizing the process of using continued fractions to find approximations.

2.2.2 Fixed points and intermediate convergents

As we build up successive images of $\mathbb{I}_0$ under the T_n transformations, the images of 0 and ∞ are alternatively fixed points of the last map in the composition as the map τ_{b_n} fixes ∞ and $\phi\tau_{b_n}\phi$ fixes 0. Each iteration generates a fixed point with respect to the previous iteration. We define the fixed points under these T_n as follows:

Definition 2.2.7. Let $T_n = t_0 t_1 \cdots t_n$ be the partial product of parabolic Möbius maps with $t_n = \tau_{b_n}$ for n even and $t_n = \phi\tau_{b_n}\phi$ for n odd, $b_n \in \mathbb{Z}$, $n \in \mathbb{N}_0$. If $T_{n-1}(p) = T_n(p)$ for some $n \in \mathbb{N}$, then $T_n(p)$ is the fixed point in the progression from $T_{n-1}(\mathbb{I}_0)$ to $T_n(\mathbb{I}_0)$ on the geodesic path.

By defining the fixed points in this way we can state the following proposition which is proved by direct calculation:

Proposition 2.2.8. For the partial product of parabolic Möbius maps $T_n = t_0 t_1 \cdots t_n$ with $t_n = \tau_{b_n}$ for n even and $t_n = \phi\tau_{b_n}\phi$ for n odd, $b_n \in \mathbb{Z}$, $n \in \mathbb{N}_0$, if n is odd, then $T_{n-1}(0) = T_n(0)$, and if n is even, then $T_{n-1}(\infty) = T_n(\infty)$.

The role of fixed point alternates between the images of 0 and ∞ for each increment of n by one.

In Figure 2.2, all geodesics in the Farey tessellation that are cut by the geodesic $\lambda_{(P,\sqrt{3}-1)}$, but are not on the geodesic path from ∞ to $\sqrt{3}-1$, are called intermediate Farey geodesics. These geodesics are images of $\mathbb{I}_0$ and are defined as follows:

Definition 2.2.9. Let t_n be one of the parabolic Möbius maps $t_n(x) = \tau_{b_n}$ or $t_n(x) = \phi\tau_{b_n}\phi$ with fixed points at $v = \infty$ and $v = 0$ respectively. In the partial product of Möbius maps $T_n = t_0 t_1 \cdots t_{n-1} t_n$, with $t_n = \tau_{b_n}$ for n even and $t_n = \phi\tau_{b_n}\phi$ for n odd, we replace t_n with t_k to get

$$T_{n,k} = t_0 t_1 \cdots t_{n-1} t_k,$$

where $t_k = \tau_k$ for k even and $t_k = \phi\tau_k\phi$ for k odd, $1 \le k \le b_n - 1$. The collection of geodesics $T_{n,k}(\mathbb{I}_0) = t_0 t_1 \cdots t_{n-1} t_k(\mathbb{I}_0)$ are called the intermediate Farey geodesics between $T_{n-1}(\mathbb{I}_0)$ and $T_n(\mathbb{I}_0)$.

Example 2.2.10. The dashed geodesics $\lambda_{(\frac{1}{2},1)} = T_{2,1}(\mathbb{I}_0)$, $\lambda_{(\frac{5}{7},\frac{3}{4})} = T_{4,1}(\mathbb{I}_0)$, $\lambda_{(\frac{19}{26},\frac{11}{15})} = T_{6,1}(\mathbb{I}_0)$ and $\lambda_{(\frac{71}{97},\frac{41}{56})} = T_{8,1}(\mathbb{I}_0)$ are all intermediate Farey geodesics in Figure 2.2.

The following proposition states the link between partial quotients and the number of intermediate geodesics.

Proposition 2.2.11. There are $|b_n| - 1$ intermediate Farey geodesics between $T_{n-1}(\mathbb{I}_0)$ and $T_n(\mathbb{I}_0)$.

Proof. The proof is based on the method of tracing geodesics of successive T_n developed in section 2.2.1 for the parabolic Möbius maps $t_n = \tau_{b_n}$ for n even and $t_n = \phi\tau_{b_n}\phi$ for n odd of Definition 2.2.4. $\square$

2.2.3 The nearest integer continued fraction

In our next example we find the *NICF* of $\sqrt{3}-1$ using the nearest integer division algorithm.

Example 2.2.12. The *NICF* for $\sqrt{3}-1$ is

$$\sqrt{3}-1=[1,-4,4,-4,4,...]=[1,\overline{-4,4}].$$

We use definition 2.2.4 to derive T_n from the *NICF* of $\sqrt{3}-1$:

$$T_n(x)=\begin{cases}\tau_1\left(\phi\tau_{-4}\phi\right)\tau_4\left(\phi\tau_{-4}\phi\right)\cdots\left(\phi\tau_{-4}\phi\right)\tau_4\left(\phi\tau_{-4}\phi\right)(x), \text{ for } n \text{ odd}\\ \tau_1\left(\phi\tau_{-4}\phi\right)\tau_4\left(\phi\tau_{-4}\phi\right)\cdots\tau_4\left(\phi\tau_{-4}\phi\right)\tau_4(x), \text{ for } n \text{ even}\end{cases} \tag{2.2}$$

where each product has $n+1$ factors. The *NICF* of example 2.2.12 has negative partial quotients and this will affect the shape of its geodesic path. The geodesic path derived from the *NICF* is $\left\langle\infty,1,\frac{3}{4},\frac{11}{15},\frac{41}{56},\frac{153}{209},\cdots\right\rangle$ and is illustrated by the solid arcs in the diagram of Figure 2.3.

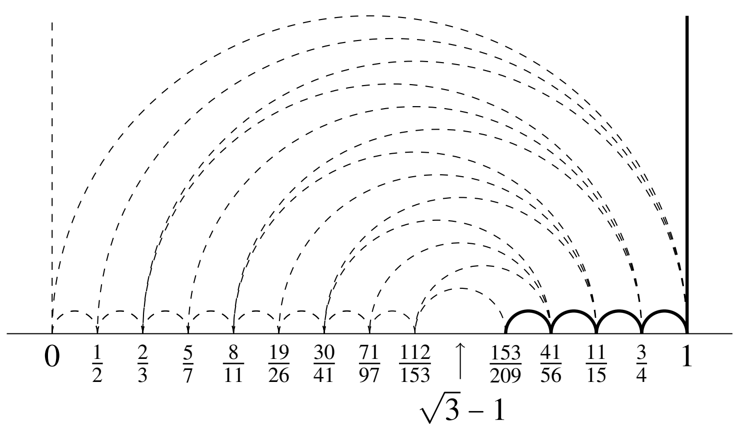

Figure 2.3: The geodesic path (solid arcs) generated by the T_n derived from the nearest node algorithm continued fraction.

We track the images of $\mathbb{I}_0$ under the T_n derived from the $NICF$ shown in Figure 2.3. For each progression from $T_{n-1}(\mathbb{I}_0)$ to $T_n(\mathbb{I}_0)$ hand movements proceed as follows:

i) Start with $T_0(\mathbb{I}_0) = \lambda_{(1,\infty)}$ by placing the right hand at 1 and the left hand at ∞.

ii) Moving from $T_0(\mathbb{I}_0)$ to $T_1(\mathbb{I}_0)$: right hand stays fixed at $x = 1$ and the left hand moves from ∞ through the end points of the three intermediate geodesics starting at 1 and ending at 0, $\frac{1}{2}$ and $\frac{2}{3}$, and stopping at $\frac{3}{4}$;

iii) Moving from $T_1(\mathbb{I}_0)$ to $T_2(\mathbb{I}_0)$: The next step keeps a fixed point at $\frac{3}{4}$ as the other hand moves from 1, through the three points $\frac{2}{3}$, $\frac{5}{7}$ and $\frac{8}{11}$ to $\frac{11}{15}$ and so on...;

In this process, there are $3 = |\pm 4| - 1$ intermediate geodesics where the partial quotients alternate between -4 and 4. The connection between the partial quotients of the $NICF$ and the number of intermediate geodesics satisfies Proposition 2.2.11 as we are again using Definition 2.2.4 to find T_n. This shows that the partial quotients are linked directly to the process underlying the generation of convergents using the $NICF$. However, this process is more awkward to visualise as the end points of the intermediate geodesics seems to go "the long way around" to get from one convergent to the next on the geodesic path.

The procedure of tracking convergents using Möbius maps acting on the Farey tessellation is visually pleasing. For the geodesic path generated with the RCF, the target ξ always lies between the endpoints of each geodesic $T_n(\mathbb{I}_0)$ in the path and each new endpoint is closer to ξ than its predecessors. The geodesic path resulting from the $NICF$ is one of the shortest geodesic paths according to Beardon, Hockman and Short in [7], but the associated dynamic progression is not entirely satisfactory as the target $\sqrt{3} - 1$ does not lie between the images of ∞ and 0 for any T_n, that is between the end points of the arcs forming the geodesic path. For both the RCF and the $NICF$ the convergents are the fixed points between successive Farey geodesics in the geodesic path.

We now reformulate our approach of using Möbius maps to generate a new dynamic for the $NICF$, with features that are as pleasing as the features revealed for the RCF.

2.3 Generating new dynamics for the nearest integer continued fraction

In the algorithm of Schmidt, described in [17] and [40], each $\xi \in \mathbb{R}$ is associated with a sequence of matrices $M_n(\xi)$ with 'integer' entries, whose inverses also have 'integer' entries. We get 3 distinct points in $\mathbb{C}$ from each $M_n(\xi)$. Using these points we focus on two aspects of the process, namely the tessellation of the complex plane by Farey sets and the generation of rational approximants. Each Farey set consists of either a circular region or a triangular region (a 'mesh triangle' bound by 3 mutually tangential circular regions) and is uniquely determined by the three points (see Fig. 1.17). These same three points in turn are candidate approximations for ξ, if ξ is located inside the Farey set.
Following the approach of Schmidt, we use images of the 3 vertices 0, 1 and ∞ under the maps derived from the $NICF$ to match the movements of the 3 vertices v_1, v_2 and v_3 used by Schmidt in [40].

2.3.1 Comparing the Möbius maps to the maps of Schmidt

We adapt Schmidt's method for generating real approximations by using only Möbius maps generated from the $NICF$. We identify both parabolic and elliptic Möbius maps as factors of T_n. According to Beardon [3], while parabolic Möbius maps fix a single point on $\partial\mathbb{H}$, elliptic Möbius maps fix a single point in $\mathbb{H}$. In particular, we replace Schmidt's maps

$$v_1 : z \mapsto z + i, \quad v_2 : z \mapsto \frac{z}{-iz+1} \quad \text{and} \quad v_3 : z \mapsto \frac{(1-i)z+i}{-iz+1+i},$$

which fix ∞, 0 and 1 respectively, with the parabolic Möbius maps

$$\tau_{b_n} \quad \text{and} \quad \phi\tau_{b_n}\phi, \quad b_n \in \mathbb{Z}, \quad n \in \mathbb{N}_0$$

which fix ∞ and 0 respectively.

Lemma 2.3.1. The trajectories of v_1 and v_2 are orthogonal to the trajectories of τ_{b_n} and $\phi\tau_{b_n}\phi$, with $b_n \in \mathbb{Z}$, $n \in \mathbb{N}_0$, respectively.

Proof. It is easy to see that v_1 is a translation in the vertical direction while τ_{b_n} is a horizontal translation. In both cases ∞ is the fixed point on the boundary.
For the maps v_2 and $\phi\tau_{b_n}\phi$ a quick calculation shows that 0 is the fixed point. The map v_2 leaves the imaginary axis invariant (shown in Figure 1.12 of Schmidt contribution in 1.2.4 of Chapter 1) while $\phi\tau_{b_n}\phi$ leaves the real axis invariant. The trajectories for v_2 lie along circles tangent to the imaginary axis at 0 and the trajectories for $\phi\tau_{b_n}\phi$ lie along circles tangent to the real axis at 0. The intersection of any pair of trajectories for v_2 and $\phi\tau_{b_n}\phi$ is orthogonal. □

Lemma 2.3.2. There is no parabolic map derived from the $NICF$ that fixes 1.

Proof. The maps τ_{b_n} and $\phi\tau_{b_n}\phi$ both move 1 and these two maps are the only parabolic maps that appear in definition 2.2.4. □

Lemma 2.3.3. Schmidt's homographic map

$$s : z \mapsto \frac{-1}{z-1}$$

has the same effect as the map

$$\tau_1 \left(\phi\tau_{-1}\phi\right).$$

Proof. $\tau_1\phi\tau_{-1}\phi\,(z) = \tau_1\phi\tau_{-1}\left(\frac{1}{z}\right) = \tau_1\phi\left(\frac{1}{z} - 1\right) = \tau_1\phi\left(\frac{1-z}{z}\right) = \tau_1\left(\frac{z}{1-z}\right) = \frac{z}{1-z} + 1 = \frac{1}{1-z}$ □

The map

$$\tau_1 \left(\phi\tau_{-1}\phi\right)$$

which appears among the parabolic Möbius factors in the product of maps generated from the $NICF$.

2.3.2 Describing the dynamics generated by Möbius maps

Schmidt describes the map S as the "non-euclidean rotation to an angle $\frac{2\pi}{3}$ around $\frac{1}{2}\left(1 + i\sqrt{3}\right)$ of the non-euclidean plane in the Poincaré model" [40], but continues thereafter to work in the extended complex plane without any further reference to hyperbolic geometry. All

Möbius maps are isometries of $\mathbb{H} = \{z \in \mathbb{C} : Im(z) > 0\}$, defined with the Poincare metric $ds^2 = \frac{dx^2+dy^2}{y^2}$, while Schmidt's maps v_1, v_2 and v_3 are not.

We introduce the following notation:

The parabolic Möbius map that fixes ∞ is	$p_\infty = \tau_1$,
and the parabolic Möbius map that fixes 0 is	$p_0 = (\phi\tau_1\phi)$.
The elliptic Möbius maps are	$s = \tau_1\,(\phi\tau_{-1}\phi)$,
and its inverse	$s^{-1} = (\phi\tau_{-1}\phi)\,\tau_1$.

In the following theorem we show that $\tau_1\,(\phi\tau_{-1}\phi)$ acts as an elliptic Möbius map on $\mathbb{H}$ and summarise the procedure for finding the elliptic maps in the product of parabolic Möbius maps of definition 2.2.4.

Theorem 2.3.4. The only elliptic maps found among the product of parabolic Möbius transformations generated from the $NICF$ are $[\tau_1\,(\phi\tau_{-1}\phi)] = s$ and $[(\phi\tau_1\phi)\,\tau_{-1}] = s^{-1}$. The maps s and s^{-1} permute the vertices 0, 1 and ∞.

Proof: The product T_n derived from the $NICF$, where

$$T_n(x) = \begin{cases} \tau_{b_0}\,(\phi\tau_{b_1}\phi)\,\tau_{b_2}\,(\phi\tau_{b_3}\phi)\cdots(\phi\tau_{b_{n-2}}\phi)\,\tau_{b_{n-1}}\,(\phi\tau_{b_n}\phi)\,(x), \text{ for } n \text{ odd} \\ \tau_{b_0}\,(\phi\tau_{b_1}\phi)\,\tau_{b_2}\,(\phi\tau_{b_3}\phi)\cdots\tau_{b_{n-2}}\,(\phi\tau_{b_{n-1}}\phi)\,\tau_{b_n}(x), \text{ for } n \text{ even,} \end{cases} \tag{2.3}$$

needs to be expressed in terms of the Möbius maps p_0, p_∞, s and s^{-1} as follows. Clearly the map $\phi\tau_{b_n}\phi$ can be writen as $\phi\tau_{\pm1}\tau_{b_n}\tau_{\mp1}\phi = (\phi\tau_{\pm1+b_n}\phi)\,(\phi\tau_{\mp1}\phi) = (\phi\tau_{\pm1}\phi)\,(\phi\tau_{b_n\mp1}\phi)$ since ϕ^2 and $\tau_{\pm1\mp1} = \tau_0$ are both the identity map. Anywhere in the product $T_n(x)$ where $b_k > 0$ and $b_{k+1} < 0$ we replace the factors involving b_k and b_{k+1} with the following Möbius maps:

- $\cdots\tau_{b_k}\,(\phi\tau_{b_{k+1}}\phi)\cdots$ is written as $\cdots\tau_{b_k-1}\,[\tau_1\,(\phi\tau_{-1}\phi)]\,(\phi\tau_{b_{k+1}+1}\phi)\cdots$ which becomes $\cdots p_\infty^{b_k-1}sp_0^{b_{k+1}+1}\cdots$ when k is even.
- $\cdots(\phi\tau_{b_k}\phi)\,\tau_{b_{k+1}}\cdots$ is written as $\cdots(\phi\tau_{b_k-1}\phi)\,[(\phi\tau_1\phi)]\,\tau_{-1}]\tau_{b_{k+1}+1}\cdots$ which becomes $\cdots p_0^{b_k-1}s^{-1}p_\infty^{b_{k+1}+1}\cdots$ when k is odd.

After that, all remaining $(\phi\tau_b\phi)$ are replaced with p_0^b and all remaining τ_b are replaced with p_∞^b to produce the product of Möbius maps called T_M.

The product T_n derived from the $NICF$ yields only 2 elliptic Möbius maps as factors. They both appear as a product of 2 parabolic Möbius maps, $p_\infty p_0^{-1} = \tau_1 (\phi\tau_{-1}\phi)$ and $p_0 p_\infty^{-1} = (\phi\tau_1\phi)\,\tau_{-1}$, which are the elliptic maps s and s^{-1} respectively.
Next, both s and s^{-1} fix the single point $\dfrac{1+\sqrt{3}i}{2}$ in $\mathbb{H}$. The calculations

$$s(0) = 1, s(1) = \infty, s(\infty) = 0 \text{ and } s^{-1}(0) = \infty, s^{-1}(1) = 0, s^{-1}(\infty) = 1$$

show that s and s^{-1} are maps of order 3 that permute the vertices 0, 1 and ∞. □

Using Möbius maps allows us to identify new geometrical aspects embedded in the process of finding rational approximants using continued fractions.

Example 2.3.5. From the product of parabolic Möbius maps derived from the $NICF$ of $\sqrt{3}-1$ we treat $\tau_1 (\phi\tau_{-1}\phi)$ as a single factor and rewrite the product

$$T = \tau_1 (\phi\tau_{-4}\phi)\, \tau_4 (\phi\tau_{-4}\phi) \cdots$$

as a product of elliptic and parabolic Möbius maps by parsing as follows:

$$T = [\tau_1 (\phi\tau_{-1}\phi)]\, (\phi\tau_{-3}\phi)\, \tau_3 [\tau_1 (\phi\tau_{-1}\phi)]\, (\phi\tau_{-3}\phi)\, \tau_3 [\tau_1 (\phi\tau_{-1}\phi)] \cdots. \tag{2.4}$$

We replace T for $\sqrt{3}-1$ in equation (2.4) with the product of Möbius maps

$$T_M = sp_0^{-3}p_\infty^3 sp_0^{-3}p_\infty^3 sp_0^{-3}p_\infty^3 \cdots = \overline{sp_0^{-3}p_\infty^3}. \tag{2.5}$$

The partial products derived from equation (2.5) are

$$T_{M(n)} = sp_0^{-3}p_\infty^3 sp_0^{-3}p_\infty^3 sp_0^{-3}p_\infty^3 \cdots t_{M(n)}$$

where $t_{M(n)}$ represents the nth factor in the product of Möbius maps T_M, and

$$t_{M(3k-2)} = s, \quad t_{M(3k-1)} = p_0^{-3} \text{ and } t_{M(3k)} = p_\infty^3 \text{ for } k \in \mathbb{N}.$$

In example 2.3.6 we track the images of the vertices 0, 1 and ∞ to demonstrate the effects of the partial products $T_{M(n)}$ on $\mathbb{R}$.

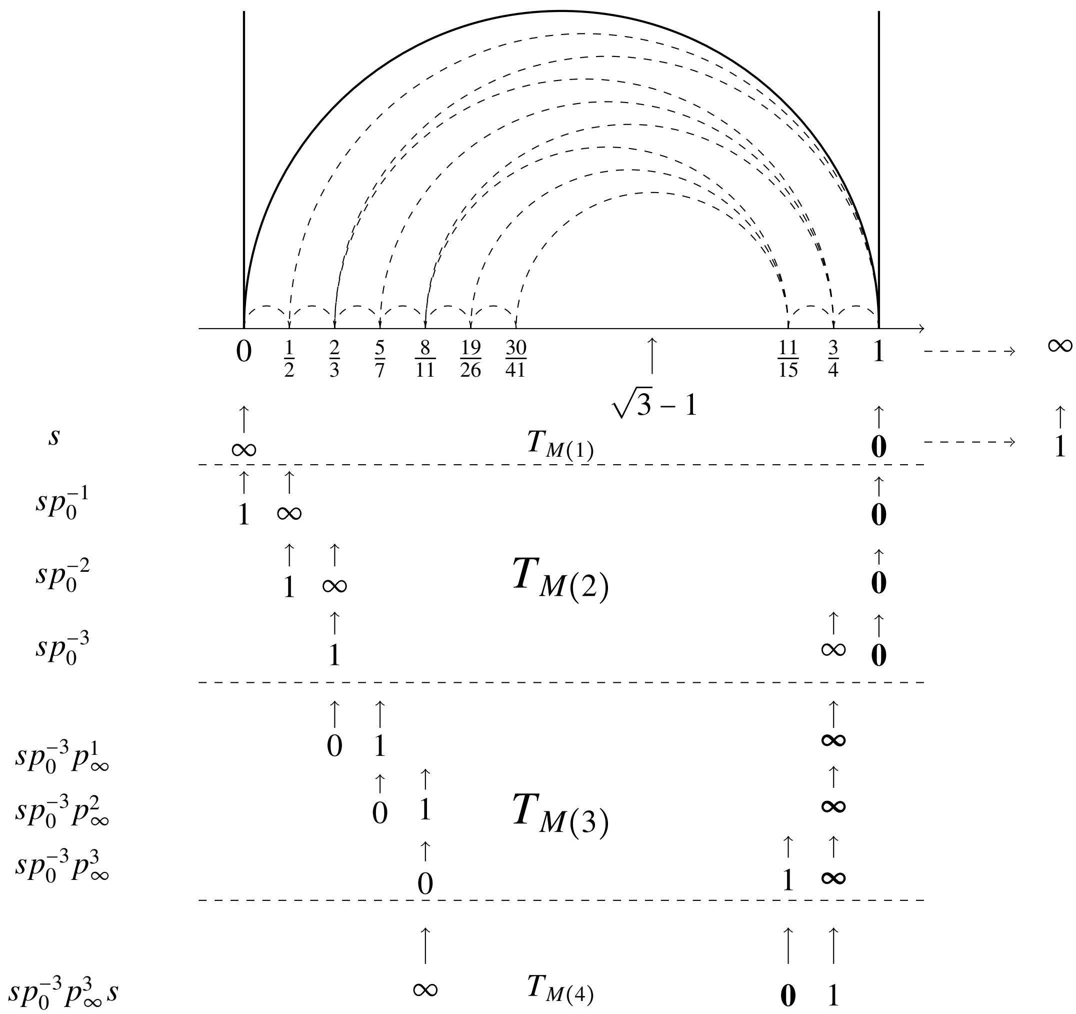

Figure 2.4: Tracing the iterates $T_{M(n)}(0)$, $T_{M(n)}(1)$ and $T_{M(n)}(\infty)$ for $\sqrt{3}-1$

Example 2.3.6. Each line under the diagram of Figure 2.4 shows the images of 0, 1 and ∞ under successive $T_{M(n)}$ of $\sqrt{3}-1$, where $T_{M(1)} = s$, $T_{M(2)} = sp_0^{-3}$, $T_{M(3)} = sp_0^{-3}p_\infty^3$, $T_{M(4)} = sp_0^{-3}p_\infty^3 s$ and so on. The effects of $T_{M(2)}$ and $T_{M(3)}$ are elaborated over three lines below the image. We describe the movement under successive $T_{M(n)}$ as follows:

- Start with the vertices 0, 1 and ∞. Of these 3 vertices, 1 is the closest to ξ, so we permute the vertices using s. In the line with s on the left hand side, in Figure 2.4, we note that images of 0, 1 and ∞ are the 3 vertices permuted by $T_{M(1)} = s$, so $s(\infty) = 0$ and $s(0) = 1$. Here $s(1) = \infty$ as indicated.

- The image of 0 under $T_{M(1)}$ is now closest to the target ξ, so it should be fixed under t_2. Since $t_2 = \phi\tau_{-3}\phi$, the image of 0 is fixed under $T_{M(2)}$, as illustrated by the next 3 lines in Figure 2.4, while the images of 1 and ∞ approach $T_{M(1)}(0) = T_{M(2)}(0) = 1$ from the left.

- The image of ∞ under $T_{M(2)}$ is closest to ξ, and this point will be fixed by $t_3 = \tau_3$. The images of 0 and 1 approach $T_{M(2)}(\infty) = T_{M(3)}(\infty) = \frac{3}{4}$ from the left under $T_{M(2)}$, as shown in the next 3 lines in Figure 2.4.

- After the last iteration, $T_{M(3)}(1)$ is closest to ξ. The map s is used to permute the images of 0, 1 and ∞ again, so that $T_{M(4)}(0)$ is closest to ξ and the process is continued in the same way.

The process illustrated in the diagram of Figure 2.4 focuses on the orbits of the 3 vertices 0, 1 and ∞. These movements are summarised in example 2.3.8, in terms of movements of hyperbolic triangles, using images of the fundamental triangle defined as follows:

Definition 2.3.7. The fundamental triangle $\mathbb{T}_0$ is the hyperbolic triangle with vertices at 0, 1 and ∞ in $\partial\mathbb{H}$. It is bounded by 3 Farey geodesic edges in $\mathbb{H}$ that join the vertices pairwise.

Example 2.3.8. The images of $\mathbb{T}_0$ move as shown in the diagram of Figure 2.5 under the successive factors of the $T_{M(n)}$, $n \in \mathbb{N}$ derived for $\sqrt{3}-1$. The descriptions of the movements follow below.

- For $T_{M(1)} = s$: The map s permutes the vertices of $\mathbb{T}_0$, in particular $T_0(0) = 1$ becomes the fixed point of the next map. (The arrow on the right indicates the change of fixed point (from ∞ to 1) as 1 becomes the image of 0.)

- For $T_{M(2)} = sp_0^{-3}$: The intermediate images of $\mathbb{T}_0$ have a fixed point at $x = 1 = T_1(0)$ and the other 2 vertices of $\mathbb{T}_0$ move toward 1 from the left as indicated by the arrow next to p_0^{-3}. (The arrow from 1 to $\frac{3}{4}$ indicates the change of fixed point from 1 to $\frac{3}{4}$)

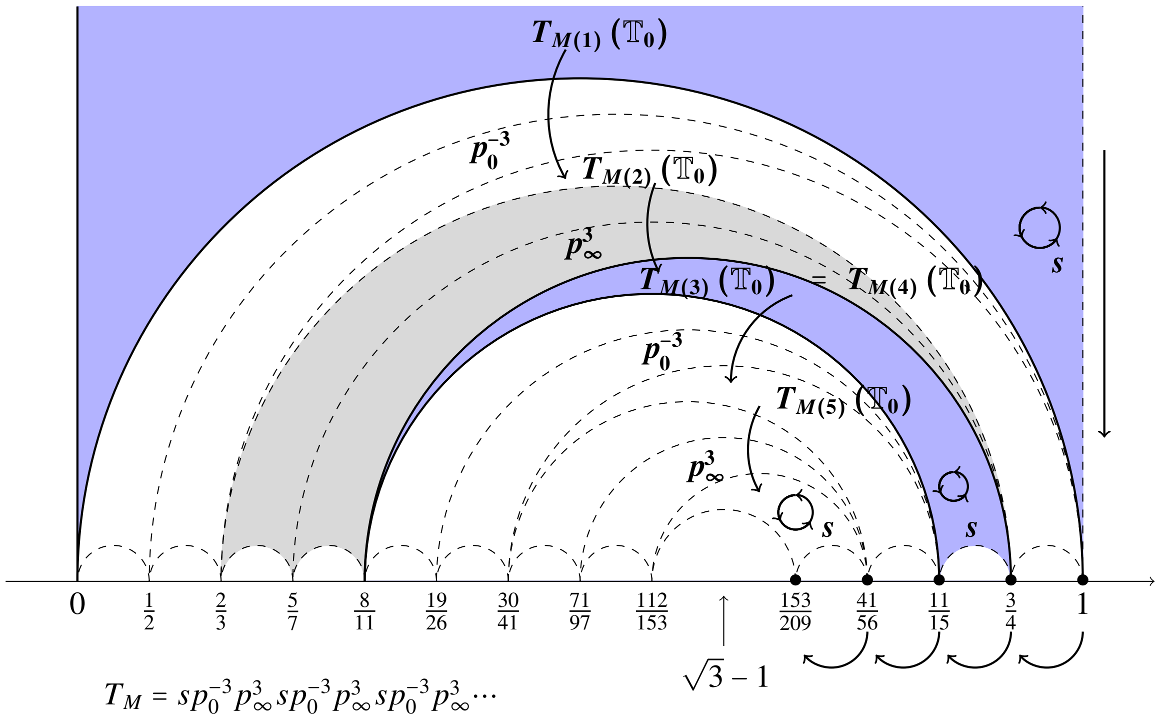

Figure 2.5: Counting movements of triangles about fixed points for $\sqrt{3}-1$

- For $T_{M(3)} = sp_0^{-3}p_\infty^3$: The images of $\mathbb{T}_0$ have a fixed point at $T_1(\infty) = \frac{3}{4}$ and move the other 2 vertices of toward $\frac{3}{4}$ from the left as indicated by the arrow next to p_∞^3. (No natural change of fixed points happens here as $\frac{11}{15}$ is the image of 1, so the next map must permute the vertices.)

- For $T_{M(4)} = sp_0^{-3}p_\infty^3 s$: The map s permutes the vertices of $\mathbb{T}_0$, in particular $T_2(0) = \frac{11}{15}$ becomes the fixed point for the next map.

We have shown the movement of images of $\mathbb{T}_0$ under the $T_{M(n)}$ generated from the $NICF$ using maps p_0 and p_∞ next to the arrow that represents the movement that they cause in the diagram of Figure 2.5. An s is placed in the triangle whose vertices have been permuted by the s map.

Example 2.3.8 serves to highlight the new roles adopted by vertices, geodesics and Farey triangles in the process of generating approximations. The roles of geometrical elements depends on whether we work with the RCF or the $NICF$.

- For the RCF, we use the image of $\mathbb{I}_0$ under successive T_n to link coefficients derived from the RCF to the number of intermediate geodesic between the Farey geodesics that make up the geodesic path from ∞ to ξ.
- For the $NICF$ we use the image of $\mathbb{T}_0$ under successive $T_{M(n)}$ to link coefficients derived from the $NICF$ to the number of Farey triangles that share a vertex.

2.4 Using Möbius maps derived from the nearest integer continued fraction

The exponents of p_0 and p_∞ in the product of Möbius maps T_M found in Theorem 2.3.4 satisfy the first main theorem of this chapter:

Theorem 2.4.1. In the product of Möbius maps T_M derived from the $NICF$ of ξ, the exponents of p_∞ and p_0 give the number of triangles that we move through about each fixed point as we approach the target.

Proof. Let $t_{M(n)}$ be a parabolic Möbius map raised to k, a non-zero integer, in T_M. For the images of 0, ∞ and 1 under the partial product $T_{M(n)}$:

1. if $t_{M(n)}$ is p_∞ raised to some $k \in \mathbb{Z} - \{0\}$ and:
   (a) the image of 0 is closest to ξ then the following map will be p_0 raised to a nonzero integer so that the image of 0 will be the fixed point of $T_{M(n+1)}$.
   (b) the image of 1 is closest to ξ then the following map will be s and the vertices will be permuted so that the image of 0 will be closest to ξ.
2. if $t_{M(n)}$ is p_0 raised to some $k \in \mathbb{Z} - \{0\}$ and:
   (a) the image of ∞ is closest to ξ then the following map will be p_∞ raised to a nonzero integer so the image of that ∞ will be the fixed point of $T_{M(n+1)}$.

(b) the image of 1 is closest to ξ then the following map will be s^{-1} and the vertices will be permuted so that the image of ∞ will be closest to ξ.

In Theorem 2.3.4, the factors of the maps s and s^{-1} are extracted directly from the parabolic Möbius factors in T_n whenever a positive partial quotient is followed by a negative one, and the value of k is an adjusted value every time an elliptic Möbius map appears in T_M. This adjustment of the value of k ensures that no triangles, other than the ones crossed by the geodesic from a point on the imaginary axis to the target on the real axis, become images of $\mathbb{T}_0$ under the partial products of Möbius maps $T_{M(n)}$. □

The examples so far have all had periodic $NICF$s as we have worked with square roots. In the next example we see one of the types of patterns associated with the number e. We give the conversion from the product of parabolic Möbius maps T to the product of Möbius maps T_M for $e-2$.

Example 2.4.2. We use the RCF of $e-2$ given by $= [0,1,2,1,1,4,1,1,6,1,1,8,\cdots]$ to find the configuration of the Farey triangles for the number $e-2$. The pattern in the partial quotients, $\cdots,1,2n,1,1,2n+2,1,\cdots$ for $n \in \mathbb{N}$ continues to infinity, so the continued fraction expression for e has a pattern advantage over its decimal representation. The path along the solid geodesics in the diagram of Figure 2.6 are easily linked to the partial quotients of the RCF by simply counting left and right cuts across the Farey triangles.
We now consider the $NICF$ of $e-2$ given as $e-2 = [1,-4,2,5,-2,-7,2,9,-2,-11,\cdots]$, which is linked to the product of maps

$$T = \tau_1\left(\phi\tau_{-4}\phi\right)\tau_2\left(\phi\tau_5\phi\right)\tau_{-2}\left(\phi\tau_{-7}\phi\right)\tau_2\left(\phi\tau_9\phi\right)\tau_{-2}\cdots.$$

For the Möbius maps we get

$$T_M = sp_0^{-3}p_\infty^2 p_0^4 s^{-1}p_\infty^{-1}p_0^{-7}p_\infty^2 p_0^8 s^{-1}p_\infty^{-1}p_0^{-11}p_\infty^2 p_0^{12}s^{-1}\cdots.$$

The effects of the partial products $T_{M(n)}$ acting on $\mathbb{T}_0$ are recorded in Table 2.2 and illustrated in the diagram of Figure 2.6.

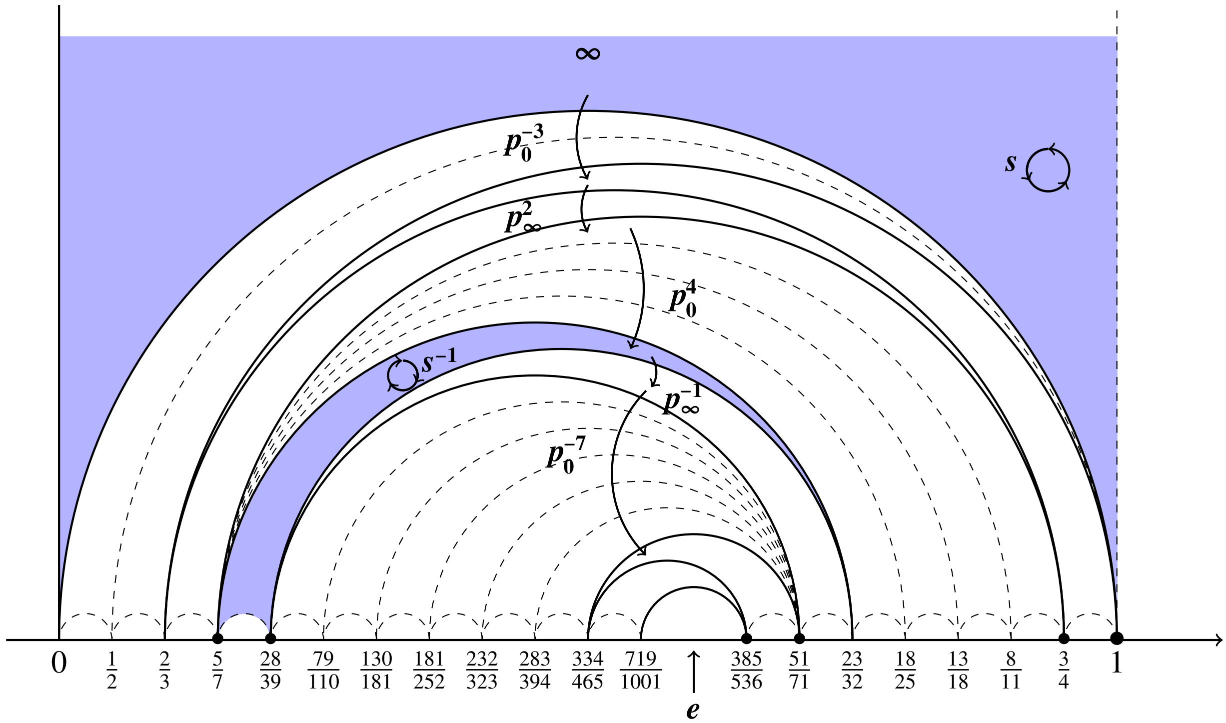

$$T_{M(n)} = s p_0^{-3} p_\infty^{2} p_0^{4} s^{-1} p_\infty^{-1} p_0^{-7} p_\infty^{2} p_0^{8} s^{-1} p_0^{-1} p_\infty^{-11} p_\infty^{2} p_0^{12} s^{-1} \cdots$$

Figure 2.6: Tracking images of $\mathbb{T}_0$ for $e-2$

$T_{M(n)}$	$t_{M(n)}$	fixed point	action on image of $\mathbb{T}_0$ under $T_{M(n)}$
$T_{M(1)}$	s	(1 becomes image of 0)	permute vertices of $\mathbb{T}_0$ to the right
$T_{M(2)}$	p_0^{-3}	$T_{M(1)}(0) = T_{M(2)}(0) = 1$	move images of 1 and ∞ right toward 1
$T_{M(3)}$	p_∞^2	$T_{M(2)}(\infty) = T_{M(3)}(\infty) = 3/4$	move images of 1 and 0 right toward 3/4
$T_{M(4)}$	p_0^4	$T_{M(3)}(0) = T_{M(4)}(0) = 5/7$	move images of 1 and ∞ left toward 5/7
$T_{M(5)}$	s^{-1}	(28/39 becomes image of ∞)	permute vertices of $\mathbb{T}_0$ to the left
$T_{M(6)}$	p_∞^{-1}	$T_{M(5)}(\infty) = T_{M(6)}(\infty) = 28/39$	move images of 1 and 0 left toward 28/39
$T_{M(7)}$	p_0^{-7}	$T_{M(6)}(0) = T_{M(7)}(0) = 51/71$	move images of 1 and ∞ right toward 51/71
$T_{M(8)}$	p_∞^2	$T_{M(7)}(\infty) = T_{M(8)}(\infty) = 385/536$	move images of 1 and 0 right toward 385/536
$T_{M(9)}$	p_0^8	$T_{M(8)}(0) = T_{M(9)}(0) = \cdots$	move images of 1 and ∞ left toward $\cdots$

Table 2.2: The effect of successive partial products $T_{M(n)}$ on $\mathbb{T}_0$ for $e-2$

All fractions on the real axis in the diagram of Figure 2.6 are approximations derived from the process of Farey subdivision, while the fractions along the solid geodesic path are convergents of the RCF. Approximations that are marked by bullets in the diagram of Figure 2.6 are convergents of the $NICF$. The exponents of the p_∞ and p_0 give the number of triangles that we move through about each fixed point under successive $T_{M(n)}$ derived from the $NICF$ and the sign of the exponent indicates the direction of the movement for the triangles about the fixed point.

The following two Lemmas regarding the images of $\mathbb{T}_0$ under the partial products $T_{M(n)}$ emerge from the discussion in Example 2.4.2.

Lemma 2.4.3. The sign of the partial quotient determines the direction of movement for the non-fixed points toward the fixed point.

Lemma 2.4.4. The s and s^{-1} maps move the images of 0, 1 and ∞ in the same direction as the maps immediately before and after them if the partial quotients b_k and b_{k+1} from which s or s^{-1} are derived satisfy $b_k \geq 2$ and $b_{k+1} \leq -2$.

When using continued fractions to find rational approximations of irrational reals the RCF is useful to get the configuration of the Farey triangles for the irrational number, but the $NICF$ gives us a method to find a shortest geodesic path. By reinterpreting the Möbius maps of the $NICF$ we become aware of the roles of the images of 0, 1 and ∞. Using the partial product $T_{M(n)} = t_{M(1)}t_{M(2)}\cdots t_{M(n)}$ it is easy to establish which of the three images is closest to the target by looking at $t_{M(n+1)}$.

- If $t_{M(n+1)} = p_\infty^b$ then $T_{M(n)}(\infty)$ is closest to the target and becomes the fixed point of $T_{M(n+1)}$
- If $t_{M(n+1)} = p_0^b$ then $T_{M(n)}(0)$ is closest to the target and becomes the fixed point of $T_{M(n+1)}$
- If $t_{M(n+1)} = s$ or $t_{M(n+1)} = s^{-1}$ then $T_{M(n)}(1)$ is closest to the target, and since neither of the parabolic maps use 1 as a fixed point the images of 0, 1 and ∞ must be permuted.

Once the Möbius maps for the $NICF$ of ξ are established, the adjustment to the exponents of p_∞ and p_0 when incorporating the maps s and s^{-1} to form the product T_M ensure that the second main theorem is satisfied.

Theorem 2.4.5. For the product of Möbius maps T_M derived from the $NICF$, the partial products of Möbius maps $T_{M(n)}$ generate images of the fundamental triangle $\mathbb{T}_0$ where:

(a) the exponents of p_∞ and p_0 count triangles that each share the fixed point of a parabolic map as a common vertex.

(b) the target ξ lies between the smallest and the largest of the 3 vertices $T_{M(n)}(0)$, $T_{M(n)}(1)$ and $T_{M(n)}(\infty)$ of triangle $T_{M(n)}(\mathbb{T}_0)$, if $t_{M(n)}$ is equal to either p_∞ or p_0, raised to a non-zero integer.

(c) the 3 vertices $T_{M(n)}(0)$, $T_{M(n)}(1)$ and $T_{M(n)}(\infty)$ of triangle $T_{M(n)}(\mathbb{T}_0)$ are permuted if the map $t_{M(n+1)}$ is equal to s or s^{-1}.

This result establishes the link similar to that developed by Series in [41, 42] between the partial quotients of the $NICF$ and the number of triangles encountered in the Farey tessellation near ξ.

2.5 Partial quotients and the link between adjusted coefficients and counting triangles

In order to simplify the link between coefficients in T_M and triangles in the Farey tessellation we define the following product:

Definition 2.5.1. Let b_n^* be the adjusted coefficient of the partial quotient b_n after all the elliptic factors s and s^{-1} have been accommodated in the factors of T to form T_M. The adjusted product of T for the $NICF$ is $T_A = t_0^* t_1^* t_2^* \cdots$, where each $t_n^*, n \in \mathbb{N}_0$ is a product of an elliptic map (e the identity map, s or s^{-1}) and a parabolic map $\tau_{b_n^*}$ or $\phi\tau_{b_n^*}\phi$. The partial adjusted product is $T_A = t_0^* t_1^* t_2^* \cdots t_n^*$.

In the following two examples we show the adjusted product of $\sqrt{3}-1$ and $e-2$, of Examples 2.3.5 and 2.4.2 respectively, in comparison with the original product of parabolic Möbius maps T.

Example 2.5.2. For $\sqrt{3}-1$:

$$\begin{array}{ccccccc} T & = & \tau_1 & (\phi\tau_{-4}\phi) & \tau_4 & (\phi\tau_{-4}\phi) & \cdots \\ T_A & = & \tau_0 & s\,(\phi\tau_{-3}\phi) & \tau_3 & s\,(\phi\tau_{-3}\phi) & \cdots \\ & = & p_\infty^0 & sp_0^{-3} & p_\infty^3 & sp_0^{-3} & \cdots \end{array}$$

Each coefficient is adjusted by the s factors that are accommodated.

Example 2.5.3. For $e-2$:

$$\begin{array}{ccccccccccccc} T & = & \tau_1 & (\phi\tau_{-4}\phi) & \tau_2 & (\phi\tau_5\phi) & \tau_{-2} & (\phi\tau_{-7}\phi) & \tau_2 & (\phi\tau_9\phi) & \tau_{-2} & \cdots \\ T_A & = & \tau_0 & s\,(\phi\tau_{-3}\phi) & \tau_2 & (\phi\tau_4\phi) & s^{-1}\tau_{-1} & (\phi\tau_{-7}\phi) & \tau_2 & (\phi\tau_8\phi) & s^{-1}\tau_{-1} & \cdots \\ & = & p_\infty^0 & sp_0^{-3} & p_\infty^2 & p_0^4 & s^{-1}p_\infty^{-1} & p_0^{-7} & p_\infty^2 & p_0^8 & s^{-1}p_\infty^{-1} & \cdots \end{array}$$

In Examples 2.5.2 and 2.5.3, we see the modulus of the exponents b_n^* of the factors p_0 and p_∞ directly before and after s or s^{-1} are simply one less than their associated b_n in T, as a direct result of Theorem 2.3.4. Since the adjusted coefficients in T_A is $b_n^*, n \in \mathbb{N}_0$, the link between and the number of intermediate Farey triangles that share a fixed point, confirmed in Theorem 2.4.5, stays the same.

The factors written as the adjusted product T_A make it easier to discuss the comparison between partial quotients of the $NICF$ and values of the adjusted coefficients. It is also easier to discuss how to find approximations using this notation, which will become useful in Chapter 4. The factors of T_M are more suitable for the geometric discussion.

2.6 Conclusion

The understanding of how a process works is often linked to the images we use to visualise the process. In the case of continued fractions the dominant images are those that involve the regular continued fraction. However, as we extend work on continued fractions to higher dimensions the $NICF$ is the most viable option, so it is essential that we have suitable images that illustrate its underlying process.

Changing the focus from the RCF to the $NICF$ changes the following parts of the process:

- The Euclidean division algorithm was replaced by the nearest integer division algorithm.

- Reading off values of partial quotients of the RCF is replaced by an analysis of Möbius maps derived from the $NICF$, requiring that we separate the elliptic maps s and s^{-1} from the parabolic maps.

- Counting left and right cuts along a geodesic has been replaced by counting movements of hyperbolic triangles about successive fixed points.

Chapter 3

Geometric structures and the action of Möbius maps in the complex case

In this chapter, we describe the geometry associated with the nearest integer continued fraction ($NICF$) when it is used to approximate complex irrationals. The definition of Farey fractions and Farey neighbours is generalised to $\mathbb{C}$ in the context of the extended Schmidt arrangement. Then, we show that parabolic Möbius maps preserve the relationship between any pair of Farey neighbours. In our two main theorems, we illustrate the effect of parabolic and elliptic Möbius maps on vertices in $\left\{\infty, 0, 1, i, 1+i, \dfrac{1+i}{2}\right\}$ using images of particular Farey quadrilaterals. We show that the circles of the Schmidt arrangement $\hat{S}_{\mathbb{Q}(\sqrt{-1})}$ become the paths along which the images of the four vertices of the Farey quadrilaterals move under successive partial products of Möbius maps. The process renders observable trajectories, in the extended Schmidt arrangement, for images of the vertices of ∇ under parabolic and elliptic Möbius maps.

3.1 Introduction

Firstly, we introduce the set of 6 vertices $\nabla = \left\{\infty, 0, 1, i, 1+i, \dfrac{1+i}{2}\right\}$. We then extend the definition of Farey fractions and Farey neighbours in $\mathbb{C}$ and establish their geometric representation. Specific pairs of Farey neighbours among the vertices of ∇ are used to define a Farey quadrilateral. We call it a Farey quadrilateral as it is bound by arcs that lie on the boundaries of the Farey sets and dual Farey sets of Schmidt in [40]. Farey quadrilaterals play a fundamental role in this thesis. We illustrate the effect of parabolic Möbius maps using images of Farey quadrilaterals in the extended Schmidt arrangement. The notion of 'intermediate images of Farey quadrilaterals' is introduced for each partial product to facilitate the visualization of movements of the Farey quadrilaterals that result due to parabolic Möbius maps. Next, from the product of parabolic Möbius maps derived from the partial quotients of the $NICF$, we reveal the elliptic Möbius maps that are present among the ϕ and τ factors of the parabolic Möbius maps and illustrate their effect on the vertices of ∇ as permutations.

3.2 Geometric structures in the extended Schmidt arrangement

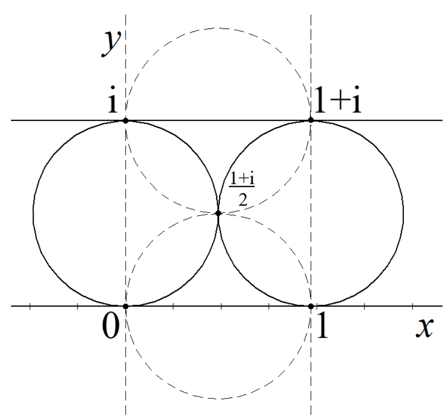

Figure 3.1: The vertices of ∇ and the Nabla configuration

The bounding circles of the Farey sets and dual Farey sets of Schmidt are called Farey circles and dual Farey circles respectively. The configuration shown in Figure 3.1 consists of four Farey (solid) circles and four (dashed) dual Farey circles that are each defined by exactly 3 vertices in ∇, where the straight lines pass through the vertex at ∞. All intersections between Farey circles and dual Farey circles are orthogonal.

The Farey circles shown in the diagram of Figure 3.1 are used as the generating circles in Theorem 3.2.1. In Definitions 3.2.11 and 3.2.12, we use the same configuration to define 2 of 6 possible Farey quadrilaterals. Each Farey quadrilateral has four vertices in ∇ and is bounded by arcs of the Farey circles and dual Farey circles that each pass through exactly 3 of those vertices.

In the Schmidt arrangement $S_{\mathbb{Q}(\sqrt{-1})}$, shown in the image[1] of Figure 3.2, the Farey circles are each generated using an iterative process. In Theorem 3.2.1, we describe the process and highlight important properties of the structures that emerge.

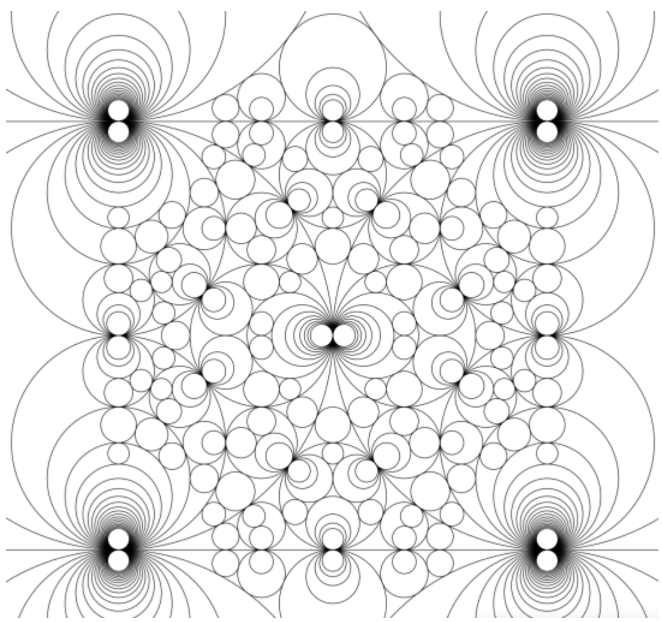

Figure 3.2: The Schmidt arrangement $S_{\mathbb{Q}(\sqrt{-1})}$

[1]reproduced with kind permission of K. Stange from [45]

Theorem 3.2.1. Each Farey circle in the Schmidt arrangement

- is tangent to exactly three external pairwise tangential Farey circles.
- circumscribes three inner pairwise tangential circles whose positions are determined by the 3 points of contact of the external pairwise tangential Farey circles.

Proof. The Farey circles of the Schmidt arrangement $S_{\mathbb{Q}(\sqrt{-1})}$ in Figure 3.2 are generated as follows:

Following Chaubey, Fuchs, Hines and Stange in [11] on Apollonian packings, we start with four circles, two Farey circles through ∞:

$$y = 0 \quad \text{and} \quad y = 1,$$

and two Farey circles tangent to each other as well as to both circles through ∞:

$$\left(y - \frac{1}{2}\right)^2 + x^2 = \frac{1}{4} \quad \text{and} \quad \left(y - \frac{1}{2}\right)^2 + (x-1)^2 = \frac{1}{4}.$$

Each of these circles is tangent to the other three circles and all these circles are external to each other. New circles are added inside the circles and in the spaces between the circles as follows:

1. We inscribe in each given circle three unique circles that have the following properties:
   - The three circles are internally tangent to the given circle and share the point of contact with one of the external tangent circles.
   - The three internal circles are pairwise tangential.
2. We inscribe into each region bounded by three existing pairwise tangent circles the unique circle that is tangent to all three.

These steps are repeated indefinitely to form the Farey circles of the Schmidt arrangement.

□

The dual Farey circles can be generated in the same way starting with the dual Farey circles

$$x = 0 \quad \text{and} \quad x = 1, \quad \left(x - \frac{1}{2}\right)^2 + y^2 = \frac{1}{4} \quad \text{and} \quad \left(x - \frac{1}{2}\right)^2 + (y-1)^2 = \frac{1}{4}.$$

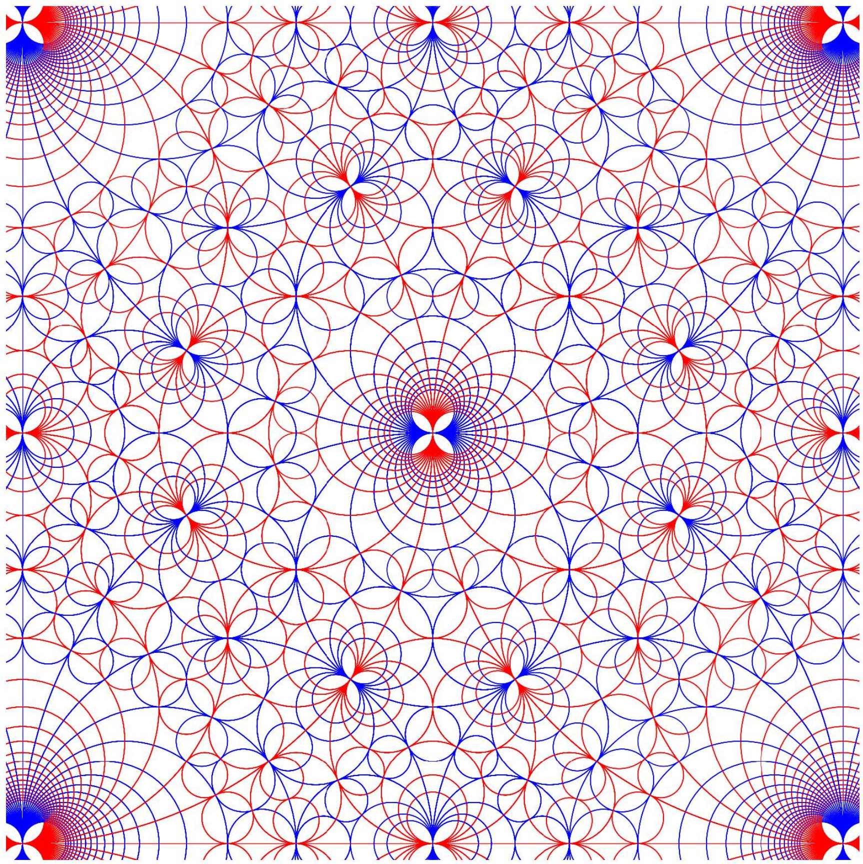

Figure 3.3: The Schmidt arrangement $\hat{S}_{\mathbb{Q}(\sqrt{-1})}$

The image [2] in Figure 3.3 shows the Farey circles of Figure 3.2, and the dual Farey circles. The dual Farey circles are a replica of the Farey circles that has been rotated through $\frac{\pi}{2}$ about the vertex $\frac{1+i}{2}$. All Farey circles and the dual Farey circles intersect orthogonally at each point of intersection [45].

[2] reproduced with kind permission of K. Stange from [45]

3.2.1 Representing Farey fractions and Farey neighbours in the extended Schmidt arrangement

The set of reduced rationals in $\mathbb{C}$ is given by

$$\mathbb{Q}^*(i) = \left\{ \frac{a}{c} \,\middle|\, a, c \in \mathbb{Z}[i],\ a \neq 0, c \neq 0, \gcd(a, c) \in U \right\}$$

where $U = \{\pm 1, \pm i\}$ and $\mathbb{Z}[i] = \{a+bi | a, b \in \mathbb{Z}\}$. We extend the concepts of Farey neighbours to the complex numbers, using the definition of Hockman in [22], as follows:

Definition 3.2.2. Two reduced rationals $\frac{a}{c}$ and $\frac{b}{d}$ in $\mathbb{Q}^*(i)$ are Farey neighbours if and only if $ad - bc \in U$. We write $\frac{a}{c} \sim \frac{b}{d}$.

The notion of Farey neighbours is used later to define Farey quadrilaterals.
Using definition 3.2.2, we see that $\infty = \frac{1}{0}$ and $0 = \frac{0}{1}$ are Farey neighbours. Any pair of Farey neighbours can be combined to generate more Farey numbers using Farey sums as defined in [22]. The Farey sum gives a set, called a Farey sum set (FSS), containing four elements and it is defined as follows:

Definition 3.2.3. The Farey sum of two Farey neighbours $\frac{a}{c}$ and $\frac{b}{d}$ in $\mathbb{Q}^*(i)$ is the set

$$\frac{a}{c} \oplus \frac{b}{d} = \left\{ \frac{au + b}{cu + d}, u \in U \right\}.$$

An important property of the FSS is proved in the following lemma:

Lemma 3.2.4. Each element in the FSS of $\frac{a}{c} \oplus \frac{b}{d}$ is a Farey neighbour of both $\frac{a}{c}$ and $\frac{b}{d}$.

Proof. For $\frac{au+b}{cu+d}$ and $\frac{a}{c}$ we have $(au + b)c - (cu + d)a = -(ad - bc) \in U$ so $\frac{au+b}{cu+d} \sim \frac{a}{c}$, and for $\frac{au+b}{cu+d}$ and $\frac{b}{d}$ we have $(au + b)d - (cu + d)b = (ad - bc)u \in U$ so $\frac{au+b}{cu+d} \sim \frac{b}{d}$. □

The resonance between the formulas for a Möbius map and the definition of the FSS shows that Möbius maps can be used to generate specific sequences of Farey neighbours.

Lemma 3.2.5. The Möbius map $f(z) = \dfrac{az+b}{cz+d}$, with $ad-bc \in U$ and $z = nu, n \in \mathbb{N}$, generates a sequence of Farey neighbours of $\dfrac{a}{c}$ for each value of $u \in U$ and consecutive elements in the sequence are Farey neighbours.

Proof. For $z = u \in U$: $f(u) = \dfrac{au+b}{cu+d} \sim \dfrac{a}{c}$ by Lemma 3.2.4, since $ad - bc = \pm 1$.
Let $z = ku$, with $k \in \mathbb{N}, k > 1, u \in U$: For $f(ku) = \dfrac{aku+b}{cku+d}$ and $\dfrac{a}{c}$ we get

$$(aku+b)(c) - (cku+d)(a) = -(ad-bc) \text{ so } \frac{aku+b}{cku+d} \sim \frac{a}{c}.$$

For the consecutive values $\dfrac{aku+b}{cku+d}$ and $\dfrac{a(k+1)u+b}{c(k+1)u+d}$:

$$\begin{aligned} \text{We get} \quad & (aku+b)(c(k+1)u+d) - (cku+d)(a(k+1)u+b) \\ = \quad & ack(k+1)u^2 + bc(k+1)u + adku + bd - ack(k+1)u^2 - ad(k+1)u - bcku - bd \\ = \quad & ad(ku - (k+1)u) + bc((k+1)u - ku) = ad(-u) + bc(u) = -u(ad-bc) \in U, \end{aligned}$$

so $\dfrac{aku+b}{cku+d} \sim \dfrac{a(k+1)u+b}{c(k+1)u+d}$ as required. □

Farey sum sets are linked closely to the orbit of each vertex when viewing the intermediate steps of any parabolic Möbius map.

Example 3.2.6. Farey fractions between the values $\dfrac{a}{c} = \dfrac{1}{1-i}$ and $\dfrac{b}{d} = \dfrac{i}{1}$ are generated by the map $f(z) = \dfrac{az+b}{cz+d} = \dfrac{z+i}{(1-i)z+1}$, where $ad - bc = -i$ and $z = nu$ with $n \in \mathbb{N}$, $u \in U$. In Table 3.1, we show the values of $f(n)$ and $f(ni)$ for $n = -2, -1, 1, 2, 3, 4$.

$f(z)$	$n=-2$	$n=-1$	$n=1$	$n=2$	$n=3$	$n=4$
$f(n)$	$\frac{-2+i}{-1+2i} = \frac{4+3i}{5}$	$\frac{-1+i}{i} = 1+i$	$\frac{1+i}{2-i} = \frac{1+3i}{5}$	$\frac{2+i}{3-2i} = \frac{4+7i}{13}$	$\frac{3+i}{4-3i} = \frac{9+13i}{25}$	$\frac{4+i}{5-4i} = \frac{16+21i}{41}$
$f(ni)$	$\frac{-i}{-1-2i} = \frac{2+i}{5}$	$\frac{0}{-i} = 0$	$\frac{2i}{2+i} = \frac{2+4i}{5}$	$\frac{3i}{3+2i} = \frac{6+9i}{13}$	$\frac{4i}{4+3i} = \frac{12+16i}{25}$	$\frac{5i}{5+4i} = \frac{20+25i}{41}$

Table 3.1: The values of $f(n)$ and $f(ni)$ for $n = -2, -1, 1, 2, 3, 4$

We note that $f(0) = \frac{i}{1} = i$ and $f(\infty) = \frac{1}{1-i}$, which give the original Farey neighbours. In Figure 3.4, we show the values of $f(n)$ and $f(ni)$ for $n = -2, -1, 0, 1, 2, 3, 4$. All Farey numbers generated by $f(z) = \dfrac{z+i}{(1-i)z+1}$ are Farey neighbours of $\frac{1}{1-i}$ and they lie on the Farey circle and the dual Farey circle that intersect each other at $\frac{1}{1-i}$ and $\frac{i}{1}$.

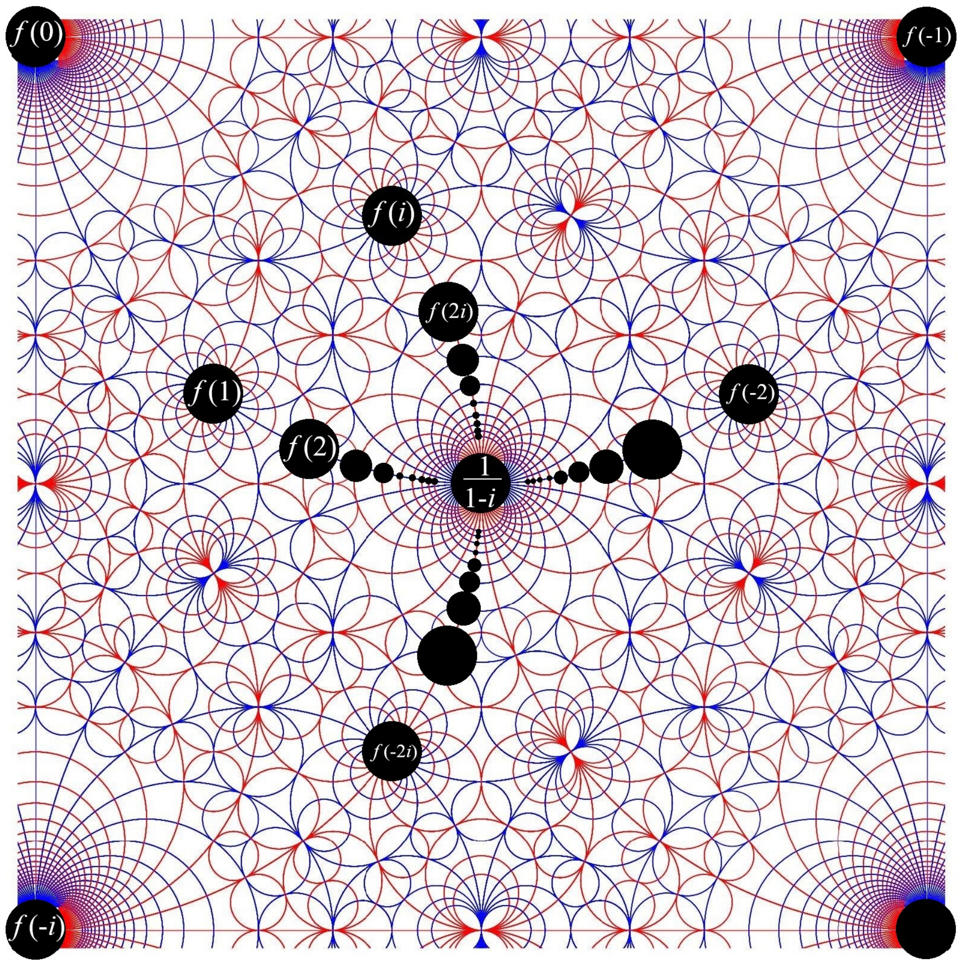

Figure 3.4: Farey neighbours of $\frac{1}{1+i}$ in $\hat{S}_{\mathbb{Q}(\sqrt{-1})}$

In the following theorem we show that Möbius transformations map a pair of Farey neighbours to a pair of Farey neighbours.

Theorem 3.2.7. If $\dfrac{m}{n}$ and $\dfrac{p}{q}$, written in reduced form, are a pair of Farey neighbours in $\mathbb{C}$ and the Möbius map $f(z) = \dfrac{az+b}{cz+d}$ satisfies $ad - bc \in U$, then $f\left(\dfrac{m}{n}\right) \sim f\left(\dfrac{p}{q}\right)$.

Proof. $f\left(\dfrac{m}{n}\right) = \dfrac{a\left(\dfrac{m}{n}\right)+b}{c\left(\dfrac{m}{n}\right)+d} = \dfrac{am+bn}{cm+dn}$ and similarly $f\left(\dfrac{p}{q}\right) = \dfrac{ap+bq}{cp+dq}$, so we have $(am+bn)(cp+dq) - (cm+dn)(ap+bq) = (ad-bc)(mq-np) \in U$, since $ad - bc \in U$ and $\dfrac{m}{n} \sim \dfrac{p}{q}$. Thus $f\left(\dfrac{m}{n}\right) \sim f\left(\dfrac{p}{q}\right)$. □

We have shown that the vertices of ∇ are the points of intersection of the generating sets of the Farey circles and the dual Farey circles. Also, since Möbius maps map circles to circles and pairs of Farey neighbours to pairs of Farey neighbours it is clear that each Farey number is represented at a point where Farey circles and dual Farey circles intersect. The two points where a Farey circle and a dual Farey circle intersect gives the location of two numbers that are Farey neighbours. In Figure 3.5, we show pairs of Farey neighbours that occur at the two points where a Farey circle and a dual Farey circle intersect.

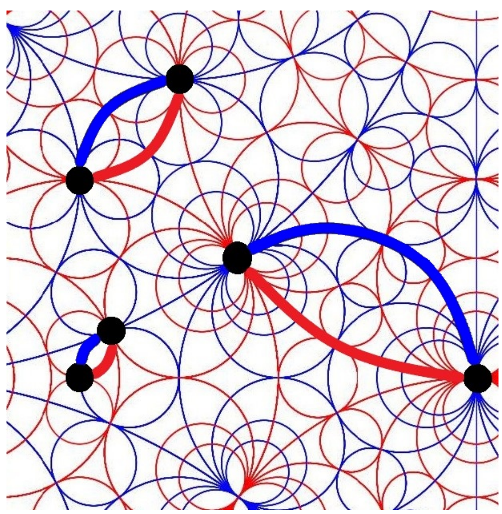

Figure 3.5: Pairs of Farey neighbours at the two points where Farey circles and dual Farey circles meet

3.2.2 Farey quadrilaterals

We introduce three subsets of ∇ whose definitions involve the Farey neighbour condition as follows:

Definition 3.2.8. The set of Farey neighbours in ∇ of $v \in \nabla$ is given by $\nabla_v = \{z \in \nabla | z \sim v\}$.

Example 3.2.9. In this example, $\gcd(1+i, 2) \notin U$ but $\frac{1+i}{2} = \frac{1}{1-i}$ with $gcd(1, 1-i) \in U$, so we work with the "reduced" expression $\frac{1}{1-i}$ instead of $\frac{1+i}{2}$. Then from Definition 3.2.8, we get $\nabla_\infty = \nabla_{\frac{1+i}{2}}$, $\nabla_0 = \nabla_{1+i}$ and $\nabla_1 = \nabla_i$.

In particular we focus on the two subsets $\nabla_\infty = \{0, 1, 1+i, i\}$ and $\nabla_0 = \{\infty, 1, \frac{1+i}{2}, i\}$. An important property of ∇_v is stated in the following lemma.

Lemma 3.2.10. The vertices of $\nabla_v = \{v_1, v_2, v_3, v_4\}$, with $v \in \nabla$, can be written as four distinct pairwise Farey neighbours $v_1 \sim v_2, v_2 \sim v_3, v_3 \sim v_4$ and $v_4 \sim v_1$.

Proof. In ∇_∞ we have $0 \sim 1, 1 \sim 1+i, 1+i \sim i$ and $i \sim 0$, in ∇_0 we have $\infty \sim 1, 1 \sim \frac{1}{1-i}, \frac{1}{1-i} \sim i$ and $i \sim \infty$, and in ∇_1 we have $\infty \sim 1+i, 1+i \sim \frac{1}{1-i}, \frac{1}{1-i} \sim 0$ and $0 \sim \infty$, where $\frac{1}{1-i}$ is the reduced form of $\frac{1+i}{2}$. $\square$

We define the Farey quadrilaterals $Q\nabla_\infty$ (quad nabla infinity) and $Q\nabla_0$ (quad nabla zero) associated respectively with ∞ and 0 as follows.

Definition 3.2.11. $Q\nabla_\infty$ is the shaded Farey quadrilateral (square in this case) in $\hat{\mathbb{C}}$ with vertices in ∇_∞, illustrated in the diagrams of Figure 3.6.

It is bounded by arcs on:

- two Farey circles, the horizontal lines $y = 0$ and $y = 1$, and
- two dual Farey circles, the vertical lines $x = 0$ and $x = 1$.

In the diagram of Figure 3.6, the shaded Farey quadrilateral $Q\nabla_\infty$ is shown in the complex plane representation and alongside, it appears bounded by 4 circular arcs in the Riemann sphere model of $\hat{\mathbb{C}}$.

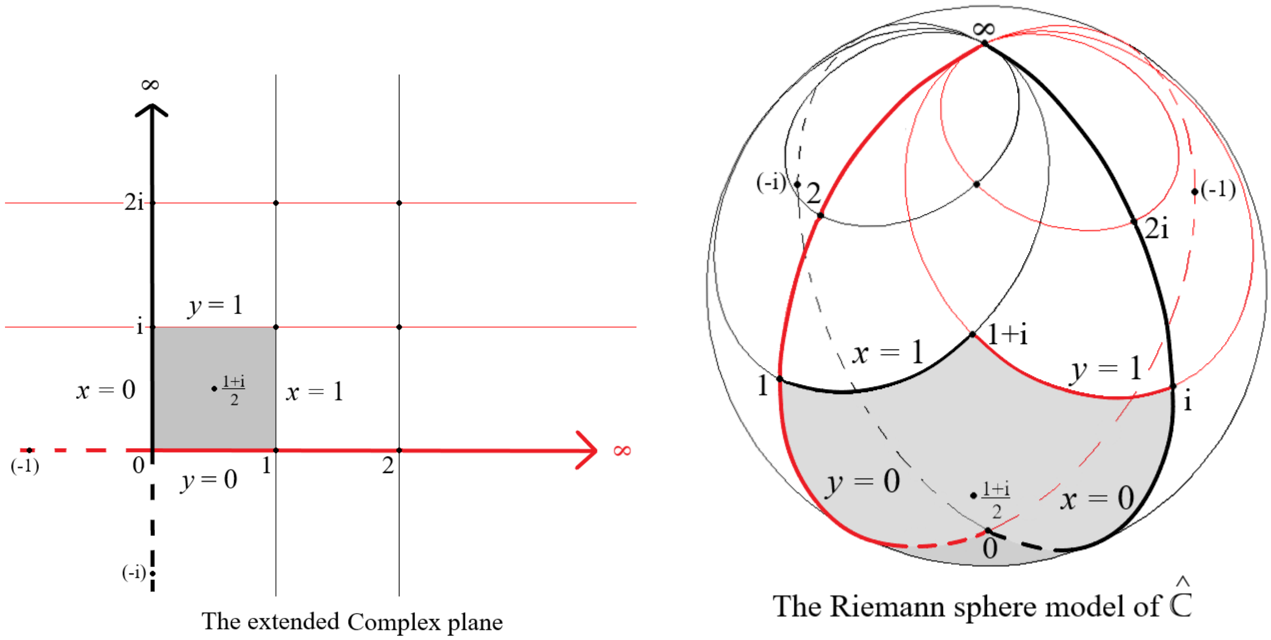

Figure 3.6: The quadrilateral $Q\nabla_\infty$ in $\hat{\mathbb{C}}$ and in the projection of $\hat{\mathbb{C}}$ onto the unit sphere

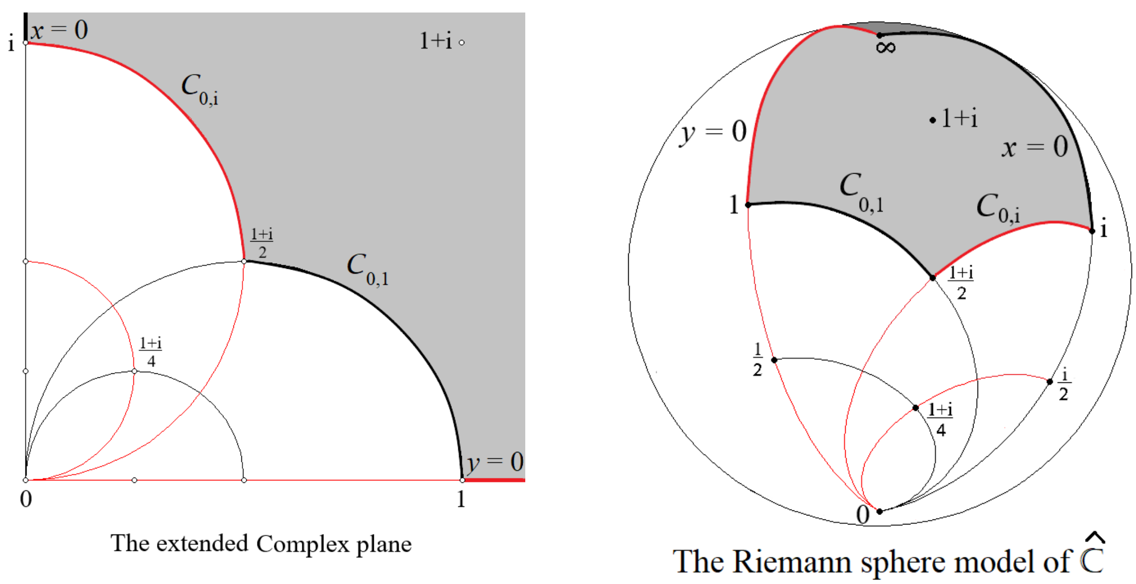

Figure 3.7: The quadrilateral $Q\nabla_0$ in $\hat{\mathbb{C}}$ and in the projection of $\hat{\mathbb{C}}$ onto the unit sphere

Definition 3.2.12. $Q\nabla_0$ is the shaded Farey quadrilateral with vertices in ∇_0, illustrated in both $\hat{\mathbb{C}}$ and on the Riemann sphere in diagrams of Figure 3.7.

The edges of the Farey quadrilateral $Q\nabla_0$ form part of:

- two Farey circles, the horizontal line $y = 0$ and the circle with diameter from 0 to i (called $\mathcal{C}_{0,i}$ in Figure 3.7) and
- two dual Farey circles, the vertical lines $x = 0$ and the circle with diameter from 0 to 1 (called $\mathcal{C}_{0,1}$ in Figure 3.7)

When comparing the $Q\nabla_\infty$ and $Q\nabla_0$ in Figures 3.6 and 3.7, they look very different in the complex plane model of $\hat{\mathbb{C}}$, however, their similarity is demonstrated in the Riemann sphere model, where ∞ is treated like any other point in $\hat{\mathbb{C}}$. The images of the Farey quadrilaterals $Q\nabla_\infty$ and $Q\nabla_0$ are the geometric tools used to create the visualisations developed in this thesis.

3.3 The effect of parabolic Möbius maps

The two parabolic maps that occur in the product of maps derived from the $NICF$ are τ_{b_n} and $\phi\tau_{b_n}\phi$, where $\tau_{b_n}(x) = x + b_n, b_n \in \mathbb{Z}[i]$ and $\phi(x) = \frac{1}{x}$, and they fix ∞ and 0 respectively. In the following lemma we focus our attention on the action of these two parabolic Möbius maps on the vertices of ∇. First we consider the parabolic maps that have a fixed point at ∞.

Lemma 3.3.1. The maps $\tau_{\pm 1}$ and $\tau_{\pm i}$ fix ∞ and move the images of vertices of $Q\nabla_\infty$ along Farey circles and dual Farey circles respectively. The image of $Q\nabla_\infty$ under $\tau_{\pm 1}$ and $\tau_{\pm i}$ is a Farey quadrilateral that is adjacent to $Q\nabla_\infty$ as it shares an edge with $Q\nabla_\infty$.

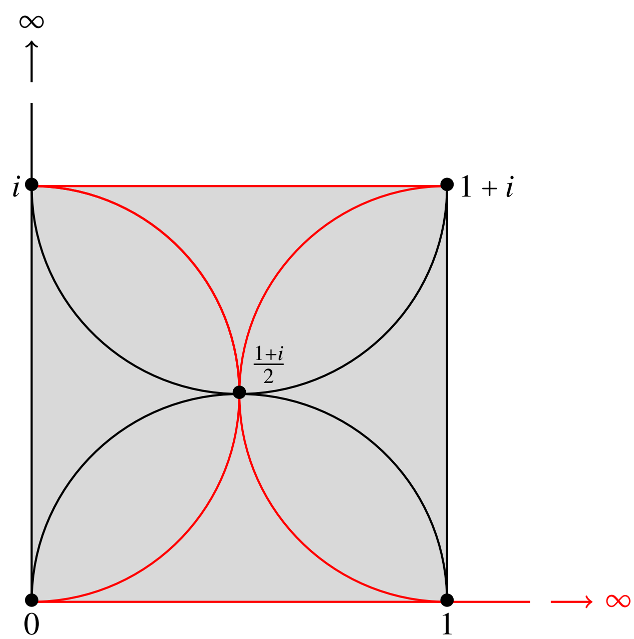

Figure 3.8: The quadrilateral $Q\nabla_\infty$ with vertices 0, 1, i and $1+i$ in ∇_∞

Proof. The shaded region illustrated in the diagram of Figure 3.8 shows the Farey quadrilateral $Q\nabla_\infty$ with vertices $0, 1, i, 1+i \in \nabla_\infty$. Clearly τ_1 and τ_i move the images of the vertices of $Q\nabla_\infty$ along the horizontal lines $y = 0$ and $y = 1$ and vertical lines $x = 0$ and $x = 1$ respectively. The horizontal lines are both Farey circles, while the vertical lines are both dual Farey circles. The Farey quadrilaterals $\tau_1(Q\nabla_\infty)$ {or $\tau_{-1}(Q\nabla_\infty)$} and $\tau_i(Q\nabla_\infty)$ {or $\tau_{-i}(Q\nabla_\infty)$} are the squares one unit to the right {or left} and one unit above {or below} $Q\nabla_\infty$ respectively. $\square$

In the next lemma we consider the parabolic maps that have a fixed point at 0. In the proof we work with the Farey quadrilateral $Q\nabla_0$. In this case we simply treat ∞ as a vertex of the quadrilateral.

Lemma 3.3.2. The maps $\phi\tau_{\pm1}\phi$ and $\phi\tau_{\mp i}\phi$ fix 0 and move the images of vertices of $Q\nabla_0$ along Farey circles and dual Farey circles respectively. The Farey quadrilateral $Q\nabla_0$ shares an edge with each one of $(\phi\tau_{\pm1}\phi)(Q\nabla_0)$ and $(\phi\tau_{\mp i}\phi)(Q\nabla_0)$.

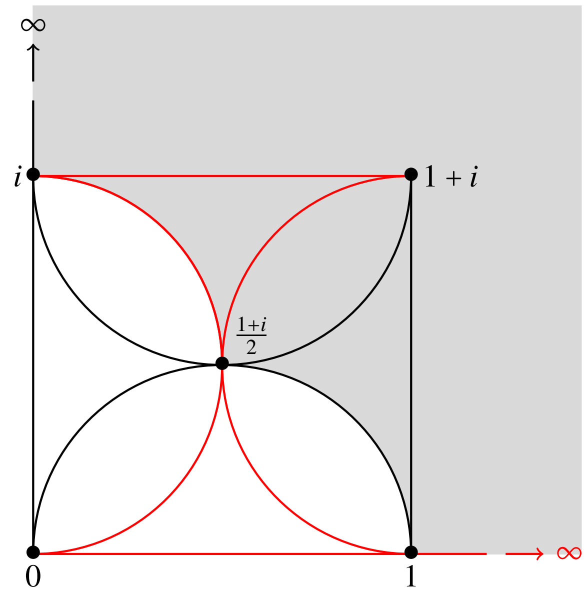

Figure 3.9: The quadrilateral $Q\nabla_0$ with vertices 0, 1, i and $\frac{1+i}{2}$ in ∇_0

z	0	1	∞	i	$\frac{1+i}{2}$
$\phi\tau_1\phi$	0	$\frac{1}{2}$	1	$\frac{1}{1-i} = \frac{1+i}{2}$	$\frac{1}{2-i} = \frac{2+i}{5}$
$\phi\tau_{-i}\phi$	0	$\frac{1}{1-i} = \frac{1+i}{2}$	i	$\frac{i}{2}$	$\frac{1}{1-2i} = \frac{1+2i}{5}$
$\phi\tau_{-1}\phi$	0	∞	-1	$\frac{1}{-1-i} = \frac{-1+i}{2}$	$\frac{1+i}{1-i} = i$
$\phi\tau_i\phi$	0	$\frac{1}{1+i} = \frac{1-i}{2}$	$-i$	∞	$\frac{1+i}{1+i} = 1$

Table 3.2: The images of 0 and the vertices of ∇_0 under $\phi\tau_{\pm 1}\phi$ and $\phi\tau_{\mp i}\phi$

Proof. The shaded region illustrated in the diagram of Figure 3.9 is the quadrilateral $Q\nabla_0$ with vertices at ∞, i, $\frac{1+i}{2}$ and 1. The images of the vertices of $Q\nabla_0$ under the maps $\phi\tau_{\pm 1}\phi$ and $\phi\tau_{\mp i}\phi$ are given in table 3.2 and are illustrated in the diagram of Figure 3.10, where each element of ∇ appears in the top row. The maps $\phi\tau_1\phi$ and $\phi\tau_{-i}\phi$ fix 0 and move the image of the vertices of $Q\nabla_0$ along the Farey circles and dual Farey circles respectively.

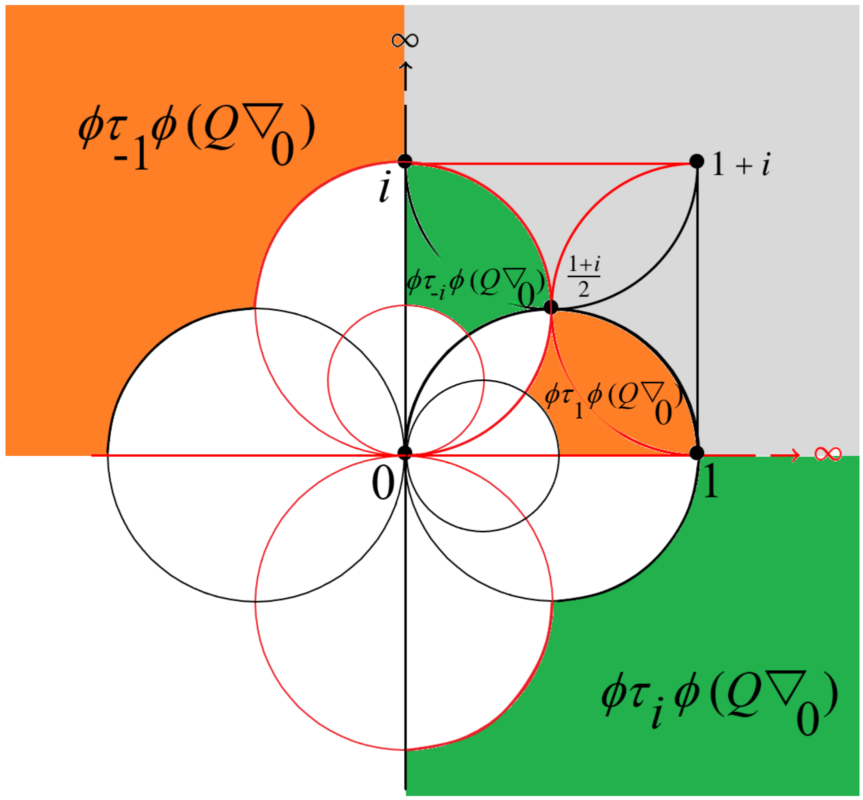

Figure 3.10: The images of $(Q\nabla_0)$ under $\phi\tau_{\pm 1}\phi$ and $\phi\tau_{\pm i}\phi$

In particular, in Figure 3.10, under $\phi\tau_1\phi$ and $\phi\tau_{-1}\phi$:

- The images of 1 and ∞ approach 0 along the Farey circle $y = 0$.
- The images of i and $\frac{1+i}{2}$ approach 0 along the Farey circle with diameter from 0 to i.
- The Farey quadrilaterals $(\phi\tau_{\pm 1}\phi)(Q\nabla_0)$ each share an edge with $Q\nabla_0$.

Similarly, in Figure 3.10, under $\phi\tau_{-i}\phi$ and $\phi\tau_i\phi$:

- The images of i and ∞ approach 0 along the dual Farey circle $x = 0$.
- The images of 1 and $\frac{1+i}{2}$ approach 0 along the dual Farey circle with diameter from 0 to 1.
- The Farey quadrilaterals $(\phi\tau_{\mp i}\phi)(Q\nabla_0)$ each share an edge with $Q\nabla_0$.

$\square$

3.3.1 Intermediate images and the representation of movements of Farey quadrilaterals induced by parabolic Möbius maps

The notion of intermediate images gives us a new tool to visualise the trajectories of the images of the vertices of ∇. Following Definition 2.2.4 in Chapter 2, we let T_n be the partial product of parabolic Möbius maps given by $T_n = t_0 t_1 \cdots t_n$ with $t_n = \tau_{b_n}$ for n even and $t_n = \phi\tau_{b_n}\phi$ for n odd, $n \in \mathbb{N}_0$, but now $b_n \in \mathbb{Z}[i]$. By decomposing the last factor t_n of T_n we create a set of intermediate images of $Q\nabla_\infty$ for n even and of $Q\nabla_0$ for n odd using the following definition:

Definition 3.3.3. Let t_n be one of the parabolic Möbius maps $t_n = \tau_{b_n}$, for n even, or $t_n = \phi\tau_{b_n}\phi$, for n odd, with fixed points at $v = \infty$ and $v = 0$ respectively. In the partial product of parabolic Möbius maps $T_n = t_0 t_1 \cdots t_{n-1} t_n$ we replace t_n with $t_{n,k} = \tau_k$ or $t_{n,k} = \phi\tau_k\phi$, keeping the same fixed point, to get $T_{n,k} = t_0 t_1 \cdots t_{n-1} t_{n,k}$.
For $b_n = p + qi$, we have

$$k \in \left\{ c + di \in \mathbb{Z}[i] \;\middle|\; 0 \leq \frac{c}{p} \leq 1, \quad 0 \leq \frac{d}{q} \leq 1, \quad k \neq 0 \text{ and } k \neq b_n \right\}.$$

The collection of Farey quadrilaterals $T_{n,k}(Q\nabla_v)$ are called the intermediate images of $Q\nabla_v$ under T_n.

In Example 3.3.4, we illustrate intermediate images for $Q\nabla_0$ under T_1 where $T_1 = t_0 t_1$ is a product of two parabolic Möbius maps. We then track the movement of the images of $Q\nabla_0$ for the progression from $T_0 = t_0$ to $T_1 = t_0 t_1$ to illustrate the effect of the parabolic Möbius map t_1 on the vertices of ∇_0.

Example 3.3.4. Consider the partial product of two parabolic Möbius maps $T_1 = t_0 t_1$, with $t_0 = \tau_{b_0}$ for some $b_0 \in \mathbb{Z}[i]$, and $t_1 = \phi\tau_{1-2i}\phi$.

In the diagram of Figure 3.11, the point $T_0(0) = T_1(0)$ is the fixed point in the progression from T_0 to T_1 and the quadrilaterals $T_0(Q\nabla_0)$ and $T_1(Q\nabla_0)$ are shown. The other four

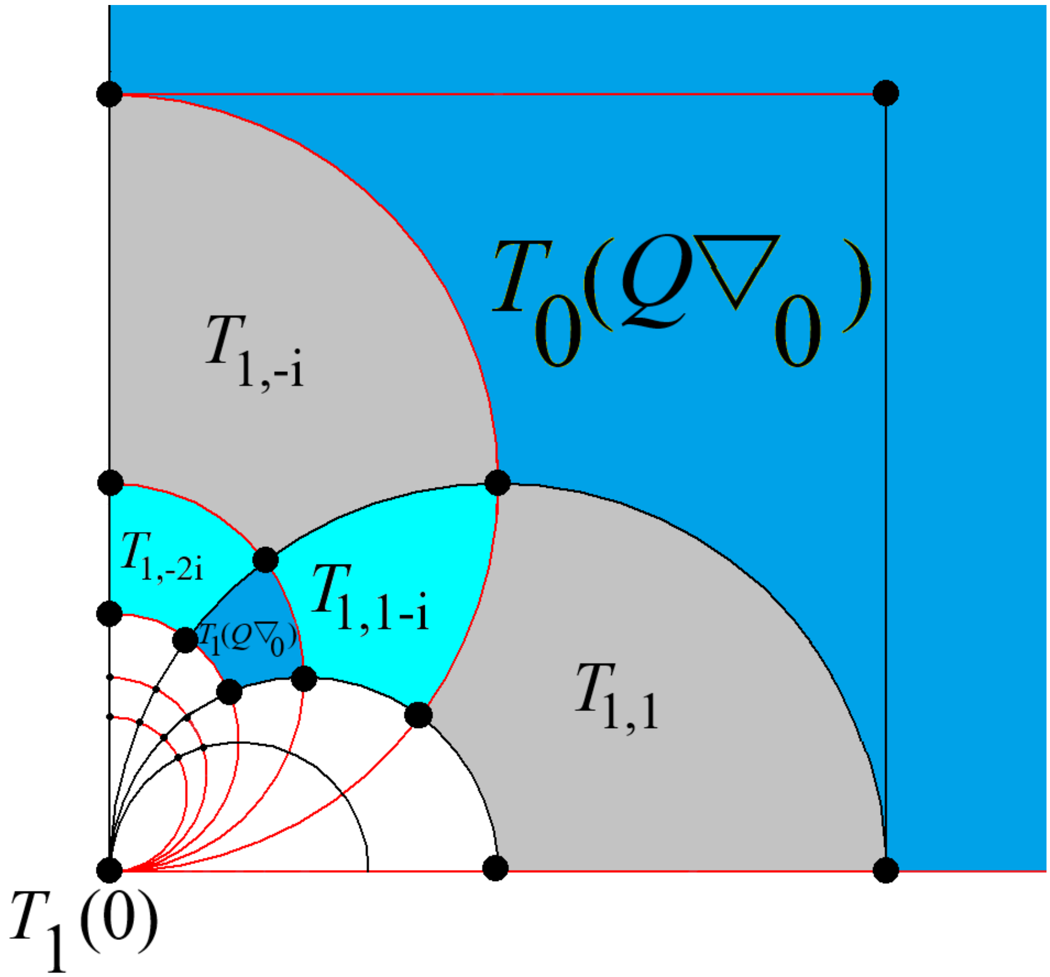

Figure 3.11: All intermediate images of $Q\nabla_0$ in the progression from T_0 to T_1

shaded quadrilaterals are the intermediate images $T_{1,k}(Q\nabla_0)$ for the k-values 1, $-i$, $1-i$ and $-2i$. These are all the possible values of k under the map $T_{1,k}$ with the restrictions on k given in definition 3.3.3. From the Farey quadrilateral $T_0\,(Q\nabla_0)$ there are two directions along which the images of intermediate quadrilaterals can approach the Farey quadrilateral $T_1\,(Q\nabla_0)$.

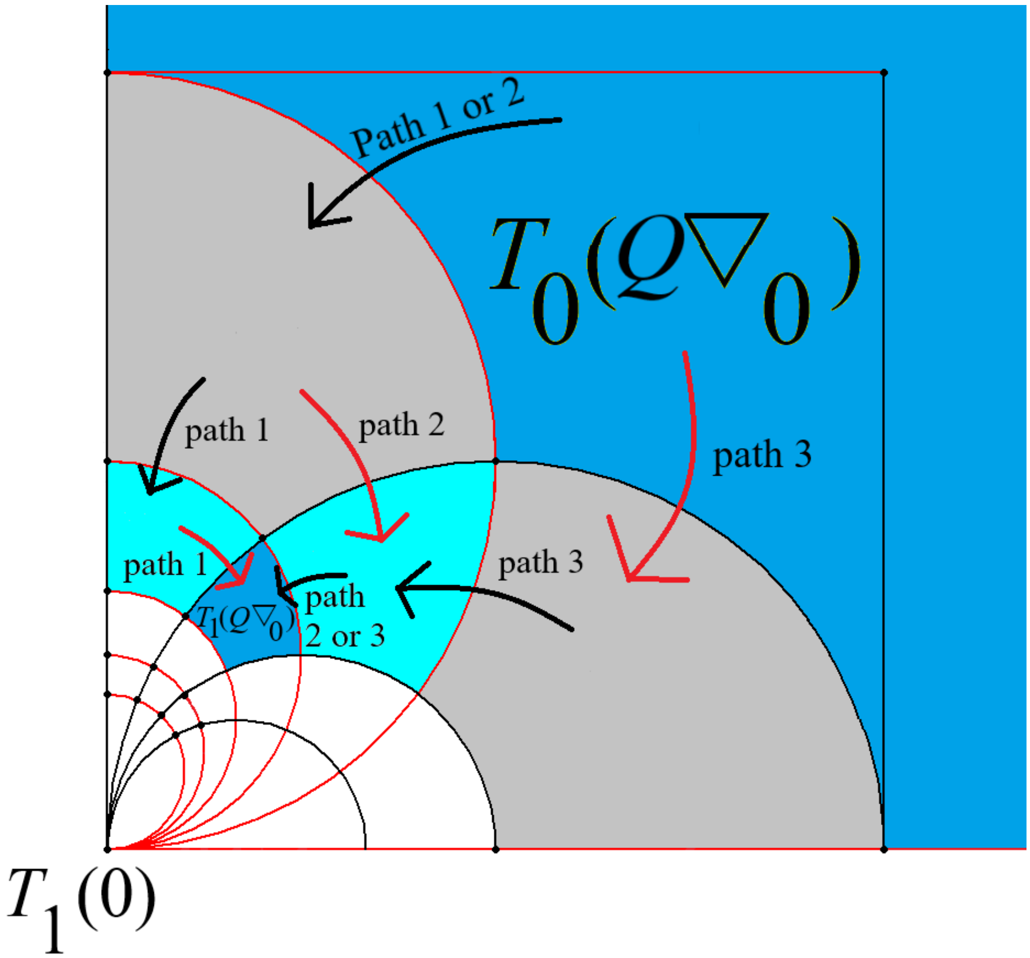

Figure 3.12: Movement from $T_0\,(Q\nabla_0)$ to $T_1\,(Q\nabla_0)$ through the intermediate images of $Q\nabla_0$

The effect of $t_1 = \phi\tau_{1-2i}\phi$ can be split up into:

- Path 1: $\phi\tau_{-2i}\phi$ followed by $\phi\tau_1\phi$ or
- Path 2: $\phi\tau_{-i}\phi$ followed by $\phi\tau_1\phi$ followed by $\phi\tau_{-i}\phi$ or
- Path 3: $\phi\tau_1\phi$ followed by $\phi\tau_{-2i}\phi$.

These 3 possible paths are illustrated in the diagram of Figure 3.12 and they link the partial quotient $1 - 2i$ to the number of intermediate Farey quadrilaterals in each direction along any path chosen from $T_0\,(Q\nabla_0)$ to $T_1\,(Q\nabla_0)$.

Example 3.3.4 shows how the effects of parabolic Möbius maps illustrated in Lemmas 3.3.1 and 3.3.2 is extended to represent the movement of Farey quadrilaterals under the effect of any product of parabolic Möbius maps. This leads us to the first main theorem of this chapter:

Theorem 3.3.5. Let t_n be the last parabolic Möbius map in the partial product of parabolic Möbius maps $T_n = t_0 t_1 \cdots t_{n-1} t_n$, with $t_n = \tau_{b_n}$ for n even and $t_n = \phi\tau_{b_n}\phi$ for n odd. With $v = \infty$ for n even and $v = 0$ for n odd, if $b_n = p + qi$ with $p, q \in \mathbb{Z}$, then:

1. there are $|p|$ intermediate images of $Q\nabla_v$ under T_n between the two Farey circles whose arcs form 2 edges of $T_{n-1}(Q\nabla_v)$ and $|q|$ intermediate images of $Q\nabla_v$ under T_n between the two dual Farey circles whose arcs form the other 2 edges of $T_{n-1}(Q\nabla_v)$.
2. part 1. is also true if we replace $T_{n-1}(Q\nabla_v)$ with $T_n(Q\nabla_v)$.
3. the number of intermediate images of $Q\nabla_v$ under T_n is $(p+1)(q+1) - 2$.

Proof. 1. From Lemmas 3.3.1 and 3.3.2 we know that the vertices of $Q\nabla_v$ are moved along Farey circles under $t_n = \tau_{b_n}$ for $v = \infty$ and $t_n = \phi\tau_{b_n}\phi$ for $v = 0$ if $b_n = 1$, and along dual Farey circles under $t_n = \tau_{b_n}$ for $v = \infty$ and $t_n = \phi\tau_{b_n}\phi$ for $v = 0$ if $b_n = -i$. There are four cases depending on the signs of p and q. The proofs for each case are similar. We consider $p \geq 0$ and $q \leq 0$, but not both 0: Now $\tau_{p+qi} = \tau_p\tau_{qi} = \underbrace{\tau_1 \ldots \tau_1}_{\text{p times}}\underbrace{\tau_{-i} \ldots \tau_{-i}}_{\text{q times}}$. The p τ_1 factors generate p intermediate images of $Q\nabla_v$ between the two Farey circles that bound $T_{n-1}(Q\nabla_v)$, where the first one is adjacent to $T_{n-1}(Q\nabla_v)$ and each of the following images of $Q\nabla_v$ are adjacent to the one before. This results in a sequence of $p+1$ Farey quadrilaterals, namely

$$T_{n-1}(Q\nabla_v), T_{n-1}t_{n,1}(Q\nabla_v), T_{n-1}t_{n,2}(Q\nabla_v), \ldots T_{n-1}t_{n,p}(Q\nabla_v)$$

between the two Farey circles bounding $T_{n-1}(Q\nabla_v)$.

The q τ_{-i} factors generate q intermediate images of $Q\nabla_v$ between the two dual Farey circles that bound $T_{n-1}(Q\nabla_v)$, where the first one is adjacent to $T_{n-1}(Q\nabla_v)$ and each of the following images of $Q\nabla_v$ are adjacent to the one before. This results in a sequence of $q+1$ Farey quadrilaterals, namely

$$T_{n-1}\left(Q\nabla_v\right), T_{n-1}t_{n,-i}\left(Q\nabla_v\right), T_{n-1}t_{n,-2i}\left(Q\nabla_v\right), \ldots T_{n-1}t_{n,qi}\left(Q\nabla_v\right)$$

between the two dual Farey circles bounding $T_{n-1}\left(Q\nabla_v\right)$.

2. Part 2. is established similarly to part 1.

3. In part 1. we established that there are $p+1$ Farey quadrilaterals between the two Farey circles bounding $T_{n-1}\left(Q\nabla_v\right)$ and $q+1$ Farey quadrilaterals between the two dual Farey circles bounding $T_{n-1}\left(Q\nabla_v\right)$. Thus, in total, there are $(p+1)(q+1)$ Farey quadrilaterals. We remove $T_{n-1}\left(Q\nabla_v\right)$ and $T_n\left(Q\nabla_v\right)$ to get $(p+1)(q+1)-2$ intermediate images of $Q\nabla_v$ under T_n.

□

3.4 The effect of Elliptic Möbius maps

There are sequences of maps, in the product of maps derived from the $NICF$, that leave ∇ invariant. These are the maps we discuss in this section.

3.4.1 The effect of the map ϕ on $\mathbb{C}_\infty$

In the case of the reals the map $\phi(z) = \frac{1}{z}$ behaves like an inversion. In $\mathbb{C}$, however, it is an elliptic map, of order 2, with 2 fixed points, one at $z=1$ and the other at $z=-1$. The action of ϕ is illustrated in the diagram of Figure 3.13. Each element of $\mathbb{C}$ is mapped to its reciprocal, in particular for the vertices in ∇:

$$\phi(\infty) = 0,\ \phi(0) = \infty,\ \phi(i) = -i,\ \phi(1+i) = \frac{1-i}{2} \text{ and } \phi\left(\frac{1+i}{2}\right) = 1-i.$$

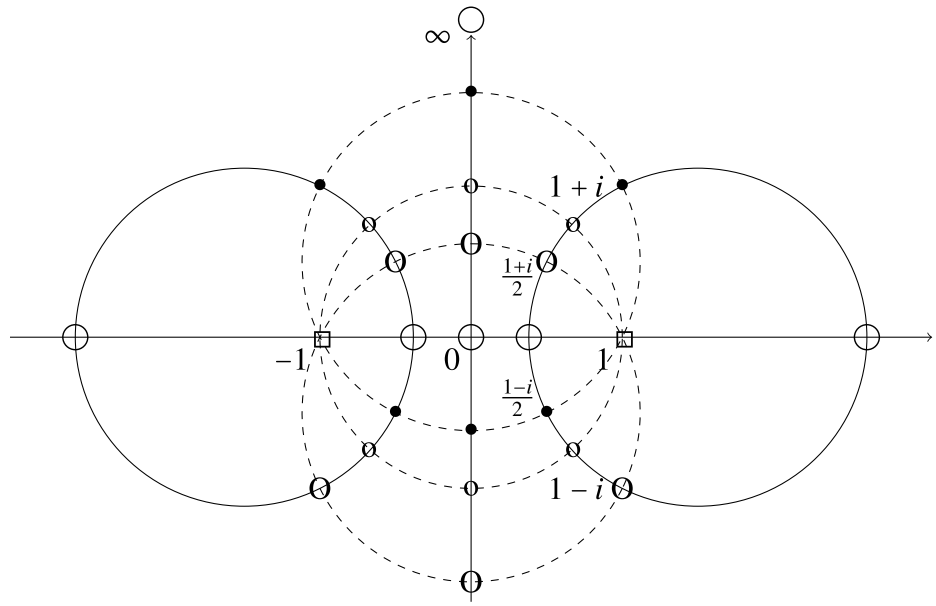

Figure 3.13: The action of ϕ on $\mathbb{C}_\infty$

In general we consider the 2 pencils of circles illustrated in the diagram of Figure 3.13:

- the elliptic pencil through the 2 points $z = 1$ and $z = -1$, the dashed circles in Figure 3.13, and
- the hyperbolic pencil of circles with a diameter from $z = x$ to $z = \frac{1}{x}$, $x \in \mathbb{R}$, the solid circles in Figure 3.13.

The action of ϕ maps any circle in the elliptic pencil to itself. In addition, any circle in the hyperbolic pencil of circles is mapped to itself. Each circle in the elliptic pencil cuts each circle in the hyperbolic pencil at two points, and the map ϕ swaps these two points in each case.

3.4.2 The influence of partial quotients with negative real or imaginary coefficients

Firstly, we define the following set of maps.

Definition 3.4.1. Let $\Xi = \{A, A^{-1}, B, B^{-1}, C, C^{-1}, D, D^{-1}, E, F, G, I\}$ where:

$$A = \phi\tau_{-i},\ A^{-1} = \tau_i\phi,\ B = \phi\tau_1\phi\tau_{-1},\ B^{-1} = \tau_1\phi\tau_{-1}\phi,\ C = \tau_{1+i}\phi\tau_{-1},\ C^{-1} = \tau_1\phi\tau_{-1-i},$$

$$D = \tau_{1+i}\phi\tau_{-1}\phi\tau_{-i},\ D^{-1} = \tau_i\phi\tau_1\phi\tau_{-1-i},\ E = \tau_{1+i}\phi\tau_{-1+i}\phi,\ E^{-1} = \phi\tau_{1-i}\phi\tau_{-1-i},$$

$$F = \tau_1\phi\tau_{-1-i}\phi\tau_{-i},\ F^{-1} = \tau_i\phi\tau_{1+i}\phi\tau_{-1},\ G = \phi\tau_1\phi\tau_{-1}\phi\tau_{-i},\ G^{-1} = \phi\tau_i\phi\tau_1\phi\tau_{-1}$$

and I is the identity map.

name	map	permutation
A	$\phi\tau_{-i}$	$\begin{pmatrix} 0 & i & \infty \end{pmatrix}\begin{pmatrix} 1+i & 1 & \frac{1+i}{2} \end{pmatrix}$
A^{-1}	$\tau_i\phi$	$\begin{pmatrix} 0 & \infty & i \end{pmatrix}\begin{pmatrix} 1+i & \frac{1+i}{2} & 1 \end{pmatrix}$
B	$\phi\tau_1\phi\tau_{-1}$	$\begin{pmatrix} 0 & \infty & 1 \end{pmatrix}\begin{pmatrix} 1+i & \frac{1+i}{2} & i \end{pmatrix}$
B^{-1}	$\tau_1\phi\tau_{-1}\phi$	$\begin{pmatrix} 0 & 1 & \infty \end{pmatrix}\begin{pmatrix} 1+i & i & \frac{1+i}{2} \end{pmatrix}$
C	$\tau_{1+i}\phi\tau_{-1}$	$\begin{pmatrix} 0 & i & \frac{1+i}{2} \end{pmatrix}\begin{pmatrix} 1+i & 1 & \infty \end{pmatrix}$
C^{-1}	$\tau_1\phi\tau_{-1-i}$	$\begin{pmatrix} 0 & \frac{1+i}{2} & i \end{pmatrix}\begin{pmatrix} 1+i & \infty & 1 \end{pmatrix}$
$D = CA$	$\tau_{1+i}\phi\tau_{-1}\phi\tau_{-i}$	$\begin{pmatrix} 0 & \frac{1+i}{2} & 1 \end{pmatrix}\begin{pmatrix} 1+i & \infty & i \end{pmatrix}$
$D^{-1} = A^{-1}C^{-1}$	$\tau_i\phi\tau_1\phi\tau_{-1-i}$	$\begin{pmatrix} 0 & 1 & \frac{1+i}{2} \end{pmatrix}\begin{pmatrix} 1+i & i & \infty \end{pmatrix}$
$E = CA^{-1}$, $E^{-1} = AC^{-1}$	$\tau_{1+i}\phi\tau_{-1+i}\phi$, $\phi\tau_{1-i}\phi\tau_{-1-i}$	$\begin{pmatrix} 0 & 1+i \end{pmatrix}\begin{pmatrix} \infty & \frac{1+i}{2} \end{pmatrix}$
$F = C^{-1}A$, $F^{-1} = A^{-1}C$	$\tau_1\phi\tau_{-1-i}\phi\tau_{-i}$, $\tau_i\phi\tau_{1+i}\phi\tau_{-1}$	$\begin{pmatrix} \frac{1+i}{2} & \infty \end{pmatrix}\begin{pmatrix} 1 & i \end{pmatrix}$
$G = BA$, $G^{-1} = A^{-1}B^{-1}$	$\phi\tau_1\phi\tau_{-1}\phi\tau_{-i}$, $\tau_i\phi\tau_1\phi\tau_{-1}\phi$	$\begin{pmatrix} 0 & 1+i \end{pmatrix}\begin{pmatrix} 1 & i \end{pmatrix}$
I	the identity map	$(\quad)$

Table 3.3: The elements of Ξ: maps and permutations

The permutations of the vertices of ∇ in Table 3.3 can be established by simple calculation.

A fundamental property of the maps in Ξ is proved in the following lemma.

Theorem 3.4.2. The elements of Ξ form the set of even permutations of the Farey octahedron with the elements of ∇ as it vertices.

Proof. We consider the Farey octahedron with the elements of ∇ as it vertices as shown in the diagram of Figure 3.14.

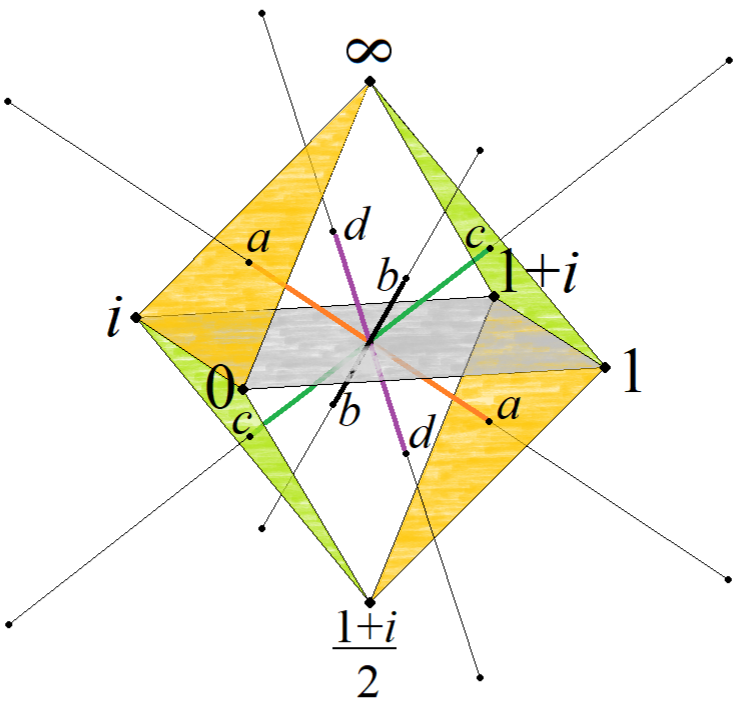

Figure 3.14: Permuting the octahedron defined by the vertices of ∇.

We draw its axes, the lines joining centroids of opposite triangular faces, and label them aa, bb, cc and dd in the diagram of Figure 3.14. We will simply call these axes a, b, c and d. All possible rigid motions of the Farey octahedron result from considering the permutations of a, b, c and d.

We consider the rotation through $\frac{2\pi}{3}$ about a, the axis between the centroid of the triangle with vertices 0, i and ∞ and the triangle with vertices $1+i$, 1 and $\frac{1+i}{2}$. The permutation

$(b\ c\ d)$ of the axes results the permutation $(0\ i\ \infty)(1+i\ 1\ \frac{1+i}{2})$ of the vertices of ∇. We call this permutation A. We label all the other rotations and their inverses about the axes a, b, c and d similarly, as given in Table 3.3.

When we compose a rotation about c with a rotation about a, namely $(a\ b\ d)$ and $(c\ b\ d)$ respectively, we get $(a\ b\ d)(c\ b\ d) = (a\ b)(c\ d)$ which corresponds with a rotation through π about the axis passing though 1 and i and we call it $E = CA^{-1}$. The rotations through π about the axes passing through ∞ and $\frac{1+i}{2}$ and the axes passing through 0 and $1+i$ are determined in a similar way. □

We have labeled the maps with capital letters, starting with the ones that occur more frequently in the product of Möbius maps derived from the $NICF$. The maps B and B^{-1} were used in chapter 2 for the case of continued fractions with real non-zero integer partial quotients. The maps A and A^{-1} are potentially useful whenever there is an imaginary integer coefficient present in the partial quotient. The maps C, C^{-1}, E and E^{-1} also occur frequently, while the maps D, D^{-1}, F, F^{-1}, G and G^{-1} do not.

We introduce the set $\nabla + a + bi$ which is defined as follows:

Definition 3.4.3. The set $\nabla + a + bi, a, b \in \mathbb{Z}$ is given by $\{z + a + bi | z \in \nabla\}$.

We use the sets $\nabla - 1$, $\nabla - i$ and $\nabla - 1 - i$ to develop the discussion about elliptic maps. In our second main theorem we show that the elliptic Möbius maps in Ξ preserve the vertices of ∇.

Theorem 3.4.4. The maps in Ξ preserve ∇.

Proof. The following equations can be confirmed by simple calculation:

$$\phi(\nabla) = \nabla - i,\ \ \phi(\nabla - i) = \nabla\ ,\ \ \phi(\nabla - 1) = \nabla - 1 - i,\ \ \phi(\nabla - 1 - i) = \nabla - 1,$$

$$\tau_{-i}(\nabla) = \nabla - i,\ \ \tau_i(\nabla - i) = \nabla,\ \ \tau_{-i}(\nabla - 1) = \nabla - 1 - i,\ \ \tau_i(\nabla - 1 - i) = \nabla - 1$$

$$\tau_{-1-i}(\nabla) = \nabla - 1 - i,\ \ \tau_{1+i}(\nabla - 1 - i) = \nabla,\ \ \tau_{1-i}(\nabla - 1) = \nabla - i\ \text{ and }\ \tau_{-1+i}(\nabla - i) = \nabla - 1.$$

Using these equations we have that:

$$A(\nabla) = \phi\tau_{-i}(\nabla) = \phi(\nabla - i) = \nabla, \quad A^{-1}(\nabla) = \tau_i\phi(\nabla) = \tau_i(\nabla - i) = \nabla$$

$$B(\nabla) = \phi\tau_1\phi\tau_{-1}(\nabla) = \phi\tau_1\phi(\nabla - 1) = \phi\tau_1(\nabla - 1 - i) = \phi(\nabla - i) = \nabla$$

$$B^{-1}(\nabla) = \tau_1\phi\tau_{-1}\phi(\nabla) = \tau_1\phi\tau_{-1}(\nabla - i) = \tau_1\phi(\nabla - 1 - i) = \tau_1(\nabla - 1) = \nabla$$

$$C(\nabla) = \tau_{1+i}\phi\tau_{-1}(\nabla) = \tau_{1+i}\phi(\nabla - 1) = \tau_{1+i}(\nabla - 1 - i) = \nabla$$

$$C^{-1}(\nabla) = \tau_1\phi\tau_{-1-i}(\nabla) = \tau_1\phi(\nabla - 1 - i) = \tau_1(\nabla - 1) = \nabla$$

The remainder of the functions in Ξ are compositions of A, B, C and their inverses.

$$D(\nabla) = \tau_{1+i}\phi\tau_{-1}\phi\tau_{-i}(\nabla) = CA(\nabla) = \nabla, \quad D^{-1}(\nabla) = \tau_i\phi\tau_1\phi\tau_{-1-i}(\nabla) = A^{-1}C^{-1}(\nabla) = \nabla$$

$$E(\nabla) = \tau_{1+i}\phi\tau_{-1+i}\phi(\nabla) = CA^{-1}(\nabla) = \nabla, \quad E^{-1}(\nabla) = \phi\tau_{1-i}\phi\tau_{-1-i}(\nabla) = AC^{-1}(\nabla) = \nabla$$

$$F(\nabla) = \tau_1\phi\tau_{-1-i}\phi\tau_{-i}(\nabla) = C^{-1}A(\nabla) = \nabla, \quad F^{-1}(\nabla) = \tau_i\phi\tau_{1+i}\phi\tau_{-1}(\nabla) = A^{-1}C(\nabla) = \nabla$$

$$G(\nabla) = \phi\tau_1\phi\tau_{-1}\phi\tau_{-i}(\nabla) = BA(\nabla) = \nabla, \quad G^{-1}(\nabla) = \tau_i\phi\tau_1\phi\tau_{-1}\phi(\nabla) = A^{-1}B^{-1}(\nabla) = \nabla$$

□

The products of factors ϕ and τ_d with $d \in \{-1-i, -1, -i, -1+i, 1-i, 1, i, 1+i\}$, that appear in the elements of Ξ, emerge naturally among the parabolic Möbius maps in T_n. These elements of Ξ need to be treated as separate factors in the product in order to develop the link between partial quotients of the NICF and the geometry of the extended Schmidt arrangement.

3.5 The Farey quadrilaterals of v

The images of $\{\alpha\} \cup \nabla_\alpha$, with $\alpha = \infty$ or 0, under partial products of Möbius maps T_n are Farey quadrilaterals in $\mathbb{C}$ with the same properties as $Q\nabla_\alpha$, since Möbius maps conformally map circles to circles and Farey neighbours to Farey neighbours. If $T_n(\alpha) = v$ and $T_n(\nabla_\alpha) = \{v_1, v_2, v_3, v_4\}$ we can visualise a Farey quadrilateral of v with vertices at

$v_i, i = 1,2,3,4$. The Farey quadrilateral is bounded by arcs on the pair of Farey circles and the pair of dual Farey circles that each pass through v and a distinct pair of Farey neighbours in $\{v_1, v_2, v_3, v_4\}$. The pair of Farey circles are tangential at v and are orthogonal to the pair of dual Farey circles that are tangential at v.

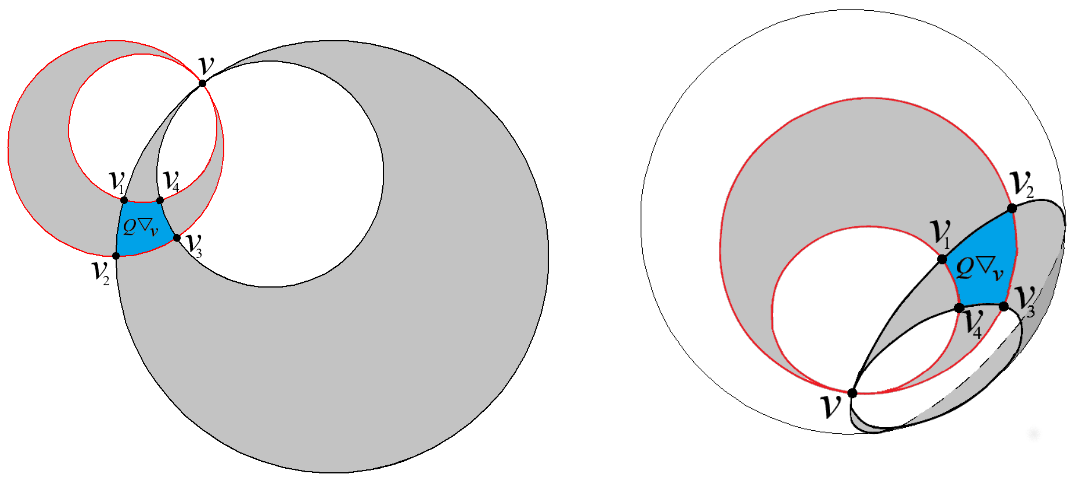

Figure 3.15: The configuration of v and $Q\nabla_v$ in $\hat{\mathbb{C}}$ (generic image) and in the projection of $\hat{\mathbb{C}}$ onto the Riemann sphere

We now define Farey quadrilaterals that are related to each vertex $v \in \mathbb{Q}[i] \cup \{\infty\}$ as follows:

Definition 3.5.1. Let $v \in \mathbb{Q}[i] \cup \{\infty\}$, with the elements of $\{v_1, v_2, v_3, v_4\} \subset \mathbb{Q}[i] \cup \{\infty\}$ satisfying the conditions

- $v \sim v_i, i = 1,2,3,4$ and
- $v_1 \sim v_2, v_2 \sim v_3, v_3 \sim v_4$ and $v_4 \sim v_1$.

The region shown in Figure 3.15 bounded by the four arcs not containing v on:

- the circle through points v, v_2 and v_3 and the circle through points v, v_1 and v_4 and
- the circle through points v, v_1 and v_2 and the circle through points v, v_3 and v_4

is a Farey quadrilateral related to v.

The illustration of one of the Farey quadrilaterals of v in $\hat{\mathbb{C}}$ shown in Figure 3.15 is generic as ∞ may possibly be one of the vertices.

The 4 circles in Definition 3.5.1 subdivide $\hat{\mathbb{C}}$ into 9 regions and the hyperbolic quadrilateral that does not have v as a vertex is the Farey quadrilaterals of v in the configuration.

Example 3.5.2. The possible configurations of v and ∇_v are illustrated in Figure 3.16.

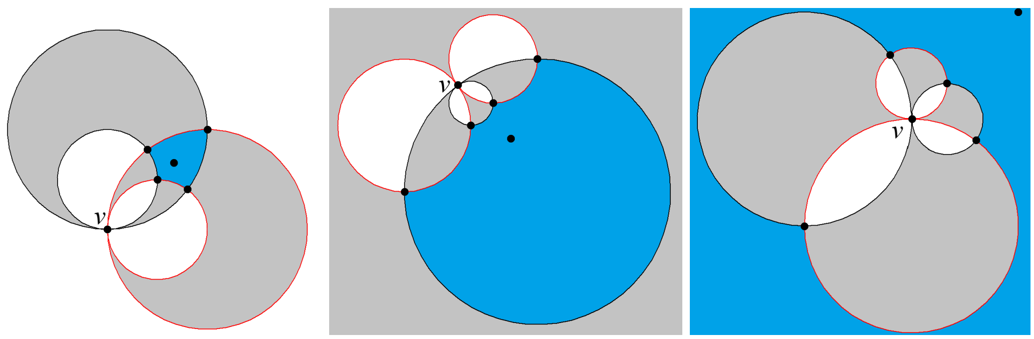

Figure 3.16: The configurations of v and ∇_v in $\hat{\mathbb{C}}$ with 3 different choices of v

In each diagram the 6 vertices are in identical positions in relation to each other. We show 3 different choices of v used to illustrate the resulting ∇_v, where the "sixth" vertex is not a Farey neighbour of v and is always located in a Farey quadrilateral of v.

3.6 Conclusion

In this chapter, we developed a new geometrical perspective from which we can study continued fractions. The connections between geometric structures embedded in the extended Schmidt arrangement and the arithmetic generated by the Möbius maps derived from the NICF become more concrete. The intermediate images of Farey quadrilaterals align with coefficients of the parabolic Möbius maps and the elliptic Möbius maps permute the vertices of the Farey quadrilateral in between these movements.

Chapter 4

Parsing products of Möbius maps using a geometrical perspective

In this chapter, we reinterpret the products of Möbius maps derived from the $NICF$ of square roots of elements in the Gaussian integers $\mathbb{Z}[i] = \{a + bi | a, b \in \mathbb{Z}\}$. We show the geometrical effects of these Möbius maps when the product is composed of:

- only parabolic factors,
- parabolic factors, interspersed with distinct elliptic factors, and
- parabolic factors interspersed with merged elliptic factors.

By analysing the movements of Farey quadrilaterals (FQs) in the extended Schmidt arrangement $\hat{S}_{\mathbb{Q}(\sqrt{-1})}$ due to parabolic Möbius maps, and permutation of vertices of ∇ that result from the use of the elliptic Möbius maps, we set out a procedure for parsing T, the original product of parabolic Möbius maps derived from the $NICF$. The main theorem of this chapter describes specific factoring techniques to obtain partial products of Möbius maps that yield a set of nested Farey quadrilaterals containing the target being approximated.

4.1 Introduction

We use the functions $\tau_{b_n}(z) = z + b_n$ and $\phi(z) = \frac{1}{z}$ as before, but now $b_n \in \mathbb{Z}[i]$. As in definition 2.2.4, the partial product of parabolic Möbius maps $T_n = t_0 t_1 \cdots t_n$ has $t_n = \tau_{b_n}$ for n even and $t_n = \phi\tau_{b_n}\phi$ for n odd, $n \in \mathbb{N}_0$. We use FQs as the geometric tools for illustrating the effects of successive partial products. The product T needs to be analysed to reveal the elliptic Möbius maps embedded in the product. These elliptic maps emerge when we extract consecutive factors involving specific combinations of the factors ϕ and τ_d with $d \in \{-1-i, -1, -i, -1+i, 1-i, 1, i, 1+i\}$. The process links Möbius maps derived from the $NICF$ and the sequence of nested FQs that contain the target ξ. We denote the FQ in this sequence as $FQ1, FQ2, \ldots FQN \ldots$ where $N \in \mathbb{N}$. We get observable trajectories that make it possible to count FQs that are intermediate images between consecutive FQN, and thus we can illustrate the connection to the coefficients of the parabolic Möbius maps in T.

4.2 The effect of parabolic Möbius maps on the vertices of $\triangledown$ in the extended complex plane.

In this chapter we work with the square roots of complex integers near

$$3 + 4i = (2 + i)^2,$$

as the geometry being illustrated is deeply connected to square roots.

In Example 4.2.1, we start with the square root of $3 + 5i$, which is one unit above $3 + 4i$ in $\mathbb{C}$. The NICF of $\sqrt{3 + 5i}$ yields T, a product of parabolic Möbius maps with no elliptic factors. We justify the statement that there are no elliptic factors in Example 4.2.2 which follows. The progression through the T_n for $n \in \mathbb{N}_0$ is illustrated. As the fixed points alternate between the images of 0 and ∞, we track the intermediate images of $Q\triangledown_0$ or $Q\triangledown_\infty$ respectively for each T_n to reveal the action of the parabolic maps, and how the partial products generate a sequence of nested hyperbolic quadrilaterals containing the target ξ.

Example 4.2.1. The number $\xi = \sqrt{3+5i} \approx 2.10130339... + i1.18973776...$ has *NICF* $[2+i, \overline{2-4i, 4+2i}]$ from which we derive the product of parabolic Möbius maps

$$T = \tau_{2+i}\ \overline{(\phi\tau_{2-4i}\phi)\ \tau_{4+2i}}.$$

In this example, we get $T_n = t_0 t_1 \ldots t_n$ with

$$t_0 = \tau_{2+i}, \quad t_1 = \phi\tau_{2-4i}\phi, \quad t_2 = \tau_{4+2i}, \quad t_{2n+1} = t_1, \quad t_{2n+2} = t_2, \quad n \in \mathbb{N}.$$

In the following diagrams, we show the progression under each successive T_n for $n \in \mathbb{N}_0$, and we link the number of intermediate FQs to the coefficients of the associated parabolic Möbius maps. The elements of ∇ are indicated next to their images in the diagrams.

1) For $T_0 = \tau_{2+i}$:
We start with the shaded quadrilateral $T_0\,(Q\nabla_\infty)$ with vertices at $T_0(0) = 2{+}i$, $T_0(i) = 2{+}2i$, $T_0(1) = 3+i$ and $T_0(1+i) = 3+2i$. $T_0\,(Q\nabla_\infty)$ is $FQ1$ for $\xi = \sqrt{3+5i}$. The target ξ is marked by an 'X' in a box, and it appears closest to the image of 0.

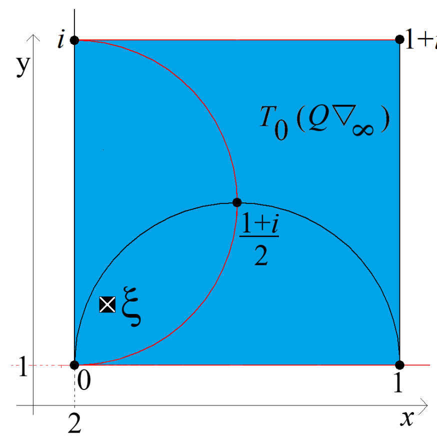

2) The next map, $t_1 = \phi\tau_{2-4i}\phi$, fixes 0, so we change our focus to the image of $Q\nabla_0$ under T_0. It is shaded region $T_0\,(Q\nabla_0)$ with vertices at ∞, i, $\frac{1+i}{2}$ and 1, and it is bounded by arcs on the 2 Farey circles (thick) and 2 dual Farey circles (thick dashed) that pass through the image of 0 as shown.

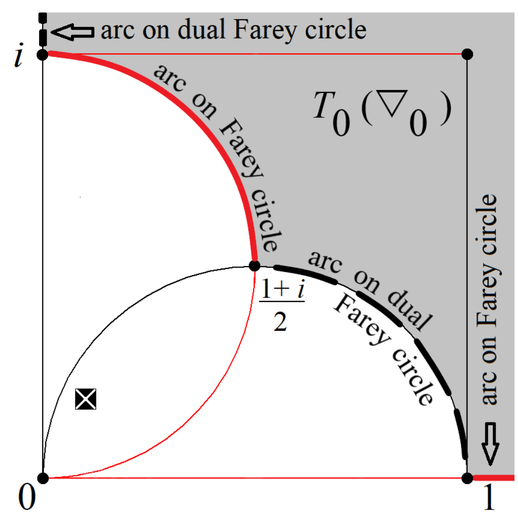

3) For $T_1 = \tau_{2+i}\,(\phi\tau_{2-4i}\phi)$:

In this diagram, we label the intermediate images of $Q\nabla_0$ under T_1 with their respective $T_{1,k}$ where k is linked to the position of the FQ. The number of intermediate FQ along any path from $T_0\,(Q\nabla_0)$ to $T_1\,(Q\nabla_0)$ matches the coefficients '$2-4i$' of t_1.

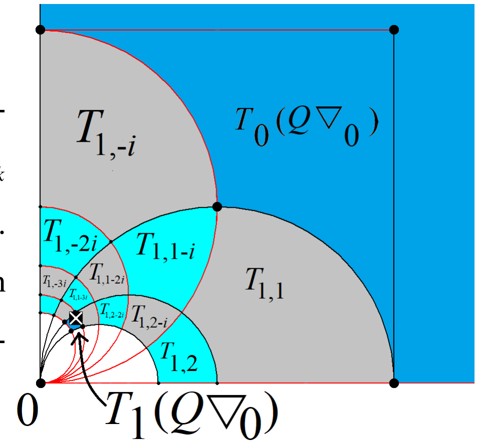

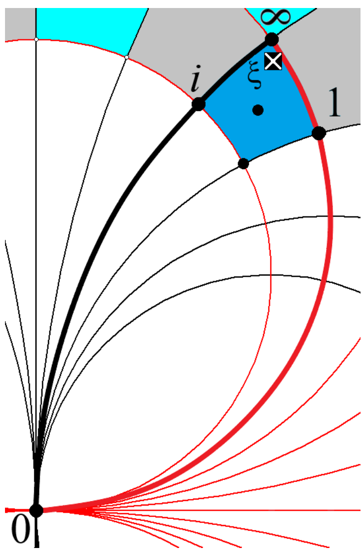

4) On the left: (enlarged)

The image $T_1(Q\nabla_0)$ is $FQ2$ for $\xi = \sqrt{3+5i}$. The target ξ appears closest to $T_1(\infty)$.

5) On the right: The next map, $t_2 = \tau_{4+2i}$, fixes ∞, so we change our focus to the shaded region $T_1\,(Q\nabla_\infty)$.

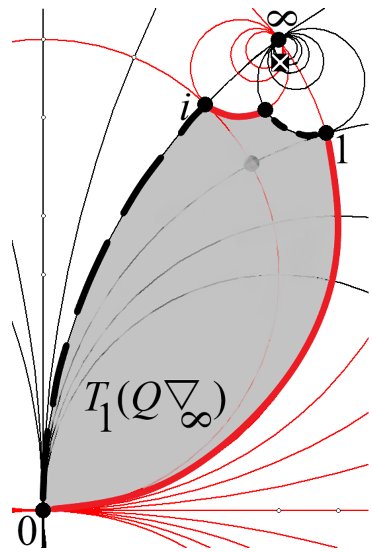

6) For $T_2 = \tau_{2+i}\,(\phi\tau_{2-4i}\phi)\,\tau_{4+2i}$: (enlarged)

In this diagram, we label the intermediate images of $Q\nabla_\infty$ under T_2 with their respective $T_{2,k}$ where k is linked to the position of the FQ. The number of intermediate FQ along any path from $T_1\,(Q\nabla_\infty)$ to $T_2\,(Q\nabla_\infty)$ matches the coefficients '$4+2i$' of t_2.

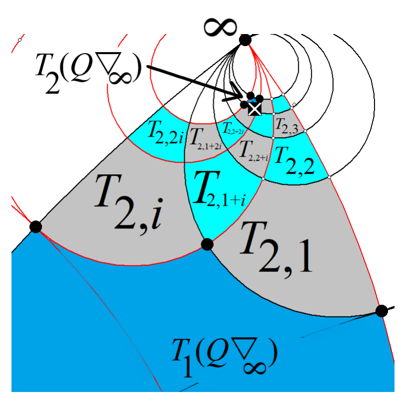

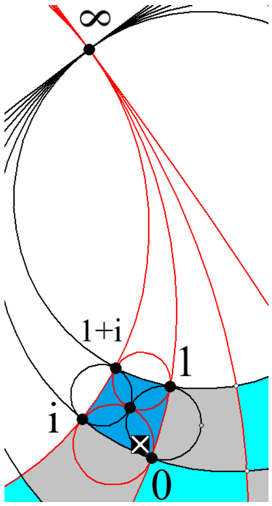

7) On the left: (enlarged) $T_2(Q\nabla_\infty)$ is $FQ3$ for $\xi = \sqrt{3+5i}$. The target ξ now appears closest to $T_2(0)$.

8) On the right: As in step 2), we change our focus to the shaded region $T_2\,(Q\nabla_0)$ shown in the diagram

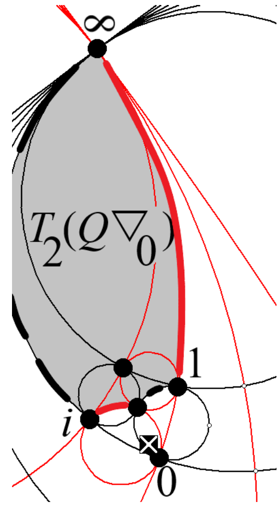

Since the fixed point alternates between the image of 0 and the image of ∞ for successive T_n we repeat the last two steps indefinitely as n increases. In this example, we have shown how the images of the vertices of ∇ move along Farey circles under the action of parabolic maps between consecutive FQNs of $\xi = \sqrt{3+5i}$, and how the number of intermediate images of Farey quadrilaterals in the progression from T_{n-1} to T_n match the coefficient of t_n, the last factor of T_n.

In the next example, we justify the statement that there are no elliptic factors in the product of Möbius maps found in Example 4.2.1. Firstly, we recall the elliptic Möbius maps in Ξ as:

$$A = \phi\tau_{-i},\ A^{-1} = \tau_i\phi,\ B = \phi\tau_1\phi\tau_{-1},\ B^{-1} = \tau_1\phi\tau_{-1}\phi,\ C = \tau_{1+i}\phi\tau_{-1},\ C^{-1} = \tau_1\phi\tau_{-1-i}$$

$$D = \tau_{1+i}\phi\tau_{-1}\phi\tau_{-i},\ D^{-1} = \tau_i\phi\tau_1\phi\tau_{-1-i},\ E = \tau_{1+i}\phi\tau_{-1+i}\phi,\ E^{-1} = \phi\tau_{1-i}\phi\tau_{-1-i}$$

$$F = \tau_1\phi\tau_{-1-i}\phi\tau_{-i},\ F^{-1} = \tau_i\phi\tau_{1+i}\phi\tau_{-1},\ G = \phi\tau_1\phi\tau_{-1}\phi\tau_{-i},\ G^{-1} = \phi\tau_i\phi\tau_1\phi\tau_{-1}.$$

Example 4.2.2. The factorization $\tau_{2+i}\ \overline{(\phi\tau_{2-4i}\phi)\,\tau_{4+2i}}$ is written without brackets as

$$\tau_{2+i}\ \phi\ \tau_{2-4i}\ \phi\ \tau_{4+2i}\ \phi\ \tau_{2-4i}\ \phi\ \tau_{4+2i}\ \phi\ \tau_{2-4i}\ \phi\ \tau_{4+2i}\ldots$$

There are no negative real parts in the $b_n, n \in \mathbb{N}$ so the maps B, C, D, E, F, G and their inverses are not present as factors in the product. We consider the possible presence of $A = \phi\tau_{-i}$ and $A^{-1} = \tau_i\phi$. In the first 3 factors

$$\tau_{2+i}\ \phi\ \tau_{2-4i}$$

the ϕ has a τ_i in front of it and a τ_{-i} after it so either A or A^{-1} could be present. But the following ϕ is located in

$$\tau_{2-4i}\ \phi\ \tau_{4+2i}$$

where neither A nor A^{-1} can be factored out. The map ϕ is an elliptic map but it does not preserve ∇, so it cannot be considered on its own, it must be included in one of the elliptic maps in Ξ or it is part of the parabolic map with the structure $(\phi\ \tau_{b_n}\ \phi)$.
We consider 3 possibilities:

- Case i) $T = \tau_2\ [\tau_i\phi]\overline{\tau_{2-4i}\left(\phi\tau_{4+2i}\phi\right)} = \tau_{2+i}\ A^{-1}\overline{\tau_{4+2i}\left(\phi\tau_{2-4i}\phi\right)}$.
- Case ii) $T = \tau_{2+i}\ [\phi\tau_{-i}]\tau_{2-3i}\overline{\left(\phi\tau_{4+2i}\phi\right)\tau_{2-4i}} = \tau_{2+i}\ A\tau_{2-3i}\overline{\left(\phi\tau_{4+2i}\phi\right)\tau_{2-4i}}$
- Case iii) $T = \tau_{2+i}\ \overline{\left(\phi\tau_{2-4i}\phi\right)\tau_{4+2i}}$

In both cases i) and ii) there are only parabolic maps in the remaining factors after A or A^{-1}, as every second ϕ must be part of a $(\phi\ \tau_{b_n}\ \phi)$ structure. For case i) the Farey quadrilateral $T_0\left(Q\nabla_\infty\right)$, with $T_0 = \tau_2$, does not contain ξ as it is the square below the one shown in step i) of Example 4.2.1. In case ii) the vertex $2 + i$ becomes the image of ∞ after $\tau_{2+i}\ A$ has been applied and the Farey quadrilateral $\tau_{2+i}\ A\tau_{2-3i}\left(Q\nabla_\infty\right)$ does not contain ξ as it is the FQ adjacent to "$T_1\left(Q\nabla_0\right)$" shown in step iii) of Example 4.2.1. The only viable choice is the original product of parabolic Möbius maps given in case iii).

In example 4.2.3, we observe a pattern, similar to the one in the $NICF$ of $\sqrt{3+5i}$, in the partial quotients of the $NICF$s of numbers that are nearer to $\sqrt{3+4i}$.

Example 4.2.3. In example 4.2.1, we worked with $\sqrt{3+5i}$ whose continued fractions has the structure $[a+bi, \overline{c-di, 2a+2bi}]$, with $a, b, c, d \in \mathbb{N}$. For examples of square roots of numbers close to $3+4i$ with a similar structure in their $NICF$s we look at $\sqrt{3+4.1i}$, $\sqrt{3+4.01i}$ and $\sqrt{3.01+4.1i}$.

ξ	$NICF$	product of parabolic maps
$\sqrt{3+4.1i} \approx 2.01+i1.02$	$[2+i, \overline{20-40i, 4+2i}]$	$\tau_{2+i}\ \overline{(\phi\tau_{20-40i}\phi)\,\tau_{4+2i}}$
$\sqrt{3+4.01i} \approx 2.001+i1.002$	$[2+i, \overline{200-400i, 4+2i}]$	$\tau_{2+i}\ \overline{(\phi\tau_{200-400i}\phi)\,\tau_{4+2i}}$
$\sqrt{3.01+4.1i} \approx 2.003+i1.001$	$[2+i, \overline{300-100i, 4+2i}]$	$\tau_{2+i}\ \overline{(\phi\tau_{300-100i}\phi)\,\tau_{4+2i}}$

These examples all yield the same structure for the Möbius maps and hence display the same movements of images $Q\nabla_0$ and $Q\nabla_\infty$ under successive T_n as in the case of $\sqrt{3+5i}$.

Some nice features of using parabolic Möbius maps occur in examples 4.2.1 and 4.2.3. Ideally, the following should occur in the progression from T_{n-1} to T_n for each partial quotient of a continued fraction:

- Fixed points for successive T_n alternate between the image of 0 and the image of ∞.
- The number of intermediate images of $Q\nabla_v$ between $T_{n-1}(Q\nabla_v)$ and $T_n(Q\nabla_v)$ is linked directly to the partial quotient b_n, with $v=0$ for n even and $v=\infty$ for n odd.
- The Farey quadrilateral $T_n(Q\nabla_v)$ contains the target ξ, with $v=0$ for n even and $v=\infty$ for n odd.

This ideal situation only occurs for $NICF$s where the product T of parabolic Möbius maps has coefficients derived from partial quotients b_n of the $NICF$ where all real parts are positive, and the imaginary parts are positive if n is even and negative if n is odd as in Example 4.2.3.
In the following example, we consider the case where the real and imaginary parts of all coefficients are positive.

Example 4.2.4. The number $\xi = \sqrt{4+4i} = 2.19736822693562...+i\,0.910179721124455...$ has $NICF$ $[2+i, \overline{4+2i}]$ from which we derive $T=\tau_{2+i}\ \overline{(\phi\tau_{4+2i}\phi)\,\tau_{4+2i}}$.

With $T_0 = \tau_{2+i}$ the quadrilateral $T_0\left(Q\nabla_\infty\right)$ does not contain the target ξ so τ_{2+i} as a choice for T_0 is not suitable. This is an indication that there is an elliptic factor among the initial factors of this product.

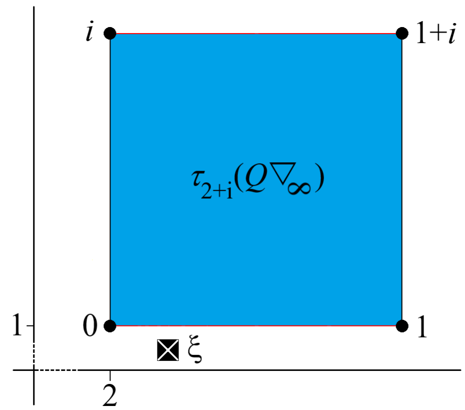

4.3 Accommodating elliptic Möbius maps

In this section, we accommodate elliptic maps in the product of Möbius maps to ensure that, when the image of v is the fixed point of T_n, the image of $Q\nabla_v$ under T_n contains ξ. The effect of elliptic maps was discussed in Chapter 3.4. We show examples of how elliptic maps are accommodated among the maps present in the product of parabolic Möbius maps derived from the NICF. Once the elliptic factors in T are isolated, the partial product of parabolic Möbius maps T_n changes into a partial product of Möbius maps $T_{M(n)}$ defined as follows:

Definition 4.3.1. Let $T_M = t_{m(1)}t_{m(2)}t_{m(3)}\dots$ be the product of Möbius maps derived from T, where each $t_{m(n)}$ is either a parabolic Möbius map that fixes ∞, a parabolic Möbius map that fixes 0 or an element in Ξ. The partial products of T_M are $T_{M(n)} = t_{m(1)}t_{m(2)}\dots t_{m(n)}$, where n is the number of parabolic and elliptic Möbius maps as separate factors.

In the following example, we show how we use brackets to isolate elements of Ξ in the product of parabolic Möbius maps T.

Example 4.3.2. As discussed in Example 4.2.4, $\tau_{2+i}\,\overline{(\phi\tau_{4+2i}\phi)\,\tau_{4+2i}}$ derived from the NICF of $\xi = \sqrt{4+4i}$ has elliptic Möbius maps among its factors. To identify the elliptic factors we first remove all brackets to get:

$$T = \tau_{2+i}\,\phi\,\tau_{4+2i}\,\phi\,\tau_{4+2i}\,\phi\,\tau_{4+2i}\,\phi\,\tau_{4+2i}\,\phi\,\tau_{4+2i}\,\phi\,\tau_{4+2i}\,\phi\,\tau_{4+2i}\dots$$

In front of every ϕ factor there is a τ_i which we separate out as follows:

$$T = \tau_2\ \tau_i\ \phi\ \tau_{4+i}\ \tau_i\ \phi\ \tau_{4+i}\ \tau_i\ \phi\ \tau_{4+i}\ \tau_i\ \phi\ \tau_{4+i}\ \tau_i\ \phi\ \tau_{4+i}\ \tau_i\ \phi\ \tau_{4+i}\ \tau_i\ \phi\ \tau_{4+i}\ldots$$

Isolating the elliptic factors, using square brackets to indicate the elements of Ξ, we get:

$$T = \tau_2\ [\tau_i\ \phi]\ \tau_{4+i}\ [\tau_i\ \phi]\ \tau_{4+i}\ [\tau_i\ \phi]\ \tau_{4+i}\ [\tau_i\ \phi]\ \tau_{4+i}\ [\tau_i\ \phi]\ \tau_{4+i}\ [\tau_i\ \phi]\ \tau_{4+i}\ [\tau_i\ \phi]\ \tau_{4+i}\ldots$$

which we now write as a product of parabolic and elliptic Möbius maps:

$$T_M = \tau_2\ \overline{[\tau_i\phi]\,\tau_{4+i}} = \tau_2\ \overline{A^{-1}\tau_{4+i}}.$$

Using Definition 4.3.1 we set

$$t_{m(1)} = \tau_2,\ t_{m(2d)} = A^{-1} \text{ and } t_{m(2d+1)} = \tau_{4+i},\ d \in \mathbb{N}.$$

For the parabolic factors in Example 4.3.2 we adjusted the value $4+2i$ to $4+i$ as the τ_i was accommodated in the elliptic map A^{-1}. We say $4+i$ is the adjusted coefficient of the parabolic map $t_{m(2d+1)} = \tau_{4+i}$ and we call it b^*_{2d+1}. We adjust the definition for intermediate images of $T_{M(n)}$, the partial products of Möbius maps, as follows:

Definition 4.3.3. Let $t_{m(n)}$ in the product T_M be either the parabolic Möbius map

$$t_{m(n)} = \tau_{b^*_n} \text{ or } t_{m(n)} = \phi\tau_{b^*_n}\phi,$$

with fixed points at $v = \infty$ and $v = 0$ respectively, where b^*_n is the adjusted coefficient of the parabolic map $t_{m(n)}$ once all the elliptic maps have been factored out. In the partial product of Möbius maps $T_{M(n)} = t_{m(1)}t_{m(2)}\ldots t_{m(n)}$ we replace $t_{m(n)}$ with $t_{m(n),k} = \tau_k$ or $t_{m(n),k} = \phi\tau_k\phi$, keeping the same fixed point, to get

$$T_{M(n),k} = t_{m(1)}t_{m(2)}\ldots t_{m(n-1)}t_{m(n),k}.$$

For $b^*_n = p + qi$, we have

$$k \in \left\{ c + di \in \mathbb{Z}[i] \,\middle|\, 0 \le \frac{c}{p} \le 1, \quad 0 \le \frac{d}{q} \le 1, \quad k \ne 0 \text{ and } k \ne b^*_n \right\}.$$

The collection of Farey quadrilaterals $T_{m(n),k}(Q\nabla_v)$ are called the intermediate images of $Q\nabla_v$ under $T_{M(n)}$.

Using FQs that are intermediate images of $T_{M(n)}$ each time $t_{m(n)}$ is a parabolic Möbius map, we show how the factorisation done in Example 4.3.2 yields the required nested FQs containing the target $\xi = \sqrt{4+4i}$.

Example 4.3.4. In the following diagrams, we show the progression under successive $T_{M(n)}$, for each $n \in \mathbb{N}$, and illustrate the associated intermediate FQs each time $t_{m(n)}$ is a parabolic Möbius map.

1) For $T_{M(1)} = \tau_2$:
We start with the shaded quadrilateral $T_{M(1)}(Q\nabla_\infty)$ with the image of 0 (bottom left hand corner) located at $z = 2$ in $\hat{\mathbb{C}}$. $T_{M(1)}(Q\nabla_\infty)$ is $FQ1$ for $\xi = \sqrt{4+4i}$. The vertex at ∞ is fixed at ∞ under $T_{M(1)}$. The target ξ appears closest to the image of i.

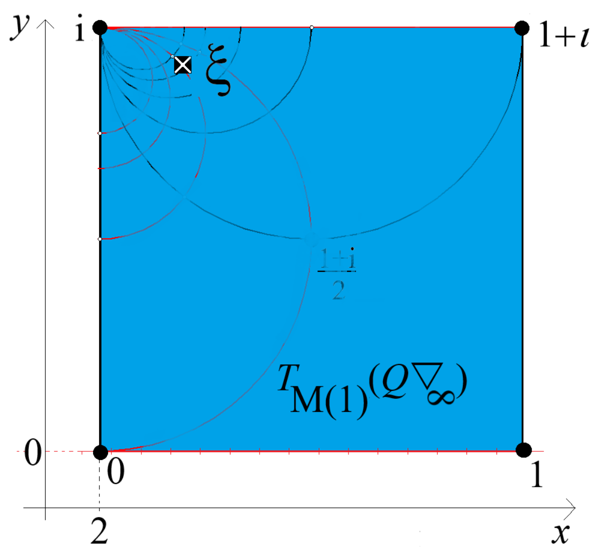

2) For $T_{M(2)} = \tau_2 A^{-1}$:
The map A^{-1} permutes the vertices of ∇. The images of 0, i and ∞ are permuted along the dual Farey circle with $x = 2$ for $z = x + iy$, and the images of 1, $1+i$ and $\frac{1+i}{2}$ are permuted along the Farey circle, as shown. In particular $A^{-1}(\infty) = \tau_i\phi(\infty) = \tau_i(0) = i$, so ξ now appears closest to $T_2(\infty)$.

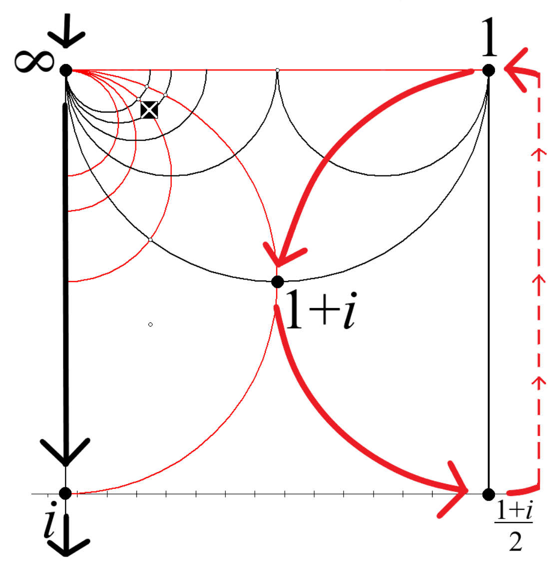

3) Since the next map $t_{m(3)} = \tau_{4+i}$, we now change our focus to $T_2(Q\nabla_\infty)$, the shaded region bounded by arcs on the 2 Farey circles (thick) and 2 dual Farey circles (thick dashed) that each pass through the images of ∞ and of 2 distinct elements in $\nabla_\infty = \{0, 1, i, 1+i\}$ as shown. The image of 0 is at ∞.

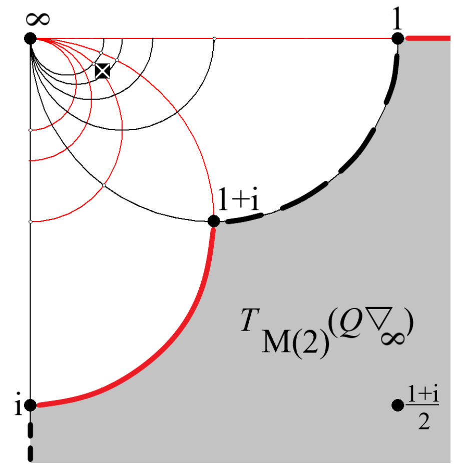

4) For $T_{M(3)} = \tau_2 A^{-1} \tau_{4+i}$:
In this diagram, we label the intermediate images of $Q\nabla_\infty$ under $T_{M(3)}$ with their respective $T_{M(3),k}$ where k is linked to the position of the FQ and $T_{M(3)}(\infty)$ is the fixed point. The number of intermediate FQ along any path from $T_{M(2)}(Q\nabla_\infty)$ to $T_{M(3)}(Q\nabla_\infty)$ matches the adjusted coefficient '$4+i$' of $t_m(3)$.

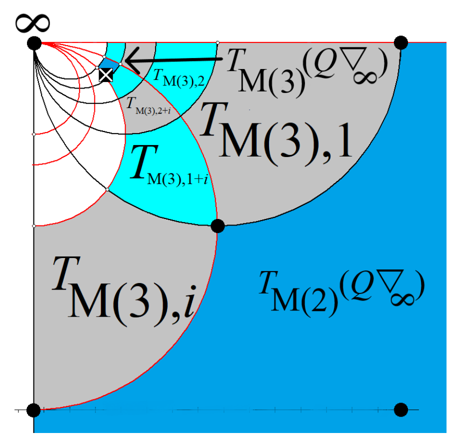

5) $T_{M(3)}(Q\nabla_\infty)$ is $FQ2$ for $\xi = \sqrt{4+4i}$. It is enlarged to show where the images of ∞, 0, 1, i and $1+i$ are located. The target ξ appears closest to the image of i.

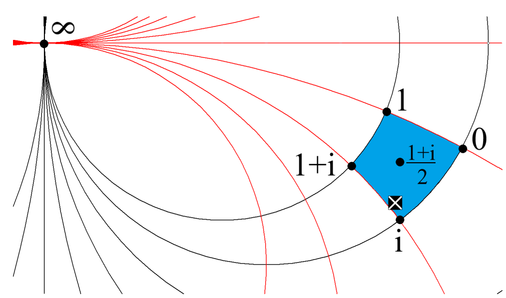

6) For $T_{M(4)} = \tau_2 A^{-1} \tau_{4+i} A^{-1}$: The map A^{-1} permutes the vertices of ∇, in particular ∞ is mapped to i, so ξ now appears closest to $T_{M(4)}(\infty)$.

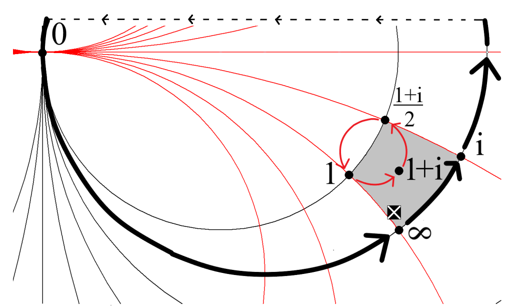

7) We change our focus to $T_{M(4)}\left(Q\nabla_\infty\right)$ which is the shaded region bounded by arcs on the 2 Farey circles (thick) and 2 dual Farey circles (thick dashed) passing through the image of ∞ and of 2 distinct elements in ∇_∞ as shown.

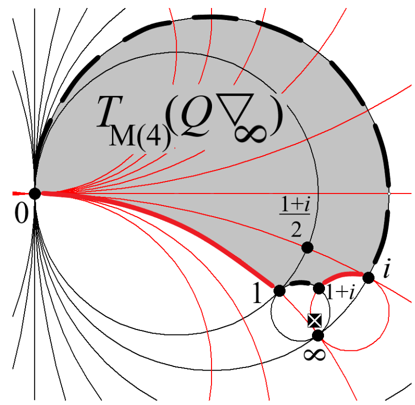

8) For $T_{M(5)} = \tau_2 A^{-1}\tau_{4+i}A^{-1}\tau_{4+i}$:
The map τ_{4+i} leaves the image of ∞ fixed in the progression from $T_{M(4)}$ to $T_{M(5)}$. $T_{M(5)}\left(Q\nabla_\infty\right)$ is $FQ3$ for $\xi = \sqrt{4+4i}$. The intermediate images of $Q\nabla_\infty$ under $T_{M(5),i}$ and $T_{M(5),1}$ are indicated.

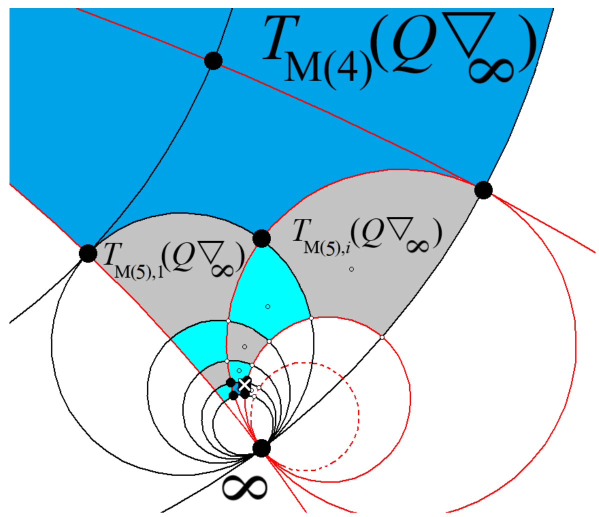

The configuration of intermediate Farey quadrilaterals for each $T_{M(n)}$ for n odd matches the adjusted coefficient '$4+i$' of $t_n = \tau_{4+i}$. Each time the target ξ lies closest to the image of i under $T_{M(n)}$ for n odd, the map $t_{n+1} = A^{-1}$ in $T_{M(n+1)}$ permutes the vertices of ∇ to put the target closest to the image of ∞.

In the next example, we illustrate the effect of the elliptic map E.

Example 4.3.5. The number $\xi = \sqrt{3+3i} = 1.90297670599502...+i\,0.788238760503214...$ has $NICF$ $[2+i, \overline{-2+4i, 4+2i}]$ from which we derive the product of parabolic Möbius maps $T = \tau_{2+i}\,\overline{\phi\tau_{-2+4i}\phi\tau_{4+2i}}$. Removing all brackets, we get:

$$T = \tau_{2+i}\,\phi\,\tau_{-2+4i}\,\phi\,\tau_{4+2i}\,\phi\,\tau_{-2+4i}\,\phi\,\tau_{4+2i}\,\phi\,\tau_{-2+4i}\,\phi\,\tau_{4+2i}\,\phi\,\tau_{-2+4i}\ldots.$$

The factors $\tau_{1+i}\ \phi\ \tau_{-1+i}$ of E are present in the first 3 factors, so we insert $(\phi)(\phi) = \phi^2$, the identity map, and rearrange the factors as shown:

$$T = \tau_1\ \tau_{1+i}\ \phi\ \tau_{-1+i}\ (\phi)(\phi)\tau_{-1+3i}\ \phi\ \tau_{3+i}\ \tau_{1+i}\ \phi\ \tau_{-1+i}\ (\phi)(\phi)\tau_{-1+3i}\ \phi\ \tau_{3+i}\ \tau_{1+i}\ \phi\ \dots .$$

The first (ϕ) completes the factor E and the second (ϕ) becomes part of $(\phi\tau_{-1+3i}\phi)$. We identify elements of Ξ present in the factors, and, using square brackets '[' and ']', we isolate the elliptic factors in the product as follows:

$$T = \tau_1\left[\tau_{1+i}\ \phi\ \tau_{-1+i}\ \phi\right](\phi\tau_{-1+3i}\phi)\,\tau_{3+i}\left[\tau_{1+i}\phi\tau_{-1+i}\phi\right](\phi\tau_{-1+3i}\phi)\,\tau_{3+i}\left[\tau_{1+i}\phi\tau_{-1+i}\phi\right](\phi\tau_{-1+3i}\phi)\dots$$

which we now write as a product of Möbius maps: $T_M = \tau_1\overline{E\,(\phi\tau_{-1+3i}\phi)\,\tau_{3+i}}$.
For the partial products, we set

$$t_{m(1)} = \tau_1,\ t_{m(3k-1)} = E,\ t_{m(3k)} = \left(\phi\tau_{-1+3i}\phi\right) \text{ and } t_{m(3k+1)} = \tau_{3+i} \text{ with } k \in \mathbb{N}.$$

In the following diagrams we show the progression under successive $T_{M(n)}$, for each $n \in \mathbb{N}$ and illustrate the associated intermediate FQs each time $t_{m(n)}$ is a parabolic Möbius map. The elements of ∇ are indicated next to the vertex that is their image in each diagram.

1) For $T_{M(1)} = \tau_1$:
We start with the shaded quadrilateral $T_{M(1)}(Q\nabla_\infty)$ with $T_{M(1)}(0) = 1$. $T_{M(1)}(Q\nabla_\infty)$ is $FQ1$ for $\xi = \sqrt{3+3i}$. The target ξ appears closest to the image of $1+i$.

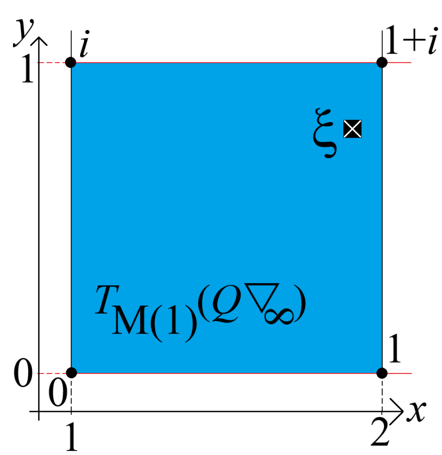

2) For $T_{M(2)} = \tau_1 E$: The map E permutes the vertices of ∇, swapping 0 and $1+i$ and swapping ∞ with $\frac{1+i}{2}$, but leaving the images of 1 and i fixed. Now ξ is closest to the image of 0 at $2+i$. We have changed our focus to the image of $Q\nabla_0$, bounded by arcs on the 2 Farey circles and 2 dual Farey circles that pass through the image of 0, as shown alongside.

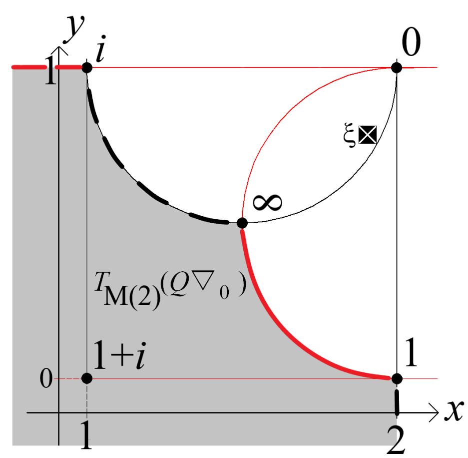

3) For $T_{M(3)} = \tau_1 E\,(\phi\tau_{-1+3i}\phi)$: The map $\phi\tau_{-1+3i}\phi$ leaves the image of 0 fixed in the progression from T_1 to T_2. We show all the intermediate images $T_{M(3),k}\,(Q\nabla_0)$, thus illustrating the link between the intermediate quadrilaterals and the coefficient '$-1+3i$'.

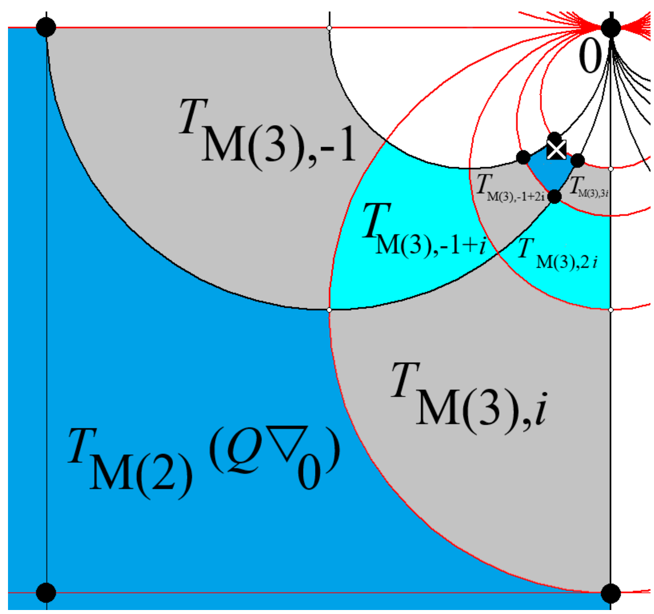

4) Enlarging, we now see $T_{M(3)}\,(Q\nabla_0)$ which is $FQ2$ for $\xi = \sqrt{3+3i}$. The target ξ appears closest to the image of ∞.

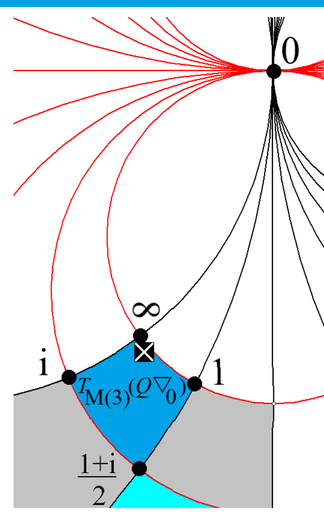

5) Since the next factor $t_{m(4)} = \tau_{3+i}$ fixes ∞, the focus changes from $T_{M(3)}(Q\nabla_0)$ to $T_{M(3)}(Q\nabla_\infty)$. $T_{M(3)}(Q\nabla_\infty)$ is bounded by the arcs on 2 Farey circles and 2 dual Farey circles that pass through the images of ∞ and of 2 distinct elements in ∇_∞, as shown alongside.

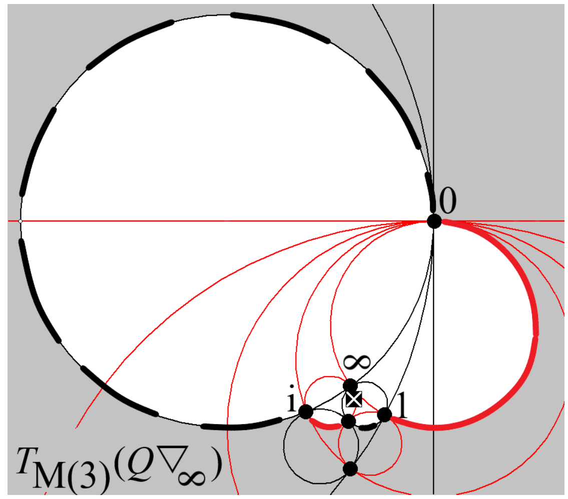

6) For $T_{M(4)} = \tau_1 E(\phi\tau_{-1+3i}\phi)\tau_{3+i}$: The image of ∞ is fixed in the progression from $T_{M(3)}$ to $T_{M(4)}$. We have shaded all intermediate images $T_{M(4),k}(Q\nabla_\infty)$ between $T_{M(3)}(Q\nabla_\infty)$ and $T_{M(4)}(Q\nabla_\infty)$.

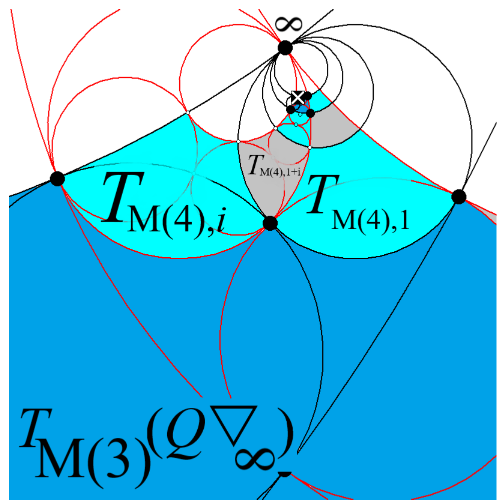

7) Enlarging, we now see $T_{M(4)}(Q\nabla_\infty)$ which is $FQ3$ for $\xi = \sqrt{3+3i}$. The target ξ appears closest to the image of $1+i$

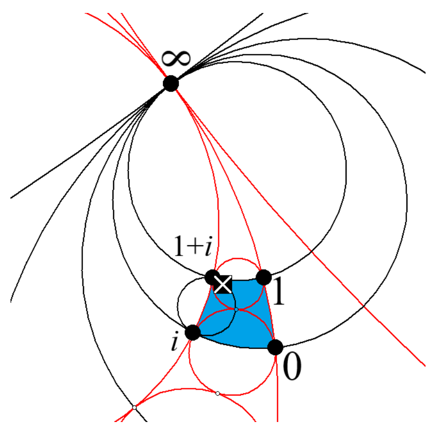

8) For $T_{M(5)} = \tau_1 E\,(\phi\tau_{-1+3i}\phi)\,\tau_{3+i}E$: The map E permutes the vertices of ∇, swapping 0 and $1+i$ and swapping ∞ with $\frac{1+i}{2}$. Now ξ is closest to the image $T_{M(5)}(0)$. Accordingly, we change our focus to the image $T_{M(5)}(Q\nabla_0)$ as shown alongside.

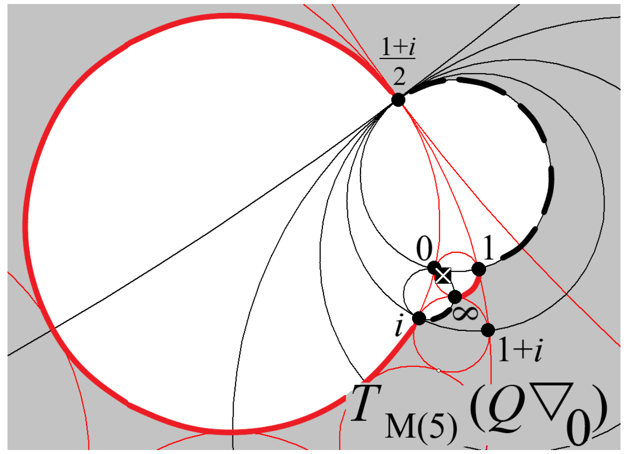

Every time the target lies closest to the image of $1+i$ under $T_{M(n)}$ the map E in $T_{M(n+1)}$ permutes the vertices of ∇, swapping the images of 0 and $1+i$. Now the image of 0 is closest to the target and the adjusted parabolic map $(\phi\tau_{-1+3i}\phi)$ can take effect in $T_{M(n+2)}$. The number of intermediate FQs on any path from one FQ containing ξ to the next FQ containing ξ matches the adjusted partial quotients of the parabolic factors in $T_{M(n)}$.

In the following example, we show the pattern that emerges in the NICF, the product of parabolic Möbius maps T, and the corresponding products of Möbius maps T_M for the first quadrant square roots of complex integers near $3+4i$, in particular

$$3+(4\pm1)i, \quad (3\pm1)+4i \text{ and } (3\pm1)+(4\pm1)i.$$

Example 4.3.6. The $NICF$ of each value in the table below has $b_0 = 2+i$ and $b_{2k} = 4+2i$ for $k \in \mathbb{N}$. The b_{2k-1} vary according to the position of ξ in relation to the number $2+i$. Note that:

- The $NICF$ of $\sqrt{4+5i}$ has the same form as $\sqrt{3+5i}$ of Example 4.2.1.
- The $NICF$ of $\sqrt{4+3i}$ has the same form as $\sqrt{4+4i}$ of Example 4.3.2.
- The $NICF$ of $\sqrt{2+3i}$ has the same form as $\sqrt{3+3i}$ of Example 4.3.5.
- The $NICF$ of $\sqrt{4+5i}$ has the same form as $\sqrt{3+5i}$, involving the maps C^{-1} and B.

$\sqrt{2+5i} \approx 1.92 + i1.30$ $[2+i, \overline{-1-3i, 4+2i}]$ $\tau_{2+i}\phi\tau_{-1-3i}\phi\tau_{4+2i}\phi\tau_{-1-3i}\dots$ $\tau_{1+i}C^{-1}\tau_{-2i}\overline{(\phi\tau_{3+2i}\phi)\,B\tau_{-3i}}$	$\sqrt{3+5i} \approx 2.10 + i1.18$ $[2+i, \overline{2-4i, 4+2i}]$ $\tau_{2+i}\phi\tau_{2-4i}\phi\tau_{4+2i}\phi\tau_{2-4i}\dots$ $\tau_{2+i}\overline{(\phi\tau_{2-4i}\phi)\,\tau_{4+2i}}$	$\sqrt{4+5i} \approx 2.28 + i1.09$ $[2+i, \overline{3-i, 4+2i}]$ $\tau_{2+i}\phi\tau_{3-i}\phi\tau_{4+2i}\phi\tau_{3-i}\dots$ $\tau_{2+i}\overline{(\phi\tau_{3-i}\phi)\,\tau_{4+2i}}$
$\sqrt{2+4i} \approx 1.79 + i1.30$ $[2+i, \overline{-4-2i, 4+2i}]$ $\tau_{2+i}\phi\tau_{-4-2i}\phi\tau_{4+2i}\phi\tau_{-4-2i}\dots$ $\tau_{1+i}C^{-1}\tau_{-3-i}\overline{(\phi\tau_{3+2i}\phi)\,B\tau_{-3-2i}}$	$\sqrt{3+4i} = 2+i$	$\sqrt{4+4i} \approx 2.19 + i0.91$ $[2+i, \overline{4+2i}]$ $\tau_{2+i}\phi\tau_{4+2i}\phi\tau_{4+2i}\phi\tau_{4+2i}\dots$ $\tau_2\overline{A^{-1}\tau_{4+i}}$
$\sqrt{2+3i} \approx 1.67 + i0.89$ $[2+i, \overline{-3+i, 4+2i}]$ $\tau_{2+i}\phi\tau_{-3+i}\phi\tau_{4+2i}\phi\tau_{-3+i}\dots$ $\tau_1\overline{E\,(\phi\tau_{-2}\phi)\,\tau_{3+i}}$	$\sqrt{3+3i} \approx 1.90 + i0.78$ $[2+i, \overline{-2+4i, 4+2i}]$ $\tau_{2+i}\phi\tau_{-2+4i}\phi\tau_{4+2i}\phi\tau_{-2+4i}\dots$ $\tau_1\,\overline{E\,(\phi\tau_{-1+3i}\phi)\,\tau_{3+i}}$	$\sqrt{4+3i} \approx 2.12 + i0.70$ $[2+i, \overline{1+3i, 4+2i}]$ $\tau_{2+i}\phi\tau_{1+3i}\phi\tau_{4+2i}\phi\tau_{1+3i}\dots$ $\tau_2\,\overline{A^{-1}\tau_{1+2i}A^{-1}\tau_{3+i}}$

The same pattern of partial quotients for the $NICF$ is found around the square root of each perfect square.

The elements of Ξ that appear in T depend on the partial quotients that occur in the $NICF$. The following theorem outlines the possible elements of Ξ that occur for each of the various arrangements of the partial quotients.

Lemma 4.3.7. Let the product $\cdots \overset{(n)th}{\phi}\ \tau_{a_n+ib_n}\ \overset{(n+1)th}{\phi}\ \tau_{a_{n+1}+ib_{n+1}}\ \overset{(n+2)th}{\phi}\ \tau_{a_{n+2}+ib_{n+2}}\dots$ be factors of T derived from the $NICF$ of a complex number ξ with $a_n, a_{n+1}, a_{n+2} \in \mathbb{Z}, a_n > 0$, $a_{n+1} \leq 0$ and $a_{n+2} > 0$. The factors of A, A^{-1}, B, B^{-1}, C, C^{-1}, E and E^{-1} in Ξ may appear in the given product, while D, D^{-1}, F, F^{-1}, G and G^{-1} do not.

Proof. From Definition 3.4.1 the elements of Ξ are

$$A = \phi\tau_{-i},\ A^{-1} = \tau_i\phi,\ B = \phi\tau_1\phi\tau_{-1},\ B^{-1} = \tau_1\phi\tau_{-1}\phi,\ C = \tau_{1+i}\phi\tau_{-1},\ C^{-1} = \tau_1\phi\tau_{-1-i}$$

$$D = \tau_{1+i}\phi\tau_{-1}\phi\tau_{-i},\ D^{-1} = \tau_i\phi\tau_1\phi\tau_{-1-i},\ E = \tau_{1+i}\phi\tau_{-1+i}\phi,\ E^{-1} = \phi\tau_{1-i}\phi\tau_{-1-i}$$

$$F = \tau_1\phi\tau_{-1-i}\phi\tau_{-i},\ F^{-1} = \tau_i\phi\tau_{1+i}\phi\tau_{-1},\ G = \phi\tau_1\phi\tau_{-1}\phi\tau_{-i},\ G^{-1} = \phi\tau_i\phi\tau_1\phi\tau_{-1}$$

and the identity I.

1. For $\overset{(n+1)th}{\phi}$, the element $A = \phi\tau_{-i}$ is possible if $b_n > 0$ and $A^{-1} = \tau_i\phi$ is possible if $b_{n+1} < 0$.

2. For $\overset{(n)th}{\phi}\ \tau_{a_n+ib_n}\ \overset{(n+1)th}{\phi}\ \tau_{a_{n+1}+ib_{n+1}}\ \overset{(n+2)th}{\phi}$ with $a_{n+1} < 0$, $B^{-1} = \left[\tau_1\left(\overset{(n+1)th}{\phi}\ \tau_{-1}\ \overset{(n+2)th}{\phi}\right)\right]$ or $B = \left[\left(\overset{(n)th}{\phi}\ \tau_1\ \overset{(n+1)th}{\phi}\right)\tau_{-1}\right]$ are both possible for any values of $b_n, b_{n+1} \in \mathbb{Z}$.

3. Otherwise, we consider 4 cases depending on the signs of b_n and b_{n+1}. The remaining possible elliptic factors for $\overset{(n+1)th}{\phi}$ are:
   - For $b_n \leq 0$, $b_{n+1} < 0$ we get $E^{-1} = \left[\left(\overset{(n)th}{\phi}\ \tau_{1-i}\ \overset{(n+1)th}{\phi}\right)\tau_{-1-i}\right]$ as a possible elliptic factor, but $C^{-1} = \left[\tau_1\ \overset{(n+1)th}{\phi}\ \tau_{-1-i}\right]$ may need to be considered instead.
   - For $b_n > 0$, $b_{n+1} < 0$ we get $C^{-1} = \left[\tau_1\ \overset{(n+1)th}{\phi}\ \tau_{-1-i}\right]$ or $C = \left[\tau_{1+i}\ \overset{(n+1)th}{\phi}\ \tau_{-1}\right]$.
   - For $b_n \leq 0$, $b_{n+1} > 0$ no further factors of Ξ are possible.
   - For $b_n > 0$, $b_{n+1} > 0$ we get $E = \left[\tau_{1+i}\left(\overset{(n+1)th}{\phi}\ \tau_{-1+i}\ \overset{(n+2)th}{\phi}\right)\right]$ as a possible elliptic factor, but $C = \left[\tau_{1+i}\ \overset{(n+1)th}{\phi}\ \tau_{-1}\right]$ may need to be considered instead.

4. For $\overset{(n)th}{\phi}\ \tau_{a_n+ib_n}\ \overset{(n+1)th}{\phi}\ \tau_{a_{n+1}+ib_{n+1}}\ \overset{(n+2)th}{\phi}$ with $a_{n+1} = 0$ only $A = \phi\tau_{-i}$ or $A^{-1} = \tau_i\phi$ are possible elliptic factors.

In each case a_n+ib_n and $a_{n+1}+ib_{n+1}$ are adjusted to $(a_n + ib_n)^* = a_n^*+ib_n^*$ and $(a_{n+1} + ib_{n+1})^* = a_{n+1}^* + ib_{n+1}^*$ respectively to accommodate the indicated factor of Ξ. By Theorem 3.4.4, all elements of Ξ preserve ∇. The maps that have appeared as possible elliptic factors are A, A^{-1}, B, B^{-1}, C, C^{-1}, E and E^{-1}. For the remaining elements of Ξ, the maps $D, D^{-1}, E, E^{-1}, F, F^{-1}, G$ and G^{-1} are compositions of the map A, B, C and their inverses:

$$D = CA,\ D^{-1} = A^{-1}C^{-1},\ E = CA^{-1},\ E^{-1} = AC^{-1}$$

$$F = C^{-1}A,\ F^{-1} = A^{-1}C,\ G = BA,\ G^{-1} = A^{-1}B^{-1}.$$

The maps E and E^{-1} are the only elements where the composition results in a composition of 2 'τ' factors that combine as a single factor. They are the only maps of order 2 that permute both 0 and ∞ among the elements of ∇.

The possibility of finding the sequence of factors for maps D, D^{-1}, F, F^{-1}, G and G^{-1} in T is lower than for the other elements of Ξ for the following reasons:

- Each of these maps involve two 'ϕ' factors and three 'τ' factors and the middle 'τ' factor would have to match exactly as no adjustments can be made for this factor.
- The second order maps F, G and their inverses also only permute 0 or ∞, but not both at the same time, unlike E and E^{-1}.

□

Example 4.3.8. The continued fractions for square roots of complex integers not located near the square roots of perfect squares are periodic, but the number of partial quotients in the period increases and the pattern among these terms is less obvious. One of the square roots of $7 + 3i$ is located in the square with vertices 2, $2 + i$, $3 + i$ and 3.[1]

$\sqrt{3+4i} = 2 + i$		$\sqrt{8+6i} = 3 + i$
	$\sqrt{7+3i} \approx 2.7033102\cdots + i0.5548752$ $[3+i, \overline{-1+2i, 2i, -2-3i, -1-3i, 1-i, 5+i}]$	
$\sqrt{4} = 2$		$\sqrt{9} = 3$

In the next example, we show that if there are successive partial quotients with non positive real parts, ξ lies does not always lie in the resulting sequence of nested hyperbolic quadrilaterals when the elliptic maps are factored out.

[1]This example is discussed in Chapter 1 under 1.3 for the method of Schmidt in [40].

Example 4.3.9. For $\sqrt{7+3i} = 2.7033102\cdots + i0.5548752\cdots$, from Schmidt [40, Example 3.2], we get the *NICF*

$$[3+i, \overline{-1+2i, 2i, -2-3i, -1-3i, 1-i, 5+i}]$$

from which we derive the product of parabolic Möbius maps T. To facilitate the process of identifying elements of Ξ in T we have done the following steps:

- Number the ϕ maps, where the 7th ϕ is a repeat of the first ϕ.
- Indicate all minus signs with $\downarrow$.
- Mark with an X all ϕs that cannot belong to an element in Ξ. There is no combination of factors in the elements of Ξ where a ϕ is preceded by τ_{-i} and followed by τ_i which happens in this example for $\overset{6th}{\phi}$.

$$T = \tau_{3+i}\left(\overset{1st}{\phi}\ \overset{\downarrow}{\tau_{-1+2i}}\ \overset{2nd}{\phi}\right)\tau_{2i}\left(\overset{3rd}{\phi}\ \overset{\downarrow\downarrow}{\tau_{-2-3i}}\ \overset{4th}{\phi}\right)\overset{\downarrow\ \downarrow}{\tau_{-1-3i}}\left(\overset{5th}{\phi}\ \overset{\downarrow\ X}{\tau_{1-i}}\ \overset{6th}{\phi}\right)\tau_{5+i}\left(\overset{1st}{\phi}\ \overset{\downarrow}{\tau_{-1+2i}}\ \overset{2nd}{\phi}\right)\tau_{2i}\ \ldots$$

$$= \tau_{2+i}\underbrace{\tau_{1+i}\ \overset{1st}{\phi}\ \tau_{-1}}\tau_i\underbrace{\tau_i\ \overset{2nd}{\phi}}\ \tau_i\underbrace{\tau_i\ \overset{3rd}{\phi}\ \tau_{-i}}\tau_{-2-2i}\underbrace{\overset{4th}{\phi}\ \tau_{-i}}\tau_{-1-2i}\underbrace{\overset{5th}{\phi}\ \tau_{-i}}\tau_1\ \overset{6th}{\phi}\ \tau_4\underbrace{\tau_{1+i}\ \overset{1st}{\phi}\ \tau_{-1}}\tau_i\underbrace{\tau_i\ \overset{2nd}{\phi}}\ \ldots$$

possibly A or A^{-1}

- The combination $\underbrace{\tau_{1+i}\ \overset{1st}{\phi}\ \tau_{-1}}\tau_i\underbrace{\tau_i\ \overset{2nd}{\phi}}$ is equal to $C\ \tau_i\ A^{-1}$, but by inserting ϕ^2, the identity map, we get $\underbrace{\tau_{1+i}\ \overset{1st}{\phi}\ \tau_{-1+i}\ \phi}\left(\phi\ \tau_i\ \overset{2nd}{\phi}\right) = E\ \left(\phi\ \tau_i\ \overset{2nd}{\phi}\right)$, which is nicer, since there is one less factor.
- For $\underbrace{\tau_i\ \overset{3rd}{\phi}\ \tau_{-i}}$ we chose $A^{-1}\ \tau_{-i}$ rather than $\tau_i\ A$. See the geometrical effects that follow.
- Considering the factors $\underbrace{\overset{4th}{\phi}\ \tau_{-i}}\tau_{-1-2i}\underbrace{\overset{5th}{\phi}\ \tau_{-i}}\tau_1\ \overset{6th}{\phi}$:

$\overset{6th}{\phi}$ cannot be part of an element of Ξ, so it must be linked to $\overset{5th}{\phi}$ in the factor $\left(\overset{5th}{\phi}\ \tau_{1-i}\ \overset{6th}{\phi}\right)$ so for $\underbrace{\overset{4th}{\phi}\ \tau_{-i}}\ \tau_{-1-2i}\ \underbrace{\overset{5th}{\phi}\ \tau_{-i}}\ \tau_1\ \overset{6th}{\phi}$ we get $A\ \tau_{-1-2i}\ \underbrace{\overset{5th}{\phi}\ \tau_{-i}}\ \tau_1\ \overset{6th}{\phi}$.

The product of Möbius maps for T becomes:

$$T_M = \tau_2 \, \overline{E \;\; (\phi\tau_i\phi) \;\; \tau_i \; A^{-1} \; \tau_{-3i-2} \; A \; \tau_{-2i-1} \;\; (\phi\tau_{1-i}\phi) \;\; \tau_4}$$

once we have accommodated all the elliptic maps A, A^{-1} and E as they appear.

We note here that the method of dealing with the factor $\underbrace{\tau_i \;\; \overset{3rd}{\phi} \;\; \tau_{-i}}$ remains unclear. We resolve the issue of whether to choose $A^{-1}\,\tau_{-i}$ or $\tau_i\,A$ by looking at the FQs that contain ξ. This issue is not considered as being serious as this particular sequence of maps does not affect our finding the next FQ in the sequence of nested FQs containing ξ.

In the diagrams that follow, ξ is indicated by a $*$. The FQ $T_0(Q\nabla_\infty) = \tau_2(Q\nabla_\infty)$ contains ξ, but the following 4 maps do not yield FQs that contain ξ. We show that each of the maps E, $(\phi\tau_i\phi)$, τ_i and A^{-1} move the images of 0, i and ∞ along the same dual Farey circle. The value ξ lies inside the dual Farey circle, but the FQs

$$\tau_2 E\,(\phi\tau_i\phi)\,(Q\nabla_0), \quad \tau_2 E\,(\phi\tau_i\phi)\,\tau_i(Q\nabla_\infty) \text{ and } \tau_2 E\,(\phi\tau_i\phi)\,\tau_i A^{-1}\tau_{-3i-2}(Q\nabla_\infty)$$

are all outside of this dual Farey circle.

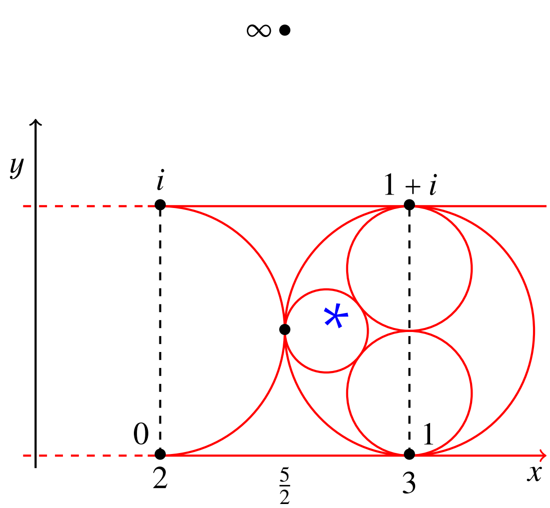

$*$ indicates the target ξ which

is in the $FQ1 = T_0(Q\nabla_\infty) = \tau_2(Q\nabla_\infty)$,

whose vertices are the images

of 0, 1, i and $1 + i$ as indicated.

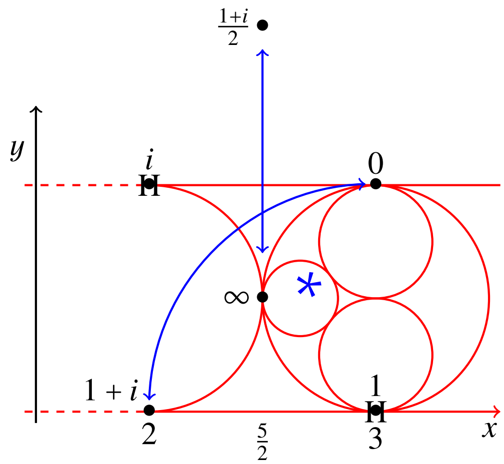

$\tau_2 E$ with $E = \tau_{1+i}\phi\tau_{-1+i}\phi$

$\ast$ indicates the target ξ

{Farey circles - red solid.}

E has swapped the images of vertices 0 with $1+i$ and ∞ with $\dfrac{1+i}{2}$.

Fixed points of E, indicated with **H**, are images of 1 and i at $z = 3$ and $z = 2+i$ respectively.

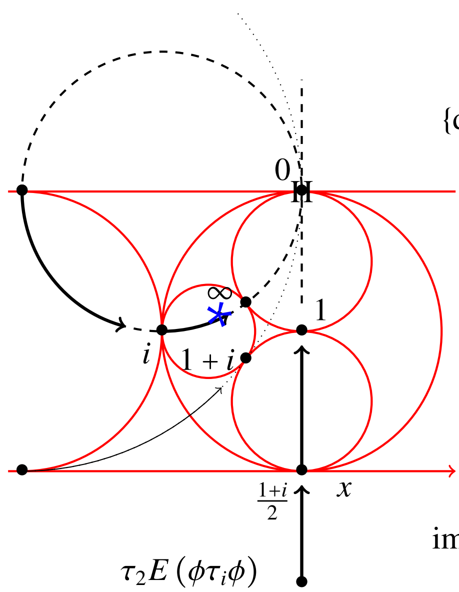

$\tau_2 E\,(\phi\tau_i\phi)$

{dual Farey circles - black dashed.}

The map $\phi\tau_i\phi$ fixes the image of 0 and moves the images of i and ∞ toward image of 0 along a dual Farey circle and the images of 1 and $\frac{1+i}{2}$ toward image of 0 along a dual Farey circle.

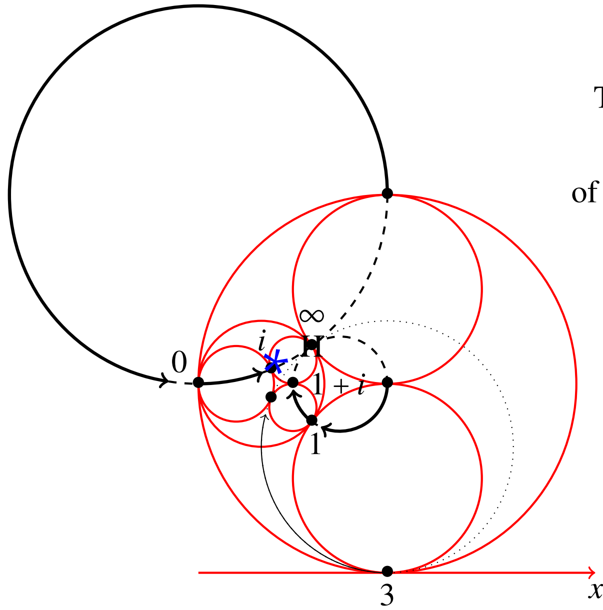

$\tau_2 E\,(\phi\tau_i\phi)\,\tau_i$

The map τ_i fixes the image

of ∞ and moves the images of

i and 0 toward image of ∞

along a dual Farey circle and

1 and $1+i$ toward image of ∞

along another dual Farey circle

The map A^{-1} permutes the images

of ∇. The images of 0, i and ∞

are permuted along a dual Farey circle

and $1+i$, 1 and $\frac{1+i}{2}$

along a Farey circle

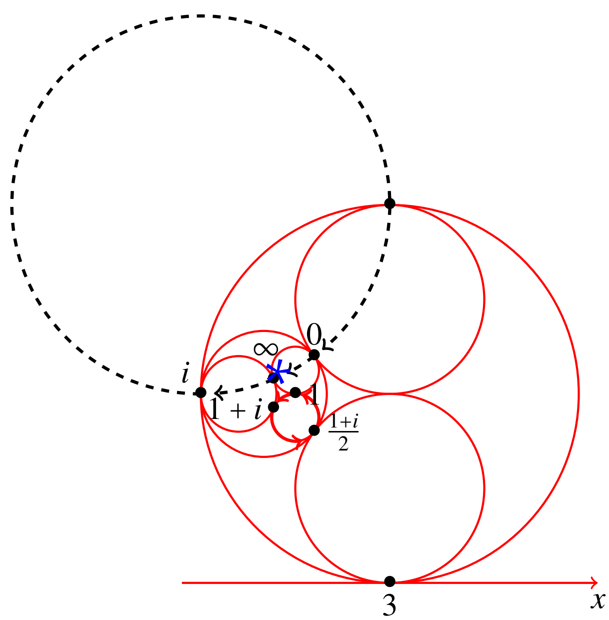

$\tau_2 E\,(\phi\tau_i\phi)\,\tau_i A^{-1}$ with $A^{-1} = \tau_i\phi$

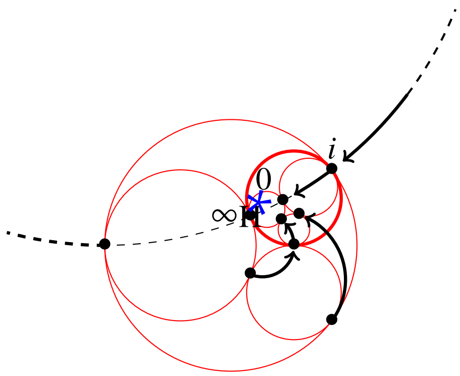

$\tau_2 E\,(\phi\tau_i\phi)\,\tau_i A^{-1}\tau_{-i}$

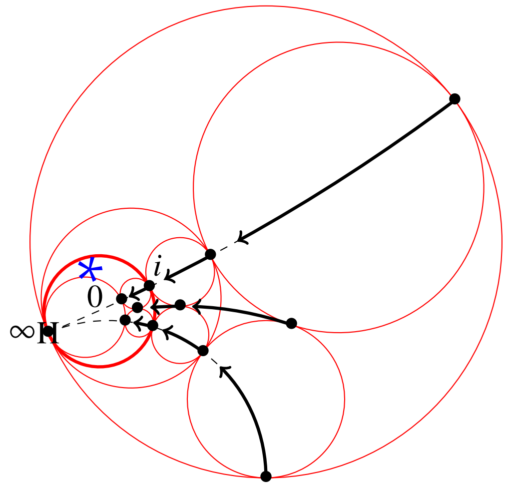

$\tau_2 E\,(\phi\tau_i\phi)\,\tau_i A^{-1}\tau_{-i}\tau_{-2i}$

The effects of τ_{-3i-2} is split over 3 images.

Above and above right: The map

τ_{-3i} moves the images of 0 and i

toward the image of ∞ along a Farey circle

Right: then τ_{-2} moves the images of 0 and i toward the

image of ∞ along a dual Farey circle

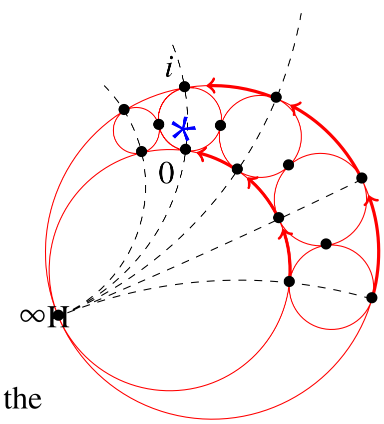

$\tau_2 E\,(\phi\tau_i\phi)\,\tau_i A^{-1}\tau_{-i}\tau_{-2i}\tau_{-2}$

In each of these diagrams, the target ξ lies inside the dual Farey circle while the Farey quadrilaterals found are all outside the circle. This is an indication that the method of identifying elliptic maps need to be adjusted when there are consecutive partial quotients with non-positive real parts.

In order to analyse the case for consecutive partial quotients with non-positive real parts, we modify the adjusted product of Definition 2.5.1 for the complex case as follows:

Definition 4.3.10. Let $a_n^* + ib_n^*$ be the adjusted coefficient of the partial quotient $a_n + ib_n$ after the elliptic factors of ∇ have been accommodated among the factors of T. The adjusted product of T for a $NICF$ is $T_A = t_0^* t_1^* t_2^* \cdots$, where each $t_n^*, n \in \mathbb{N}_0$ is a product of an elliptic map from the set ∇ and a parabolic map $\tau_{b_n^*}$ or $\phi \tau_{b_n^*} \phi$. The partial product is defined as $T_{A(n)} = t_0^* t_1^* t_2^* \cdots t_n^*$

In the following example we show the adjusted product for

$$T_M = \tau_2 \, \overline{E \ (\phi \tau_i \phi) \ \tau_i \ A^{-1} \ \tau_{-3i-2} \ A \ \tau_{-2i-1} \ (\phi \tau_{1-i} \phi) \ \tau_4}$$

found in Example 4.3.9 for $\sqrt{7 + 3i}$.

Example 4.3.11. We compare the product of parabolic Möbius maps to the adjusted product of maps for $\sqrt{7 + 3i}$ in Example 4.3.9.

$$\begin{array}{ccccccccccc} T & = & \tau_{3+i} & (\phi \tau_{-1+2i} \phi) & \tau_{2i} & (\phi \tau_{-2-3i} \phi) & \tau_{-1-3i} & (\phi \tau_{1-i} \phi) & \tau_{5+i} & \cdots \\ T_A & = & t_0^* & t_1^* & t_2^* & t_3^* & t_4^* & t_5^* & t_6^* & \cdots \\ & = & \tau_2 & E \ (\phi \tau_i \phi) & \tau_i & A^{-1} \ \tau_{-2-3i} & A \ \tau_{-1-2i} & (\phi \tau_{1-i} \phi) & \tau_4 & \cdots \end{array}$$

Each b_n in T is adjusted to b_n^* in T_A, depending on the element of Ξ immediately before or after it. All parabolic factors between the maps t_1^* and t_5^* have $Re(b_n^*) \leq 0$ and the only elliptic factors that appear are A and A^{-1}. From the images of Example 4.3.9, $\xi \notin T_{A(1)} \left(Q \nabla_0 \right) = \tau_2 E \ (\phi \tau_i \phi) \left(Q \nabla_0 \right)$ and thereafter the sequence of Farey quadrilaterals

$$T_{A(2)} \left(Q \nabla_\infty \right), \quad T_{A(3)} \left(Q \nabla_\infty \right) \text{ and } T_{A(4)} \left(Q \nabla_\infty \right)$$

do not contain ξ either.

In the following theorem, we show that consecutive partial quotients with non-positive real parts result in images of $Q \nabla_v$, under successive $T_{A(n)}$, that do not contain ξ, where $v = \infty$ or $v = 0$, whichever is the fixed point of the parabolic factor of t_n^*, the last factor of $T_{A(n)}$.

Theorem 4.3.12. Let $\cdots \overset{(n)th}{\phi} \ \tau_{a_n + ib_n} \ \overset{(n+1)th}{\phi} \ \tau_{a_{n+1} + ib_{n+1}} \ \overset{(n+2)th}{\phi} \ \cdots \ \overset{(n+k)th}{\phi} \ \tau_{a_{n+k} + ib_{n+k}} \ \overset{(n+k+1)th}{\phi} \ \ldots$ be factors of T derived from the $NICF$ of a complex number ξ, with $a_n > 0$, $a_{n+r} \leq 0, r =$

$1, \cdots, k-1$ and $a_{n+k} < 0$, all integers. Let $v = \infty$ or $v = 0$, whichever gives the fixed point of the parabolic factor of t_n^*. If $\xi \in T_{A(n)}\left(Q\nabla_v\right)$ and $\xi \notin T_{A(n+1)}\left(Q\nabla_v\right)$ then $\xi \notin T_{A(n+r)}\left(Q\nabla_v\right)$ for any $r = 1, \cdots, k$.

Proof. Consider the product $\cdots \overset{(n+1)th}{\phi} \quad \tau_{a_{n+1}+ib_{n+1}} \quad \overset{(n+2)th}{\phi} \quad \cdots \quad \overset{(n+k)th}{\phi} \quad \tau_{a_{n+k}+ib_{n+k}} \quad \overset{(n+k+1)th}{\phi} \quad \ldots$ with $a_{n+r} \in \mathbb{Z}$, $a_{n+r} \leq 0, r = 1, \cdots, k-1$ and $a_{n+k} < 0$. The only factors contained in this product between $\overset{(n+1)th}{\phi}$ and $\overset{(n+k+1)th}{\phi}$ are ϕ, τ_{-i}, τ_i and τ_{-1}. With $a_{n+k} < 0$, the image of ∇ under $\tau_{a_{n+k}}$ is

$$\tau_{a_{n+k}}\left(\nabla\right) = \tau_{a_{n+k}+1}\tau_{-1}\left(\nabla\right) = \tau_{a_{n+k}+1}\left(\nabla - 1\right)$$

which is an image of $\nabla - 1$. None of the factors present between $\overset{(n+1)th}{\phi}$ and $\overset{(n+k+1)th}{\phi}$ take $\nabla - 1$ back to the position of ∇, since only the maps in Ξ preserve ∇ by Theorem 3.4.4. This results in each $T_{A(n+r)}\left(Q\nabla_v\right)$ being the image of $\nabla - 1$, for $r = 1, \cdots, k$.

The image $T_{A(n+r)}\left(Q\nabla_v\right)$ and the value ξ will lie on opposite sides of the image of the y-axis (the 'circle' through 0, i, and ∞) as the maps $\tau_{\pm i}$, $\phi\tau_{\pm i}\phi$, A and A^{-1} all leave the image of the circle through the images of 0, ∞ and i invariant. □

4.4 The technique of insertion and deletion

The elliptic Möbius maps derived from consecutive parabolic maps with non positive real coefficients do not yield nested Farey quadrilaterals containing the target Ξ. We introduce the technique of insertion and deletion required to compensate for the consecutive negative real coefficients in the next example:

Example 4.4.1. For the product of parabolic Möbius maps

$$T = \tau_{3+i}\,\overline{\left(\phi\tau_{-1+2i}\phi\right)\ \tau_{2i}\ \left(\phi\tau_{-2-3i}\phi\right)\ \tau_{-1-3i}\ \left(\phi\tau_{1-i}\phi\right)\ \tau_{5+i}}$$

of $\sqrt{7+3i}$, we focus on the non positive real parts of the consecutive parabolic factors

$$\left(\overset{1st}{\phi}\ \tau_{-1+2i}\ \overset{2nd}{\phi}\right)\ \tau_{2i}\ \left(\overset{3rd}{\phi}\ \tau_{-2-3i}\ \overset{4th}{\phi}\right)\ \tau_{-1-3i}.$$

starting at the right

$$\tau_{3+i}\left(\overset{1st}{\phi}\ \tau_{-1+2i}\ \overset{2nd}{\phi}\right)\ \tau_{2i}\ \left(\overset{3rd}{\phi}\ \tau_{-2-3i}\ \overset{4th}{\phi}\right)\ \overset{\downarrow}{\tau_{-1-3i}}$$

$$= \tau_{3+i}\ \ \phi\tau_{-1+2i}\phi\ \ \tau_{2i}\ \ \phi\tau_{-2-3i}\ \underbrace{\overset{4th}{\phi}\ \ \tau_{-1-3i}}$$

$$\tau_{-1} \nearrow \tau_1 \nearrow$$

The combination $\overset{4th}{\phi}\ \ \tau_{-1-3i}$ needs a τ_1 in front of it to get $C^{-1} = \tau_1\phi\tau_{-1-i}$.

We insert τ_{-1} in front of τ_{-2-3i} to cancel the τ_1.

With 'inserted' and 'deleted' factors underlined we get:

$$\tau_{3+i}\ \phi\tau_{-1+2i}\phi\ \ \tau_{2i}\ \ \overset{3rd}{\phi}\ \tau_{\underline{-1}}\ \tau_{-2-3i}\ \tau_{\underline{1}}\ \ \overset{4th}{\phi}\ \ \tau_{-1-3i}$$

$$= \tau_{3+i}\ \ \phi\tau_{-1+2i}\phi\ \tau_{2i}\ \ \underbrace{\overset{3rd}{\phi}\ \tau_{\underline{-1}-i}}\ \tau_{-2-2i}\ \tau_{\underline{1}}\ \phi\ \tau_{-1-3i}$$

$$\tau_{-1} \nearrow$$

$$\tau_1 \nearrow$$

The combination $\overset{3rd}{\phi}\ \ \tau_{-1-i}$ needs a τ_1 in front of it to get $C^{-1} = \tau_1\phi\tau_{-1-i}$.

We insert τ_{-1} in front of τ_{2i} to cancel the τ_1.

With 'inserted' and 'deleted' factors underlined we get:

$$\tau_{3+i}\ \phi\tau_{-1+2i}\ \overset{2nd}{\phi}\ \ \tau_{\underline{-1}}\tau_{2i}\ \tau_{\underline{1}}\ \ \overset{3rd}{\phi}\ \ \tau_{\underline{-1}-i}\ \tau_{-2-2i}\ \tau_{\underline{1}}\ \ \overset{4th}{\phi}\ \ \tau_{-1-3i}$$

$$= \tau_{3+i}\ \phi\tau_{-1+2i}\ \underbrace{\overset{2nd}{\phi}\ \ \tau_{\underline{-1}}}\tau_{2i}\ \tau_{\underline{1}}\ \phi\tau_{\underline{-1}-i}\ \tau_{-2-2i}\ \tau_{\underline{1}}\ \phi\ \tau_{-1-3i}$$

$$\tau_{-1} \nearrow$$

$$\tau_1 \nearrow$$

The combination $\overset{2nd}{\phi}\ \ \tau_{-1}$ needs a τ_{1+i} in front of it to get $C = \tau_{1+i}\phi\tau_{-1}$, but τ_i already present,

so we put a τ_1 after τ_{-1+2i} and a τ_{-1} in front of τ_{-1+2i} to cancel the τ_1.

Thus, with 'inserted' and 'deleted' factors underlined we get:

$$\tau_2\ \tau_{1+i}\ \phi\ \tau_{\underline{-1}}\ \tau_{-1+i}\ \tau_i\ \tau_{\underline{1}}\ \ \overset{2nd}{\phi}\ \ \tau_{\underline{-1}}\tau_{2i}\ \tau_{\underline{1}}\ \ \overset{3rd}{\phi}\ \tau_{\underline{-1}-i}\ \tau_{-2-2i}\ \tau_{\underline{1}}\ \ \overset{4th}{\phi}\ \ \tau_{-1-3i}$$

which becomes:

$$\tau_2\left[\tau_{1+i}\phi\ \tau_{\underline{-1}}\right]\tau_{-1+i}\ \left[\tau_{\underline{1}+i}\phi\ \tau_{\underline{-1}}\right]\ \tau_{2i}\left[\tau_{\underline{1}}\ \phi\tau_{\underline{-1}-i}\right]\ \tau_{-2-2i}\ \left[\tau_{\underline{1}}\ \phi\ \tau_{-1-i}\right]\tau_{-2i}$$

so the product:

$$T = \tau_{3+i}\ \overline{\left(\phi\tau_{-1+2i}\phi\right)\ \tau_{2i}\ \left(\phi\tau_{-2-3i}\phi\right)\ \tau_{-1-3i}\ \left(\phi\tau_{1-i}\phi\right)\ \tau_{5+i}}$$

becomes:

$$T = \tau_2 \overline{\left[\tau_{1+i}\phi\tau_{\underline{-1}}\right] \tau_{-1+i} \left[\tau_{\underline{1}+i}\phi\tau_{\underline{-1}}\right] \tau_{2i} \left[\tau_{\underline{1}}\phi\tau_{\underline{-1}-i}\right] \tau_{-2-2i} \left[\tau_{\underline{1}}\phi\tau_{-1-i}\right] \tau_{-2i} \left(\phi\tau_{1-i}\phi\right) \tau_4}.$$

The factorisation $\tau_2 \overline{E \ (\phi\tau_i\phi) \ \tau_i \, A^{-1} \, \tau_{-3i-2} \, A \, \tau_{-2i-1} \ (\phi\tau_{1-i}\phi) \ \tau_4}$ found by just identifying and isolating elliptic maps now changes to the product of Möbius maps

$$T_M = \tau_2 \overline{C \, \tau_{-1+i} \, C \, \tau_{2i} \, C^{-1} \, \tau_{-2-2i} \, C^{-1} \, \tau_{-2i} \left(\phi\tau_{1-i}\phi\right) \tau_4}.$$

when taking into account the consecutive non-positive real coefficients in the product of parabolic Möbius maps derived from the $NICF$.

We show the progression of FQs under the partial Möbius products $T_{M(k)}$ for $k \in \mathbb{N}$, where k represents the number of factors of the product of Möbius factors present in the partial product $T_{M(k)}$.

1) For $T_{M(1)} = \tau_2$:
$FQ1$ for $\xi = \sqrt{7+3i}$ is the shaded quadrilateral $T_{M(1)}\left(Q\nabla_\infty\right)$ shown alongside. The target ξ, marked by an 'X' in a box, appears close to the dual Farey circle through the images of $\dfrac{1+i}{2}$, i and $1+i$.

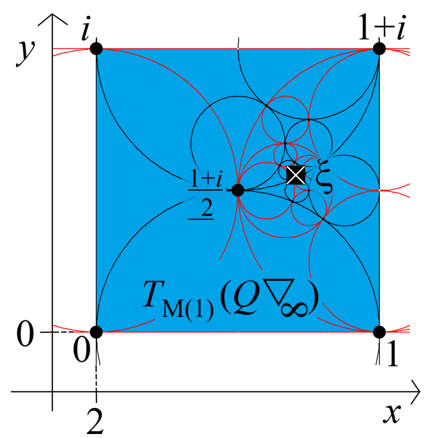

2) Below left: For $T_{M(2)} = \tau_2 C$: The map C permutes the vertices of ∇ via the permutation $\left(\begin{array}{ccc} 0 & i & \frac{1+i}{2} \end{array}\right)\left(\begin{array}{ccc} 1+i & 1 & \infty \end{array}\right)$:

The map C has permuted the vertices 0, i and $\frac{1+i}{2}$, whose images lie on a Farey circle shown, and $1+i$, 1 and ∞ whose images lie on the dual Farey circle with $x = 3$. The image of ∞ under C is $1 + i$.

The next map is τ_{-1+i} so we change our focus to $T_{M(2)}\left(Q\nabla_\infty\right)$, which is bounded by 2 Farey circles and 2 dual Farey circles passing through $T_{M(2)}\left(\infty\right)$ and the images of 2 distinct elements of ∇_∞, as shown. The image of 1 is at ∞.

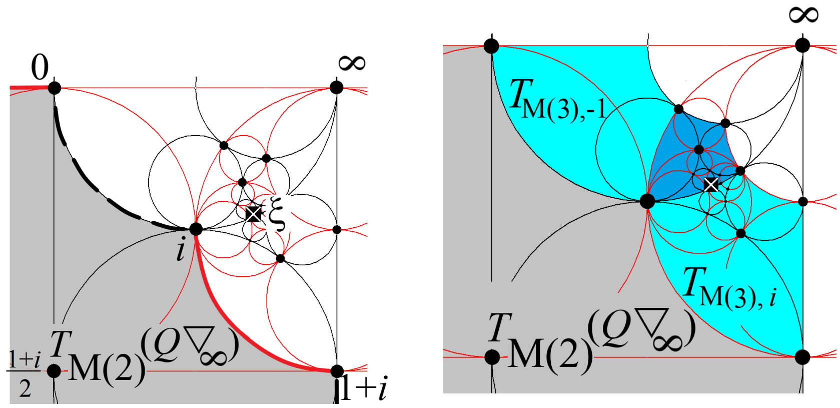

3) Above right:

For $T_{M(3)} = \tau_2\, C\, \tau_{-1+i}$:

We show the intermediate images $T_{M(3),k}\left(Q\nabla_\infty\right)$ for $k = -1$ and $k = i$.

4) $T_{M(3)}\left(Q\nabla_\infty\right)$, shown alongside, is $FQ2$ for $\xi = \sqrt{7+3i}$. The target ξ appears closest to the image of $1 + i$.

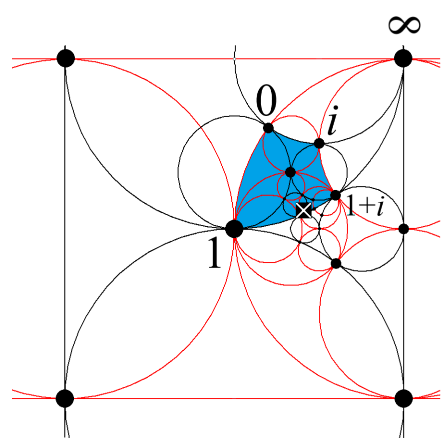

5) For $T_{M(4)} = \tau_2\, C\, \tau_{-1+i}\, C$:

The map C permutes the vertices of ∇, so the target ξ appears closest to the image of ∞. We change our focus to $T_{M(4)}\,(Q\nabla_\infty)$, which is bounded by 2 Farey circles and 2 dual Farey circles passing through $T_{M(4)}\,(\infty)$ and the images of 2 distinct elements of ∇_∞, as shown alongside.

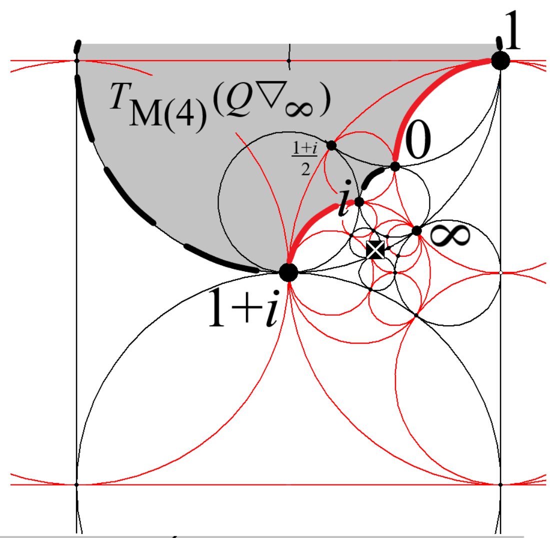

6) For

$T_{M(5)} = \tau_2\, C\, \tau_{-1+i}\, C\, \tau_{2i}$:

We show the intermediate image $T_{M(5),i}\,(Q\nabla_\infty)$. The images of 0, 1, i and $1+i$ have moved toward the image of ∞ along dual Farey circles through $T_{M(5)}\,(\infty)$.

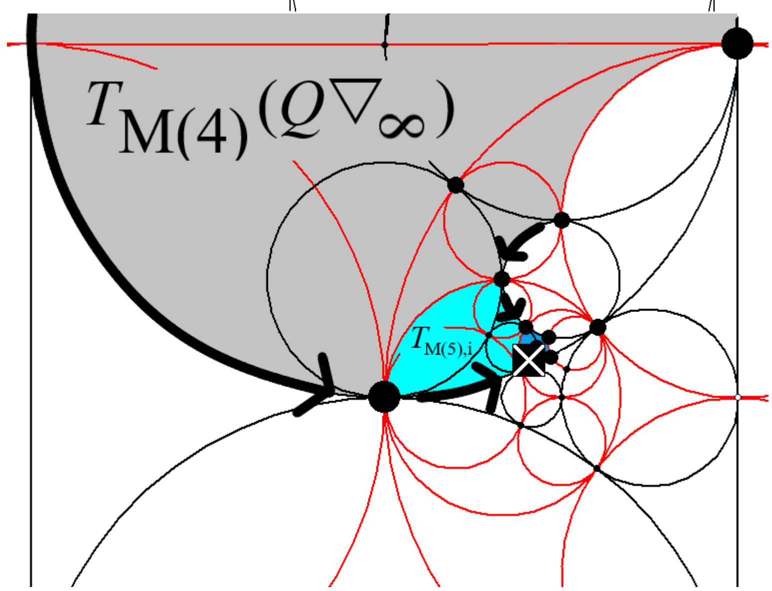

7) We now see $T_{M(5)}\,(Q\nabla_\infty)$ enlarged. $T_{M(5)}\,(Q\nabla_\infty)$ is $FQ3$ for $\xi = \sqrt{7+3i}$. The image $T_{M(5)}(1)$ is the one closest to ξ.

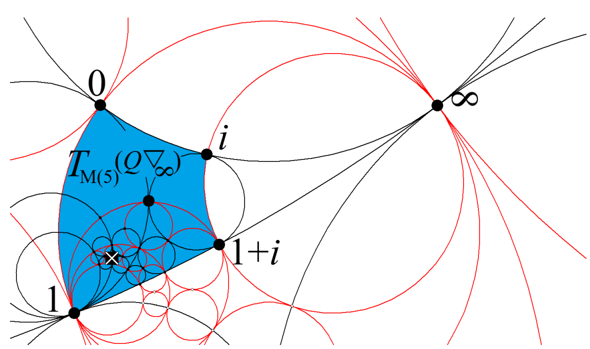

8) For $T_{M(6)} = T_{M(5)}\ C^{-1}$ and $T_{M(7)} = T_{M(6)}\ \tau_{-2-2i}$:

C^{-1} permutes the vertices of ∇ with $C^{-1}(\infty) = 1$, so the image of ∞ becomes the fixed point in the progression from $T_{M(6)}$ to $T_{M(7)}$. The intermediate images $T_{M(7),k}\,(Q\nabla_\infty)$ shown leading to $T_{M(7)}\,(Q\nabla_\infty)$ link to $-2-2i$.

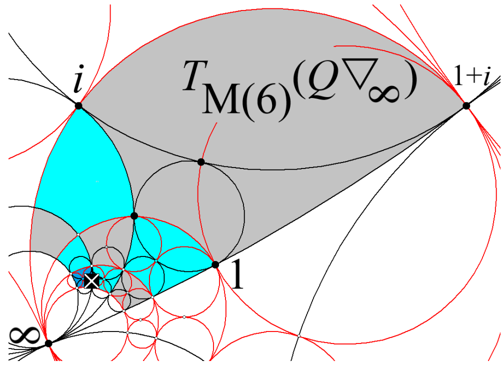

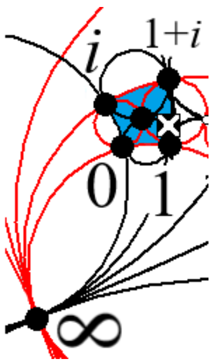

9) $T_{M(7)}\,(Q\nabla_\infty)$ is $FQ4$ for $\xi = \sqrt{7+3i}$. The target ξ now appears closest to image of 1.

10) On the right:

For $T_{M(8)} = T_{M(7)}\ C^{-1}$:

The map C^{-1} permutes the vertices of ∇ with $C^{-1}(\infty) = 1$. Now ξ is closest to the image $T_{M(8)}(\infty)$. Accordingly, we change our focus to the image of $Q\nabla_\infty$ as shown.

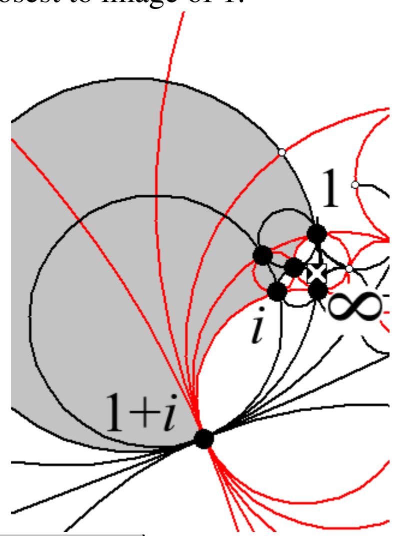

11) For $T_{M(9)} = T_{M(8)}\tau_{-2i}$:

The image of ∞ is fixed in the progression from $T_{M(8)}$ to $T_{M(9)}$. We show the single intermediate image $T_{M(9),-i}\,(Q\nabla_\infty)$ leading to $T_{M(9)}\,(Q\nabla_\infty)$, which is $FQ5$ for $\xi = \sqrt{7+3i}$.

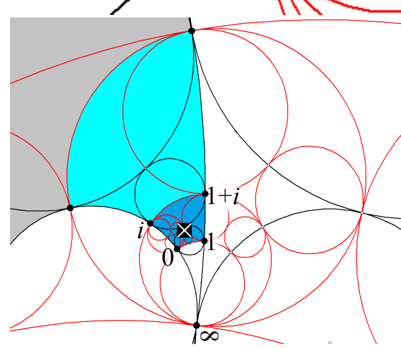

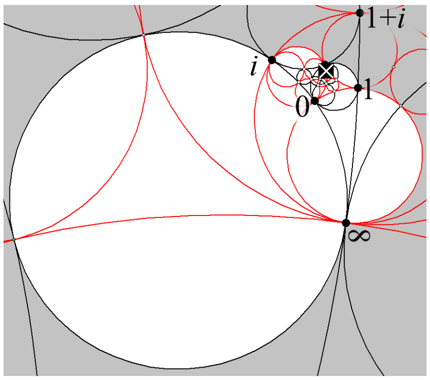

12) On the left: We change our focus to $T_{M(9)}(Q\nabla_0)$.

13) On the right: $T_{M(10)} = T_{M(9)}(\phi\tau_{-1-i}\phi)$. The intermediate images leading to $T_{M(10)}(Q\nabla_\infty)$, which is $FQ6$ for $\xi = \sqrt{7+3i}$

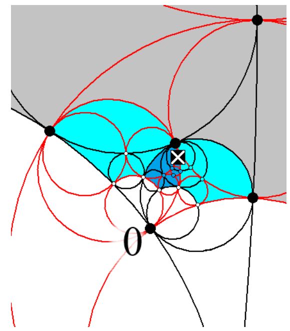

14) For $T_{M(11)} = T_{M(10)}\tau_4$: The image of ∞ is fixed in the progression from $T_{M(10)}$ to $T_{M(11)}$. We show the intermediate images $T_{M(10),k}(Q\nabla_\infty)$ for $k = 1,2,3$ between $T_{M(10)}(Q\nabla_\infty)$ and $T_{M(11)}(Q\nabla_\infty)$.

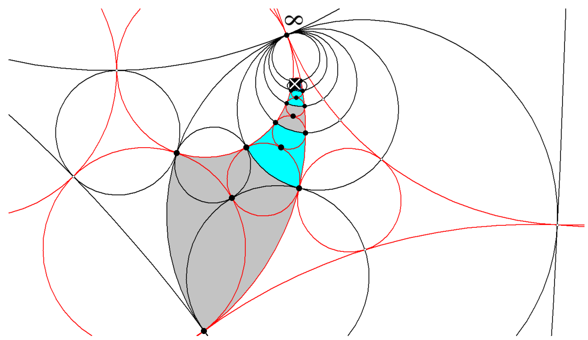

15) Enlarging, we now have $T_{M(10)}(Q\nabla_\infty)$, which is $FQ6$ for $\xi = \sqrt{7+3i}$. The target ξ lies in the same place as in step 1 of this example in terms of the configuration of Farey and dual Farey circles through the images of the vertices of ∇, as it is near the arc of the dual Farey circle between $1+i$ and $\frac{1+i}{2}$.

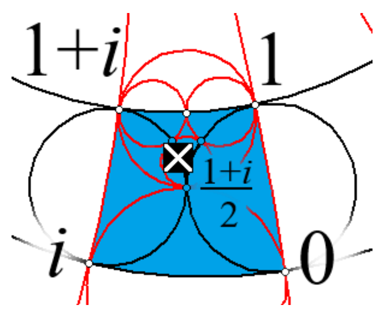

Finally, we show the comparison between T and T_A for $\sqrt{7+3i}$ to emphasize the change from the b_n of the $NICF$ to the adjusted coefficients b_n^* due to the accommodation of the elliptic maps.

$$
\begin{array}{lllllllll}
T & = & \tau_{3+i} & (\phi\tau_{-1+2i}\phi) & \tau_{2i} & (\phi\tau_{-2-3i}\phi) & \tau_{-1-3i} & (\phi\tau_{1-i}\phi) & \tau_{5+i} \quad \cdots \\
T_A & = & \tau_2 & C\,\tau_{-1+i} & C\,\tau_{2i} & C^{-1}\,\tau_{-2-2i} & C^{-1}\,\tau_{-2i} & (\phi\tau_{1-i}\phi) & \tau_4 \quad \cdots
\end{array}
$$

4.4.1 Steps in the insertion and deletion technique

The insertion and deletion technique used in Example 4.4.1 is summarised in the following theorem.

Theorem 4.4.2. For any product of $r+2$ consecutive '$\phi\tau_{b_k}$' factors

$$\overset{(n-r-1)th}{\phi} \quad \ldots \tau_{b_{n-r-1}} \quad \overset{(n-r)th}{\phi} \quad \tau_{b_{n-r}} \quad \overset{(n-r+1)th}{\phi} \quad \tau_{b_{n-r+1}} \quad \overset{(n-r+2)th}{\phi} \quad \cdots \overset{nth}{\phi}\ \tau_{b_n} \quad \overset{(n+1)th}{\phi} \quad \tau_{b_{n+1}} \ldots$$

with $Re\,(b_k) \le 0$ for $n-r \le k \le n, k \in \mathbb{N}$, $Re\,(b_{n-r-1}) > 0$ and $Re\,(b_{n+1}) > 0$, it is possible to accommodate each ϕ, in either the element C or C^{-1} in Ξ.

Proof. In the given product, we start with the last factor, $\overset{nth}{\phi}\ \tau_{b_n}$, that has a non-positive real part. Let $k = n$:

(a) Let $p + qi = b_k$

(b) If $p \le -1, q \le -1$ we put τ_1 in front of $\overset{kth}{\phi}\ \tau_{b_k}$ and we put τ_{-1} in front of $\tau_{b_{k-1}}$ to delete the effect of inserting τ_1 in the first place, to get:

$$\tau_{-1}\tau_{b_{k-1}}\tau_1 \overset{kth}{\phi}\ \tau_{b_k} = \tau_{-1}\tau_{b_{k-1}}\left[\tau_1 \overset{kth}{\phi}\ \tau_{-1-i}\right]\tau_{b_k+1+i} = \tau_{-1}\tau_{b_{k-1}}C^{-1}\tau_{b_k+1+i}.$$

The adjusted coefficient for b_k becomes $b_k^* = b_k + 1 + i$ and we set $p + qi = b_{k-1} - 1$ for the next iteration.

(c) If $p \le -1, q \ge 0$:

- For $Im(b_{k-1}) = 0$: put τ_{1+i} in front of $\overset{kth}{\phi}\ \tau_{b_k}$ and we put τ_{-1-i} in front of $\tau_{b_{k-1}}$ to delete the effect of inserting τ_{1+i} in the first place, to get

$$\tau_{-1-i}\tau_{b_{k-1}}\tau_{1+i} \overset{kth}{\phi}\ \tau_{b_k} = \tau_{-1-i}\tau_{b_{k-1}}\left[\tau_{1+i} \overset{kth}{\phi}\ \tau_{-1}\right]\tau_{b_k+1} = \tau_{-1-i}\tau_{b_{k-1}}C\tau_{b_k+1}.$$

The adjusted coefficient for b_k becomes $b_k^* = b_k + 1$ and we set $p + qi = b_{k-1} - 1 - i$ for the next iteration.

- For $Im(b_{k-1}) > 0$: put τ_1 and a τ_i from $\tau_{b_{k-1}}$ in front of $\overset{kth}{\phi}\,\tau_{b_k}$ and put τ_{-1} in front of $\tau_{b_{k-1}-i}$ to delete the effect of inserting τ_1 in the first place, to get

$$\tau_{-1}\tau_{b_{k-1}-i}\tau_{1+i}\overset{kth}{\phi}\,\tau_{b_k} = \tau_{-1}\tau_{b_{k-1}-i}\left[\tau_{1+i}\overset{kth}{\phi}\,\tau_{-1}\right]\tau_{b_k+1} = \tau_{-1}\tau_{b_{k-1}-i}C\tau_{b_k+1}$$

The adjusted coefficient for b_k becomes $b_k^* = b_k + 1$ and we set $p + qi = b_{k-1} - 1 - i$ for the next iteration.

- Finally, if none of the above options yield a quadrilateral that contains ξ, one may need to consider the presence of

$$B = \tau_1\phi\tau_{-1}\phi,\ B^{-1} = \phi\tau_1\phi\tau_{-1},\ E = \tau_{1+i}\phi\tau_{-1+i}\phi \text{ or } E^{-1} = \phi\tau_{1-i}\phi\tau_{-1-i}$$

and find the value of b_k^* and $p = qi$ for the next iteration accordingly.

Now we put $\tau_{b_{k-2}}\overset{(k-1)th}{\phi}$ in front of the new product acquired involving $\overset{(k)th}{\phi}$ in steps (b) or (c). We repeat the procedure through steps (b) and (c), using the $p+qi$ found in (b) or (c) for the next iteration. Continue in this way from $k = n-1$ to $k = n-r, k \in \mathbb{Z}$, All ϕ maps from $\overset{(n-r)th}{\phi}$ to $\overset{(n)th}{\phi}$ must be incorporated in either the element C or C^{-1} in Ξ and all coefficients of parabolic maps between $\overset{(n-r)th}{\phi}$ to $\overset{(n)th}{\phi}$ must be adjusted accordingly. In the final step a '1' from b_{n-r-1} becomes the '1' in C or C^{-1} involving $\overset{(n-r)th}{\phi}$. The partial quotient b_{n-r-1} cannot be finalised at this stage. The adjusted coefficient b^*_{n-r-1} can only be determined once all elliptic factors before $\tau_{b_{n-r-1}}$ have been established. □

This theorem exhausts all known possible combinations of partial quotients that occur in the parts of the products where successive partial quotients have non-positive real parts.

4.4.2 Steps for converting a product of parabolic Möbius maps into a product of Möbius maps

There are 3 initial steps before analysing a product of parabolic Möbius maps derived from the $NICF$ of a complex number:

1. Remove all brackets, locate all negative real and imaginary coefficients and identify the ϕ maps with a negative coefficient for i before ϕ and a positive coefficient for i after ϕ. [These ϕ maps cannot be incorporated into an element of Ξ as there is no map in Ξ that has this combination of factors. These ϕs must be either the first or the second ϕ of the parabolic Möbius map $\phi\tau_{b_n}\phi$.]

2. Link ϕ maps with a τ_i before it or a τ_{-i} after it or both with an 'underbrace'.

3. Locate all consecutive factors where the real part of the partial quotient is non-positive. Starting from the right hand side of this product, incorporate each ϕ map in an element of Ξ using insertion and deletion techniques.

Once these steps are finalised, start from the left of the whole original product identifying and isolating all possible elements of Ξ in the remaining factors not dealt with in step 3. No ϕ can be a factor on its own as it is neither a parabolic Möbius map nor an elliptic Möbius map that leaves ∇ invariant.

The product of Möbius maps that result from this analytic process are used to generate a sequence of nested Farey quadrilaterals that contain the target ξ.

For Examples 4.3.2 for $\sqrt{4+4i}$, 4.3.5 for $\sqrt{3+3i}$ and 4.4.1 for $\sqrt{7+3i}$ we have used Excel to compute the values of the images of ∇, and Wingeom to sketch the images of the vertices in ∇ along with the Farey and dual Farey circles, to confirm that ξ lies inside the Farey quadrilaterals indicated. Geometrical analysis has guided the process of identifying and isolating elliptic Möbius maps from the product of parabolic Möbius maps derived from the $NICF$ of a quadratic irrational when its continued fraction is periodic.

For complex numbers whose square roots yield periodic $NICF$s, we can state the following theorem:

Theorem 4.4.3. Let ξ be the square root of a complex number where the $NICF$ of ξ is periodic. The periodic product of parabolic Möbius maps T derived from periodic $NICF$s can be factorised into parabolic and elliptic Möbius maps such that, for all $n \in \mathbb{N}_0$:

(a) $T_{M(n)}\left(Q\nabla_v\right)$ contains the target for $v = \infty$ if $t_{m(n)}$ is a parabolic Möbius map that fixes ∞ and $v = 0$ if $t_{m(n)}$ is a parabolic Möbius map that fixes 0.

(b) $T_{M(n-1)}(\nabla) = T_{M(n)}(\nabla)$ if $t_{m(n)} \in \Xi$.

In terms of the adjusted product T_A the statement becomes: Let $v = \infty$ or $v = 0$, whichever is the fixed point of the parabolic factor of t_n^* in $T_{A(n)}$, then $\xi \in T_{A(n)}\left(Q\nabla_v\right)$ for all $n \in \mathbb{N}_0$.

Proof. Each product of parabolic Möbius maps T derived from a periodic $NICF$ has either

- no elliptic factors,
- distinct elliptic factors interspersed among the parabolic factors, or
- it has merged elliptic factors as well as distinct elliptic factors interspersed among the parabolic factors.

Once the type of $NICF$ has been identified we follow the appropriate steps for the type as follows:

(a) For no elliptic factors: leave the factors as they are, but rename T_n as $T_{M(n)}$ to indicate that it is in fact a product of Möbius maps that has no elliptic factors. Theorem 3.3.5 gives the number of intermediate Farey quadrilaterals between the the images of $Q\nabla_v$ under $T_{M(n)}$ and $T_{M(n+1)}$ as required. Also, $T_A = T$ in this case as $b_n^* = b_n$ for all $n \in \mathbb{N}_0$.

(b) For distinct elliptic factors: Make sure there are no consecutive factors with negative real parts in their coefficients, otherwise we generate Farey quadrilaterals that do not contain ξ by Theorem 4.3.12. Then, identify and isolate all elliptic factors in the product using Lemma 4.3.7. One may need to insert ϕ^2 to separate an element in Ξ from the parabolic map $\phi\tau_{b_n}\phi$.

(c) For merged elliptic factors: Identify all consecutive factors with negative real parts in their coefficients and use "insertion and deletion techniques" outlined in Theorem 4.4.2 to incorporate each ϕ among the consecutive factors into the elements C or C^{-1} of Ξ as required.

For (b) and (c) rename T_n as $T_{M(n)}$ and rename the individual factors using Definition 4.3.1. The product T_A is then generated by combining each elliptic map with the parabolic map that follows immediately after it, as in Definition 4.3.10.
Trace the Farey quadrilaterals to confirm the final rearrangement of maps yields a sequence of nested Farey quadrilaterals each time $t_{M(n)}$ is a parabolic Möbius map. Each period in T yields an identical product of Mobius maps. The geometric confirmation used in the first period of T of the product is easily repeated for the rest of the factors in $T_{M(n)}$. $\square$

4.4.3 An example involving 'e'

The example that follows concerns vertex e^i on the unit circle. Hensley mentioned the continued fraction for e^i on p71 in [17]. Its continued fraction exhibits a pattern from the fourth partial quotient. The pattern is "pseudo-periodic" as there is a pattern from one period to the next. Each period is identical, except that one of the factors in each period has a coefficient that increments to the next odd number for each successive period.

Example 4.4.4. The number $e^i = \cos 1 + i \sin 1 \approx 0.5403023059... + i\, 0.8414709848...$ has $NICF$

$$[1+i, -2+i, 1+3i, -2, -5i, 2, 7i, -2, -9i, 2, 11i \cdots].$$

We write this in terms of parabolic Möbius maps as

$$T = \tau_{1+i}\,(\phi\tau_{-2+i}\phi)\,\tau_{1+3i}\,(\phi\tau_{-2}\phi)\,\tau_{-5i}\,(\phi\tau_{2}\phi)\,\tau_{7i}\,(\phi\tau_{-2}\phi)\,\tau_{-9i}\,(\phi\tau_{2}\phi)\,\tau_{11i}\,(\phi\tau_{-2}\phi)\,\tau_{-13i}\cdots.$$

Following the steps outlined in Section 4.4.2:
Step 1: Remove brackets, locate all negatives coefficients and mark $\tau_{-i}\phi\tau_i$s with an 'X'.

$$\tau_{1+i}\ \overset{1st}{\phi}\ \overset{\overline{\Downarrow}}{\tau_{-2+i}}\ \overset{2nd}{\phi}\ \tau_{1+3i}\ \overset{3rd}{\phi}\ \overset{\overline{\Downarrow}}{\tau_{-2}}\ \overset{4th}{\phi}\ \overset{\overline{\Downarrow}}{\tau_{-5i}}\ \overset{X}{\overset{5th}{\phi}}\ \tau_2\ \overset{X}{\overset{6th}{\phi}}\ \tau_{7i}\ \overset{3rd}{\phi}\ \overset{\overline{\Downarrow}}{\tau_{-2}}\ \overset{4th}{\phi}\ \overset{\overline{\Downarrow}}{\tau_{-9i}}\ \overset{X}{\overset{5th}{\phi}}\ \tau_2\ \overset{X}{\overset{6th}{\phi}}\ \tau_{11i}\ \overset{3rd}{\phi}\ \overset{\overline{\Downarrow}}{\tau_{-2}}\ \overset{4th}{\phi}\ \cdots$$

The combination $\tau_{-i}\ \overset{5th}{\phi}\ \tau_2\ \overset{6th}{\phi}\ \tau_i$ cannot be found in any element of Ξ so we mark both of these ϕ maps with an 'X'.

Step 2: Link ϕ maps with a τ_i before it or a τ_{-i} after it or both with an 'underbrace'.

$$\tau_1 \underbrace{\tau_i \overset{1st}{\phi}} \overset{\bar{\Downarrow}}{\tau_{-2}} \underbrace{\tau_i \overset{2nd}{\phi}} \tau_{1+2i} \underbrace{\tau_i \overset{3rd}{\phi}} \overset{\bar{\Downarrow}}{\tau_{-2}} \underbrace{\overset{4th}{\phi} \overset{\bar{\Downarrow}}{\tau_{-i}}} \overset{\bar{\Downarrow}}{\tau_{-4i}} \overset{\overset{X}{5th}}{\phi} \tau_2 \overset{\overset{X}{6th}}{\phi} \tau_{6i} \underbrace{\tau_i \overset{3rd}{\phi}} \overset{\bar{\Downarrow}}{\tau_{-2}} \underbrace{\overset{4th}{\phi} \overset{\bar{\Downarrow}}{\tau_{-i}}} \overset{\bar{\Downarrow}}{\tau_{-8i}} \overset{\overset{X}{5th}}{\phi} \tau_2 \overset{\overset{X}{6th}}{\phi} \tau_{10i} \underbrace{\tau_i \overset{3rd}{\phi}} \cdots$$

The combinations $\tau_i\phi$ and $\phi\tau_{-1}$, at the very least, give A^{-1} and A. We look at other factors to decide if other elements of Ξ could be considered later.

Step 3: Locate all consecutive factors where real part of partial quotient is non-positive.

$$\tau_1 \underbrace{\tau_i \overset{1st}{\phi}} \overset{\bar{\Downarrow}}{\tau_{-2}} \underbrace{\tau_i \overset{2nd}{\phi}} \tau_{1+2i} \underbrace{\tau_i \overset{3rd}{\phi}} \overset{\bar{\Downarrow}}{\tau_{-2}} \underbrace{\overset{4th}{\phi} \overset{\bar{\Downarrow}}{\tau_{-i}}} \overset{\bar{\Downarrow}}{\tau_{-4i}} \overset{\overset{X}{5th}}{\phi} \tau_2 \overset{\overset{X}{6th}}{\phi} \underbrace{\tau_{6i} \underbrace{\tau_i \overset{3rd}{\phi}} \overset{\bar{\Downarrow}}{\tau_{-2}}}_{\text{non-positive reals}} \underbrace{\overset{4th}{\phi} \overset{\bar{\Downarrow}}{\tau_{-i}}} \overset{\bar{\Downarrow}}{\tau_{-8i}} \overset{\overset{X}{5th}}{\phi} \tau_2 \overset{\overset{X}{6th}}{\phi} \tau_{10i} \underbrace{\tau_i \overset{3rd}{\phi}} \cdots$$

Starting from the right hand side of the product with non-positive reals, by incorporating each ϕ map in an element of Ξ using insertion and deletion techniques:

We consider $\tau_2 \overset{\overset{X}{6th}}{\phi} \underbrace{\tau_{6i} \underbrace{\tau_i \overset{3rd}{\phi}} \overset{\bar{\Downarrow}}{\tau_{-2}}}$ which ends with the last negative real coefficient and starts with the first positive real coefficient before it.

For the factors $\underbrace{\tau_{6i} \underbrace{\tau_i \overset{3rd}{\phi}} \tau_{-1}\tau_{-1}}$, we need to insert a τ_1 in front of $\tau_i \overset{3rd}{\phi} \tau_{-1}$ to get $C = \tau_{1+i}\phi\tau_{-1}$, using the τ_i that is present. We then put a τ_{-1} in front of τ_{6i} to cancel the τ_1 we inserted. Underlining the inserted and deleted parts, we get

$$\tau_2 \overset{\overset{X}{6th}}{\phi} \tau_{\underline{-1}}\tau_{6i} \left[\underbrace{\tau_{\underline{1}+i} \overset{3rd}{\phi}} \tau_{-1} \right] \tau_{-1} = \tau_2 \overset{\overset{X}{6th}}{\phi} \tau_{\underline{-1}}\tau_{6i} C \tau_{-1}.$$

The $\tau_{\underline{-1}}$ inserted after $\overset{\overset{X}{6th}}{\phi}$ needs to be accommodated in an element in Ξ, but $\overset{\overset{X}{6th}}{\phi}$ is part of a parabolic Möbius map with structure $\phi\tau_{b_n}\phi$. The same is true for $\overset{\overset{X}{5th}}{\phi}$, so we put it in front and rearrange the factors $\overset{\overset{X}{5th}}{\phi} \tau_2 \overset{\overset{X}{6th}}{\phi} \tau_{\underline{-1}}$ as $\overset{\overset{X}{5th}}{\phi} \tau_1 \overset{\overset{X}{6th}}{\phi} \left[\overset{\overset{X}{5th}}{\phi} \tau_1 \overset{\overset{X}{6th}}{\phi} \tau_{\underline{-1}} \right] = (\phi\tau_1\phi)\, B.$

Now we look at the remaining factors, by starting from the left of the whole original product, identifying and isolating all possible elements of Ξ in the remaining factors not dealt with in step 3.

The factors before $\overset{\overset{X}{5th}}{\phi}$ are:

$$\tau_1 \underbrace{\tau_i \overset{1st}{\phi}}\, \overset{\overline{\Downarrow}}{\tau}_{-2} \underbrace{\tau_i \overset{2nd}{\phi}}\, \tau_{1+2i} \underbrace{\tau_i \overset{3rd}{\phi}}\, \overset{\overline{\Downarrow}}{\tau}_{-2} \underbrace{\overset{4th}{\phi}\, \overset{\overline{\Downarrow}}{\tau}_{-i}}\, \overset{\overline{\Downarrow}}{\tau}_{-4i}$$

The factors $\tau_1\tau_i \overset{1st}{\phi} \tau_{-2}\tau_i \overset{2nd}{\phi}$ can be written as $\left[\tau_{1+i} \overset{1st}{\phi} \tau_{-1+i} \overset{2nd}{\phi}\right]\left(\overset{1st}{\phi} \tau_{-1} \overset{2nd}{\phi}\right) = E\left(\phi\tau_{-1}\phi\right)$.

Then for $\tau_{1+2i} \underbrace{\tau_i \overset{3rd}{\phi}}\, \overset{\overline{\Downarrow}}{\tau}_{-2} \underbrace{\overset{4th}{\phi}\, \overset{\overline{\Downarrow}}{\tau}_{-i}}\, \tau_{-4i}$ we get

$$\tau_{2i}\tau_{1+i} \overset{3rd}{\phi} \tau_{-1}\tau_{-1} \overset{4th}{\phi} \tau_{-i}\tau_{-4i} = \tau_{2i}\left[\tau_{1+i} \overset{3rd}{\phi} \tau_{-1}\right]\tau_{-1}\left[\overset{4th}{\phi} \tau_{-i}\right]\tau_{-4i} = \tau_{2i}C\tau_{-1}A\tau_{-4i}.$$

So far the product from Step 3

$$\tau_1 \underbrace{\tau_i \overset{1st}{\phi}}\, \overset{\overline{\Downarrow}}{\tau}_{-2} \underbrace{\tau_i \overset{2nd}{\phi}}\, \tau_{1+2i} \underbrace{\tau_i \overset{3rd}{\phi}}\, \overset{\overline{\Downarrow}}{\tau}_{-2} \underbrace{\overset{4th}{\phi}\, \overset{\overline{\Downarrow}}{\tau}_{-i}}\, \overset{\overline{\Downarrow}}{\tau}_{-4i} \overset{\overset{X}{5th}}{\phi} \tau_2 \overset{\overset{X}{6th}}{\phi} \underbrace{\tau_{6i} \underbrace{\tau_i \overset{3rd}{\phi}}\, \overset{\overline{\Downarrow}}{\tau}_{-2}} \underbrace{\overset{4th}{\phi}\, \overset{\overline{\Downarrow}}{\tau}_{-i}}\, \overset{\overline{\Downarrow}}{\tau}_{-8i} \overset{\overset{X}{5th}}{\phi} \tau_2 \overset{\overset{X}{6th}}{\phi} \tau_{10i} \underbrace{\tau_i \overset{3rd}{\phi}} \cdots$$

has been rearranged up to, but not including, the second $\overset{4th}{\phi}$ as

$$= E\left(\phi\tau_{-1}\phi\right)\tau_{2i}C\tau_{-1}A\tau_{-4i}\left(\phi\tau_1\phi\right)B\tau_{6i}C\tau_{-1}$$

Since the pattern of the maps between the first $\overset{3rd}{\phi}$ and the second $\overset{3rd}{\phi}$ is repeated between every pair of consecutive $\overset{3rd}{\phi}$ maps we can complete T_M for e^i as follows:

$$E\left(\overset{1st}{\phi} \tau_{-1} \overset{2nd}{\phi}\right)$$

$$\tau_{2i} \overset{3rd}{C} \tau_{-1} \overset{4th}{A} \tau_{-4i}\left(\overset{5th}{\phi} \tau_1 \overset{6th}{\phi}\right) \overset{5th,6th}{B}$$

$$\tau_{6i} \overset{3rd}{C} \tau_{-1} \overset{4th}{A} \tau_{-8i}\left(\overset{5th}{\phi} \tau_1 \overset{6th}{\phi}\right) \overset{5th,6th}{B}$$

$$\tau_{10i} \overset{3rd}{C} \tau_{-1} \overset{4th}{A} \tau_{-12i}\left(\overset{5th}{\phi} \tau_1 \overset{6th}{\phi}\right) \overset{5th,6th}{B} \cdots$$

or simply as:

$$E\left(\phi\tau_{-1}\phi\right)\prod_{k=1}^{\infty}\tau_{(4k-2)i}C\tau_{-1}A\tau_{-4ki}\left(\phi\tau_1\phi\right)B$$

We show the progression of FQs under the partial Möbius products $T_{M(k)}$ for $k \in \mathbb{N}$, where k represents the number of factors of the product of Möbius factors present in the partial product $T_{M(k)}$.

1) For $T_{M(1)} = E$: $\xi = e^i$ is on the unit circle in the first quadrant so the square with vertices at 0, 1, $1+i$ and i is $FQ1$ for e^i.

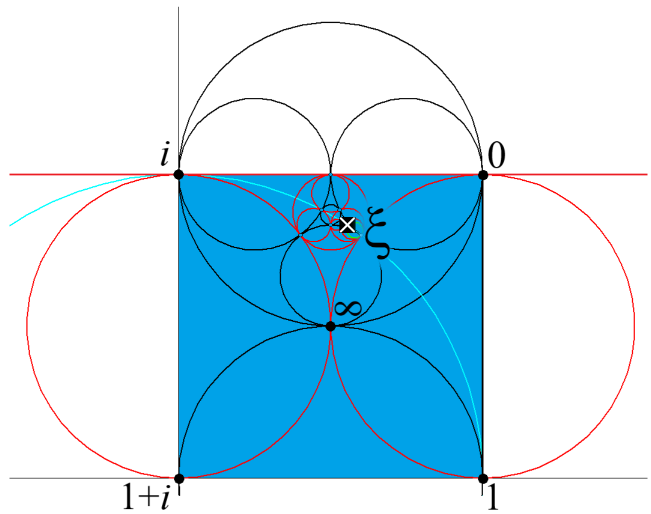

2) For $T_{M(1)} = E$: The map E permutes the vertices of ∇, swapping 0 with $1+i$ and ∞ with $\frac{1+i}{2}$. The next map fixes 0. Accordingly, we change our focus to the image of $Q\nabla_0$ as shown alongside.

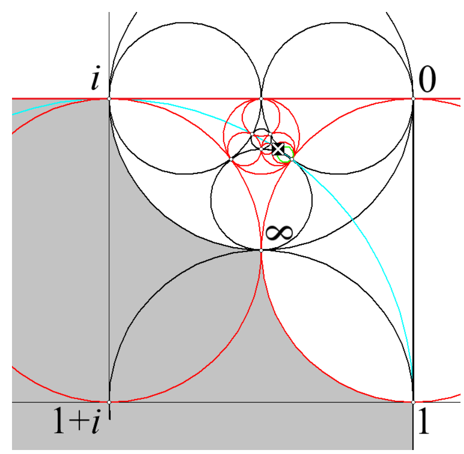

3) For $T_{M(2)} = E(\phi\tau_{-1}\phi)$: The map $\phi\tau_{-1}\phi$ fixes the image of 0 and moves the images of ∞, 1, i and $\frac{1+i}{2}$ toward the image of 0 along Farey circles. $T_{M(2)}(Q\nabla_0)$ is $FQ2$ for e^i

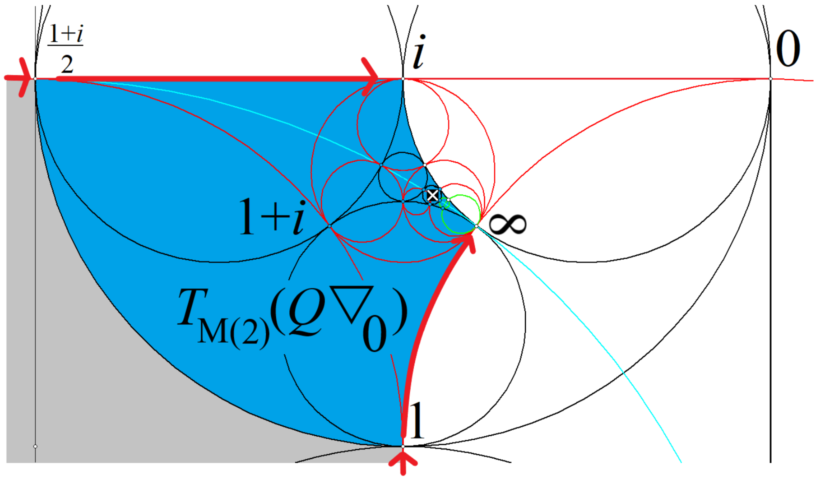

4) We switch our focus to $T_{M(2)}(Q\nabla_\infty)$ as the image of ∞ is fixed in the progression from T_1 to T_2.

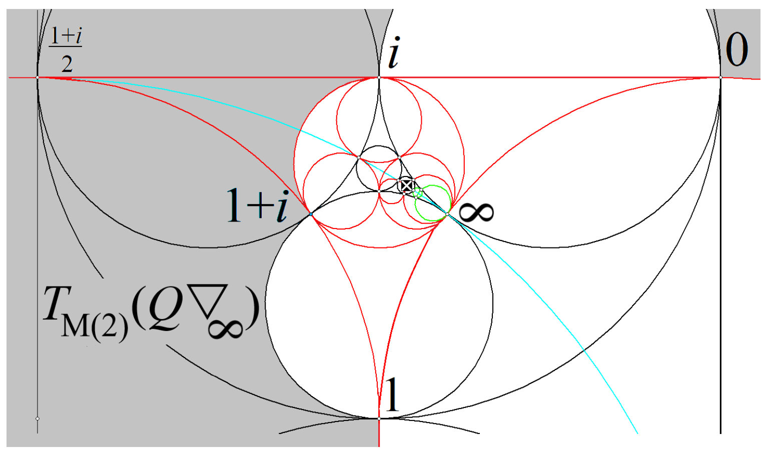

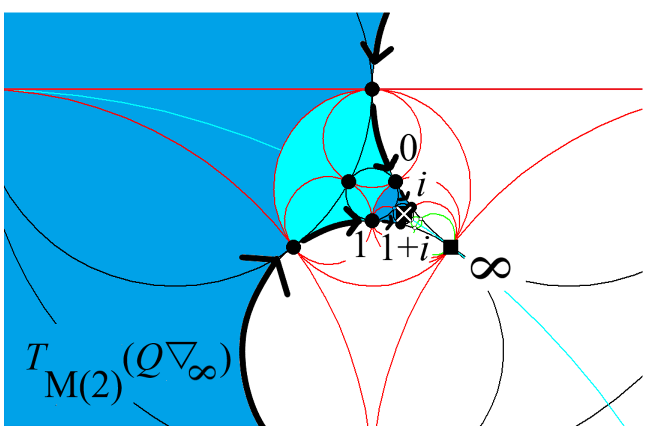

5) For $T_{M(3)} = E(\phi\tau_{-1}\phi)\tau_{2i}$: We show $T_{M(2)}(Q\nabla_\infty)$, the single intermediate image $T_{M(3),i}(Q\nabla_\infty)$ and $T_{M(3)}(Q\nabla_\infty)$.

6) Enlarging, we now see $T_{M(3)}\left(Q\nabla_{\infty}\right)$, which is $FQ3$ for e^{i}.

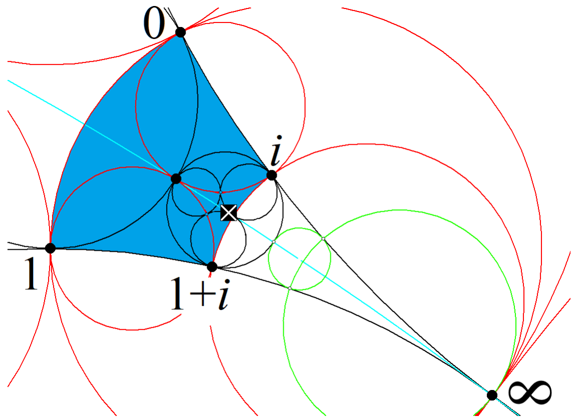

7) For $T_{M(4)} = E\left(\phi\tau_{-1}\phi\right)\tau_{2i}C$: The map C permutes the vertices. The following map is τ_{-1} so we focus on $T_{M(4)}\left(Q\nabla_{\infty}\right)$.

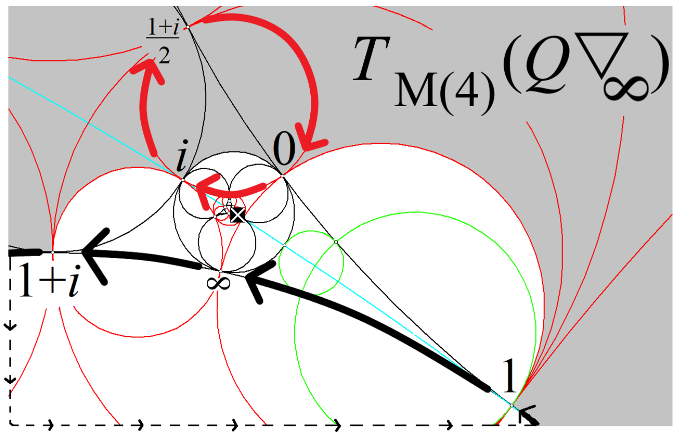

8) For $T_{M(5)} = E\left(\phi\tau_{-1}\phi\right)\tau_{2i}C\tau_{-1}$: The map τ_{-1} fixes the image of ∞ and moves the images of 0, 1, i and $1 + i$ toward the image of ∞ along Farey circles.

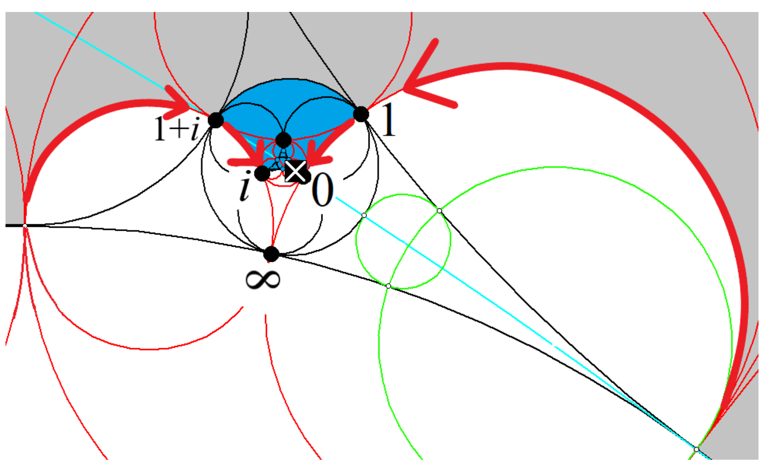

9) Enlarging, we see $T_{M(5)}(Q\nabla_\infty)$, which is $FQ4$ for e^i.

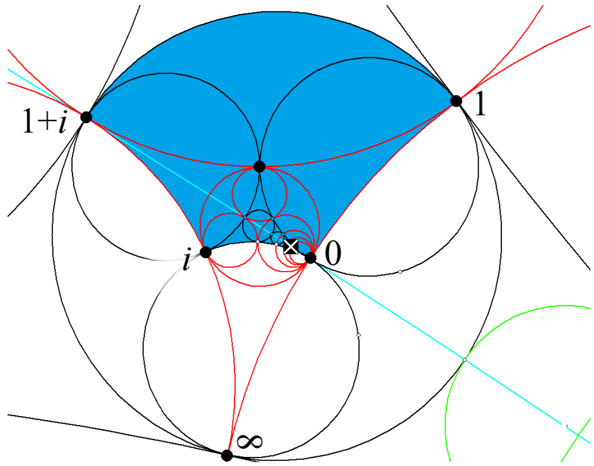

10) For $T_{M(6)} = E(\phi\tau_{-1}\phi)\tau_{2i}C\tau_{-1}A$: The map A permutes the vertices. The following map is τ_{-4i} so we focus on $T_{M(6)}(Q\nabla_\infty)$.

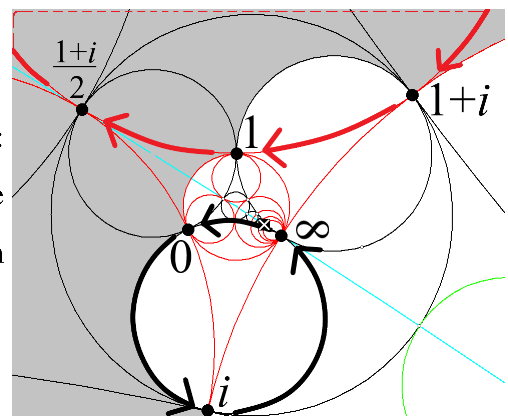

11) For $T_{M(7)} = E(\phi\tau_{-1}\phi)\tau_{2i}C\tau_{-1}A\tau_{-4i}$: The map τ_{-4i} fixes the image of ∞ and moves the images of 0, 1, i and $1+i$ toward the image of 0 along dual Farey circles.

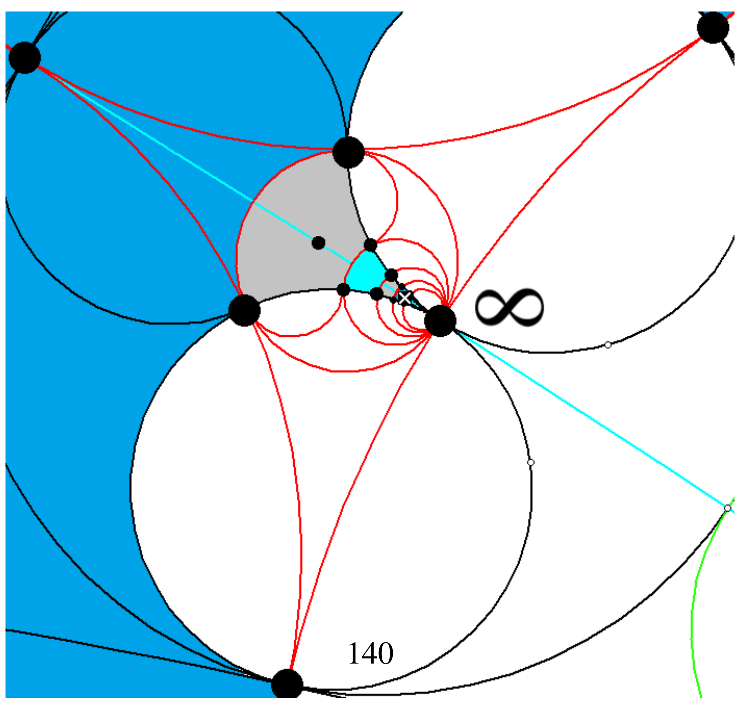

12) Enlarging, we now see $T_{M(7)}(Q\nabla_\infty)$, which is $FQ5$ for e^i.

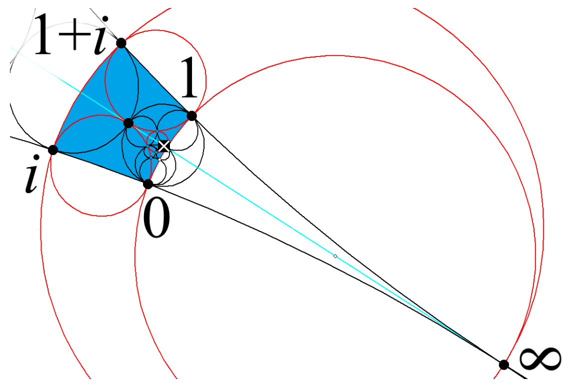

13) For $T_{M(8)} = E(\phi\tau_{-1}\phi)\tau_{2i}C\tau_{-1}A\tau_{-4i}(\phi\tau_1\phi)$: The map $(\phi\tau_1\phi)$ fixes 0 and the images of 1, ∞, i and $\frac{1+i}{2}$ are moved along dual Farey circles toward the image of 0. $T_{M(8)}(Q\nabla_0)$ is $FQ6$ for e^i.

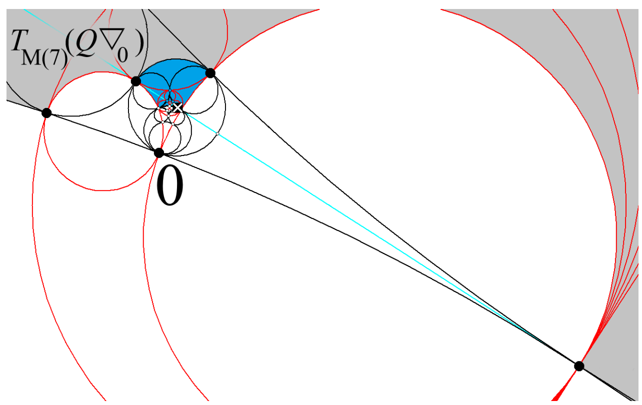

14) Enlarging, we now see $T_{M(8)}(Q\nabla_0)$, which is $FQ6$ for e^i.

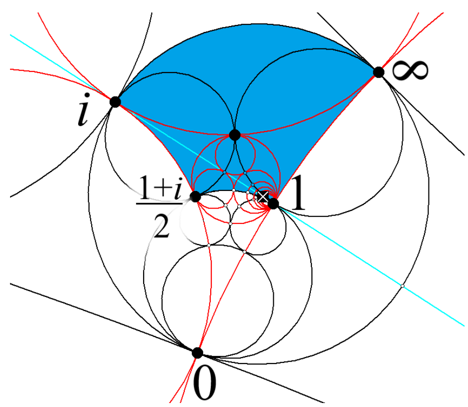

15) For $T_{M(9)} = E\,(\phi\tau_{-1}\phi)\,\tau_{2i}C\tau_{-1}A\tau_{-4i}\,(\phi\tau_1\phi)\,B$: The map B permutes the vertices of ∇. The following map is τ_{6i} so we focus on $T_{M(9)}\,(Q\nabla_\infty)$.

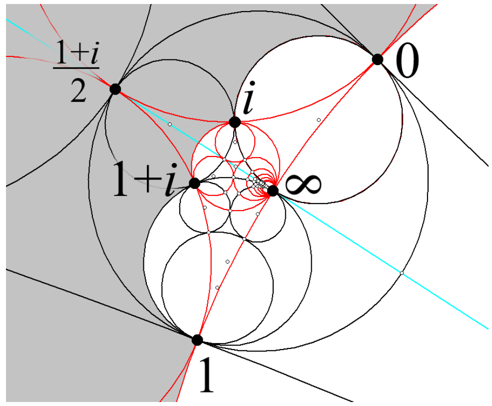

16) Below left: For $T_{M(10)} = E\,(\phi\tau_{-1}\phi)\,\tau_{2i}C\tau_{-1}A\tau_{-4i}\,(\phi\tau_1\phi)\,B\tau_{6i}$: The map τ_{6i} fixes ∞ and the images of 0, 1, i and $1+i$ are moved along dual Farey circles toward the image of ∞. $T_{M(10)}\,(Q\nabla_\infty)$ is $FQ7$ for e^i.

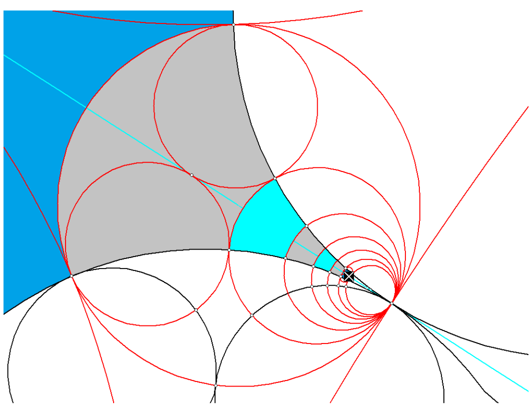

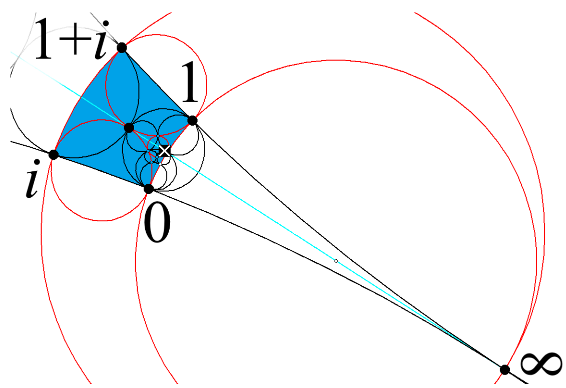

17) Above right: For $T_{M(11)} = E\,(\phi\tau_{-1}\phi)\,\tau_{2i}C\tau_{-1}A\tau_{-4i}\,(\phi\tau_1\phi)\,B\tau_{6i}C$: Enlarging, we now see $T_{M(11)}\,(Q\nabla_0)$, which is $FQ8$ for e^i.

By using the techniques employed in Example 4.4.1 for merged elliptic factors we were able to find the nested Farey quadrilaterals for e^i.

Finally, we show the comparison between T and T_A for e^i to emphasize the change from the b_n of the $NICF$ to the adjusted coefficients b_n^* due to the accommodation of the elliptic maps.

$$T = \tau_{1+i} \quad (\phi\tau_{-2+i}\phi) \quad \tau_{1+3i} \quad \prod_{k=1}^{\infty} \quad [(\phi\tau_{-2}\phi) \quad \tau_{-(4k+1)i} \quad (\phi\tau_2\phi) \quad \{\tau_{-1}\}\tau_{(4k+3)i}\{\tau_1\}]$$

$$T_A = \tau_0 \quad E\,(\phi\tau_{-1}\phi) \quad \tau_{2i} \quad \prod_{k=1}^{\infty} \quad [C\tau_{-1} \quad A\tau_{-4ki} \quad (\phi\tau_1\phi) \quad B\tau_{(4k+2)i}],$$

where the factors $C = \tau_{1+i}\phi\tau_{-1}$, $A = \phi\tau_{-i}$ and $B = \phi\tau_1\phi\tau_{-1}$, result in the change from b_n to b_n^* as required. The factors B and C use the factors $\{\tau_{-1}\}$ and $\{\tau_1\}$, 'inserted and deleted' in T, as shown.

4.5 Conclusion

In this chapter, the techniques for rearranging factors in product of parabolic Möbius maps derived from the $NICF$ of ξ, supported by geometric analysis of nested Farey quadrilaterals containing the target, have been extended to irrational values of ξ with $NICF$s where there is a pattern. Rearrangement of the maps produced a T_M whose partial products, $T_{M(n)}$, yield a sequence of nested Farey quadrilaterals each time the last factor $t_{M(n)}$ was a parabolic Möbius map. This is an area for further research.

Chapter 5

Conclusion

In conclusion to this thesis, we outline the main results of each chapter. A new geometric approach for analysing continued fractions has been developed. There are many contexts in which the Ford circles and the Farey tessellation are manifested in the approaches of other authors so we needed to be explicit about how the roles of geometric features have changed in the new approach.

In chapter 2, the pleasing links established by Series, between the partial quotients of the RCF and the triangles in the Farey tessellation $\mathcal{F}$, have been extended to the $NICF$ for the case of the real numbers. In the main result, the link is established between T_M, the product of Möbius maps derived from the $NICF$, and the triangles of the Farey tessellation of hyperbolic space. In the case where partial quotients are negative, we discovered one of the elliptic maps $s = \tau_1 \left(\phi\tau_{-1}\phi\right)$ or $s^{-1} = \left(\phi\tau_{-1}\phi\right)\tau_1$ needed to be treated as a separate factor, while adjusting the coefficient of the parabolic Mobius maps preceding and following each elliptic factor found accordingly. The action of map $t_{m(n)}$, the last factor of each partial product of Möbius maps $T_{M(n)}$, was considered as an isometry acting on $\mathcal{F}$, the Farey tessellation of the upper half plane model of hyperbolic space. The coefficient of each parabolic Möbius map in $T_{M(n)}$ is linked directly to the number of Farey triangles sharing a common vertex, where the vertex is a fixed point in the progression from $T_{M(n-1)}$ to $T_{M(n)}$ if $t_{m(n)}$ is a parabolic map.

In Chapter 3, the new approach was extended to the case of complex numbers. Farey sums and Farey neighbours were defined in the context of the extended Schmidt arrangement $\hat{S}_{\mathbb{Q}(\sqrt{-1})}$. We introduced the set $\nabla = \left\{\infty, 0, 1, i, 1+i, \frac{1+i}{2}\right\}$ and defined the Farey quadrilaterals $Q\nabla_0$ and $Q\nabla_\infty$, with vertices in ∇, associated both with 0 and with ∞ respectively. In the main theorem, Farey quadrilaterals were used to describe the effect of Möbius maps in the complex plane. The parabolic Möbius maps τ_{a+bi} and $\phi\tau_{a+bi}\phi$ resulted in the movement of the vertices of images of the Farey quadrilaterals $Q\nabla_0$ and $Q\nabla_\infty$ along Farey circles for $a \neq 0, b = 0$ and along dual Farey circles for $a = 0, b \neq 0$. In the second main theorem the role of the elliptic Möbius maps was described by showing that they permute the vertices of ∇.

In Chapter 4, examples of $NICF$s of various square roots of complex numbers were used to illustrate the different patterns that emerge among the partial quotients. We started with products of parabolic Möbius maps that had no elliptic elements present, then proceeded to the type that had distinct elliptic factors (no consecutive factors with non-positive real parts) and then we worked on the cases where elliptic factors were merged (consecutive factors with non-positive real parts present). The chapter was concluded with our main theorem which states that, if ξ is the square root of a complex number, every product of parabolic Möbius maps derived from the $NICF$ of ξ can be factorised into parabolic and elliptic Möbius maps, where the partial products $T_{M(n)}$ with:

- a parabolic map as the last factor generate the nested sequence of Farey quadrilaterals that contain the target ξ, and
- an elliptic map as the last factor permute the vertices of the nested Farey quadrilateral in the sequence derived from $T_{M(n-1)}$.

The last example shows that the technique does work for numbers involving e where the $NICF$ is pseudo periodic. It would be ideal to extend the final theorem to ξ any complex number.

5.1 Further research

In our work we consider the action of Möbius maps on the vertices in ∇. It is the images of the vertices of ∇ under the Möbius maps derived from the $NICF$ of ξ that become the approximations for the target ξ. In Chapter 4.2 we showed how the images of the vertices of ∇ moved along Farey circles under the action of parabolic maps, while the elliptic maps permuted the vertices where needed. The target ξ lies in a series of nested images $T_n\left(Q\nabla_v\right)$, where v is the fixed point of T_n.

The 6 vertices given by $T_n(\nabla)$ determine a region called the lune of T_n.

Definition 5.1.1. Given the 6 vertices in $T_n(\nabla)$, the region defined as the union of all the pairwise intersections between any two distinct circles, each drawn through any 3 points in $T_n(\nabla)$ is called the lune of T_n.

Theorem 5.1.2. If $t_{n+1} \in \Xi$ the lune of T_{n+1} is the same as the lune of T_n.

Proof. The two Farey circles that bound the lune of T_{n+1} are the same Farey circles that bound the lune of T_n, but the vertices of ∇ that define these circles have simply been permuted. □

It may be useful to use the concept of the lune of each T_n instead of the Farey quadrilaterals used in this thesis.

Secondly, while working in $\hat{\mathbb{C}}$ as a complex plane, we must bear in mind that it is the boundary of hyperbolic 3-space $\mathbb{H}^3$. The Riemann sphere model of $\hat{\mathbb{C}}$ has the advantage that the point ∞ is represented as a single point instead of the "circle at infinity" imagined in the extended complex plane model of $\hat{\mathbb{C}}$. Since Möbius maps preserve angles and map circles to circles, and ∞ can be mapped to any point in $\mathbb{C}$ using a Möbius map, every point has the same properties as ∞:

- At each point there are two pencils of circles that intersect orthogonally, a pencil of Farey circles and a pencil of dual Farey circles.

- Each point in $\hat{\mathbb{C}}$ is a one point "compactification" of some circle at infinity when the extended complex plane is viewed as the boundary of $\mathbb{H}^3$.

Furthermore, in higher dimensions simply truncating the $NICF$ has a negative impact on accuracy of the approximations. We need to understand the underlying process governed by the Möbius maps generated from the $NICF$. In the case of approximating reals we already need to track the orbits of the 3 points, namely ∞, 0 and 1, to visualise the process. As we move into approximating complex numbers using $NICF$s the number of vertices whose orbits we need to track increases to 6. To explore the extension of these ideas to the approximation of quaternion numbers there are 10 vertices which need to be tracked as they form the vertices of the pentacross discussed in [31].

Finally, there are many well known, beautifully patterned continued fraction representations of π,

$$\pi = 3 + \cfrac{1^2}{6 + \cfrac{3^2}{6 + \cfrac{5^2}{6 + \cdots}}} \quad \text{and, from [38],} \quad \frac{\pi}{2} = 1 + \cfrac{1}{1 + \cfrac{1}{\frac{1}{2} + \cfrac{1}{\frac{1}{3} + \cfrac{1}{\frac{1}{4} + \cdots}}}},$$

$$\text{but the } RCF \text{ of } \pi = 3 + \cfrac{1}{7 + \cfrac{1}{15 + \cfrac{1}{1 + \cfrac{1}{292 + \cfrac{1}{1 + \cfrac{1}{1 + \cdots}}}}}} \text{ (with all numerators equal to 1)}$$

is not one of them.

The continued fractions with

- numerators not all equal to 1, and
- numerators equal to 1, but denominators rational.

need to be explored further. We may need to use the lune of Definition 5.1.1 in order to work with both of these types.

Bibliography

[1] J. W. Anderson. *Hyperbolic Geometry*. Springer-Verlag, London, second edition, 2005. https://doi.org/10.1007/1-84628-220-9.

[2] J. F. Barrett. Minkowski space-time and hyperbolic geometry. In *MASSEE International Comgress on Mathematics MICOM 2015*, September 2015. https://eprints.soton.ac.uk/397637/2/J_F_Barrett_MICOM_2015_2018_revision_.pdf.

[3] A. F. Beardon. *The Geometry of Discrete Groups*. Springer, New York, 1983. https://doi.org/10.1007/978-1-4612-1146-4.

[4] A. F. Beardon. Continued fractions, discrete groups and complex dynamics. *Computational Methods and Function Theory*, 1(2):535–594, 2001. https://doi.org/10.1007/BF03321006.

[5] A. F. Beardon. The geometry of pringheim's continued fractions. *Geometriae Dedicata*, 84:125–134, 2001. https://doi.org/10.1023/A:1010361030641.

[6] A. F. Beardon. Mobius maps and periodic continued fractions. *Mathematics Magazine*, 88(4):272–277, 2015. https://doi.org/10.4169/math.mag.88.4.272.

[7] A. F. Beardon, M. Hockman, and I. Short. Geodesic continued fractions. *Michigan Mathematical Journal*, 61:133–150, 2012. https://doi.org/10.1307/mmj/1331222851.

[8] A. F. Beardon and I. Short. A geometric representation of continued fractions. *The American Mathematical Monthly*, 121:391–402, 2014. https://doi.org/10.4169/amer.math.monthly.121.05.391.

[9] C. Brezinski. *History of Continued Fractions and Padé approximations*. Springer-Verlag, New York, 1991. https://doi.org/10.1007/BFb0095574.

[10] J. W. S. Cassel, W. Ledermann, and K. Mahler. Farey section in k(i) and k(ρ). *Philosophical Transactions of the Royal Society of London*, 243(873):585–626, August 1951. https://doi.org/10.1098/rsta.1951.0012.

[11] S. Chaubey, E. Fuchs, R. Hines, and K. E. Stange. The dynamics of super apollonian continued fractions. *Transactions of the American Mathematical Society*, 372:2287–2334, 2019. https://doi.org/10.1090/tran/7372.

[12] R. M. Corless. Continued fractions and chaos. *The American Mathematical Monthly*, 99(3):203–215, 1992. https://doi.org/10.2307/2325053.

[13] L. R. Ford. Rational approximations to irrational complex numbers. *Transactions of the American Mathematical Society*, 19(1):1–42, 1918. https://doi.org/10.1090/S0002-9947-1918-1501085-6.

[14] L. R. Ford. Fractions. *The American Mathematical Monthly*, 45(9):586–601, 1938.

[15] C. G. Gunn. Visualizing non-euclidean geometry. 2002. https://studylib.net/doc/8090310/visualizing-non-euclidean-geometry.

[16] G. P. Hayward. *The action of the Picard Group on Hyperbolic 3-space and complex Continued Fractions*. MSc dissertation, University of the Witwatersrand, 2013. https://wiredspace.wits.ac.za/bitstream/handle/10539/15145/MSc.

[17] D. Hensley. *Continued Fractions*. World Scientific Publishing, Singapore, 2006. https://doi.org/10.1142/5931.

[18] R. Hines. *Applications of hyperbolic geometry to continued fractions and Diophantine approximation*. PHD thesis, University of Colorado, 2019. `https://math.colorado.edu/~rohi1040/research/hines_thesis.pdf`.

[19] M. Hockman. Continued fractions and the geometric decomposition of modular transformations. *Quaestiones Mathematicae*, 29(4):427–446, 2006. `https://doi.org/10.2989/16073600609486174`.

[20] M. Hockman. The geometry of gaussian integer continued fractions. *Journal of Number Theory*, pages 427–446, 2018. `https//doi.org/10.1016/j.jnt.2018.08.006`.

[21] M. Hockman. The farey octahedron graph, the poincaré polyhedron theorem and gaussian integer continued fractions. *Annales mathḿatique du Quebec*, 2019. `https//doi.org/10.1007/s40316-019-00115-4`.

[22] M. Hockman. Geodesic gaussian integer continued fractions. *Michigan Mathematical Journal*, 69:297–322, 2020. `https://10.1307/mmj/1576033219`.

[23] M. Hockman and C. M. Mennen. Orientation preserving mobius transformations in $\mathbb{R}^4_\infty$ and quaternionic determinants. *Linear Algebra and its Applications*, 505:367–386, September 2016. `https://www.sciencedirect.com/science/article/pii/S0024379516301586`.

[24] M. Hockman and R. V. Rensburg. Simple continued fractions and cutting sequences. *Quaestiones Mathematicae*, 36:1–12, 2013. `https://doi.org/10.2989/16073606.2013.779975`.

[25] R. K. James W Cannon, William J Floyd and W. J. Parry. Hyperbolic geometry. *Flavors of Geometry*, 31:59–115, 1997.

[26] W. B. Jones and W. J. Thron. *Continued Fractions: Analytic Theory and Applications*. Addison-Wesley Publishing Company, Reading Massachusetts, 1980.

[27] O. Karpenkov. Open problems in geometry of continued fractions. 12 2017. https://arxiv.org/abs/1712.01450.

[28] J. C. Lagarias and C. P. Tresser. A walk along the branches of the extended farey tree. *IBM Journal of Research and Development*, 39(3):427–446, May 1995. https://doi.org/10.1147/rd.393.0283.

[29] H. Li, D. Hestenes, and A. Rockwood. *A Universal Model for Conformal Geometries of Euclidean, Spherical and Double-Hyperbolic Spaces*, pages 77–104. Springer Berlin Heidelberg, 2001. https://doi.org/10.1007/978-3-662-04621-0_4.

[30] D. Marshall and P. Scott. A brief history of non-euclidean geometry. *The Australian Mathematics teacher*, 60(3):2–4, 2004. https://eric.ed.gov/?id=EJ717835.

[31] C. M. Mennen. The algebra and geometry of continued fractions with integer quaternion coefficients. MSc dissertation, University of the Witwatersrand, 2015. https://wiredspace.wits.ac.za/bitstream/handle/10539/17643/CMM-MSC-final.pdf?sequence=1.

[32] C. D. Olds. *Continued fractions*. The Mathematical Association of America, Washington, first edition, 1963.

[33] T. J. Osler. Lord brouncker's forgotten sequence of continued fractions for pi. *International Journal of Mathematical Education in Science and Technology*, 41(1):105–110, 2010. https://doi.org/10.1080/00207390903189195.

[34] W. F. Reynolds. Hyperbolic geometry on a hyperboloid. *The American Mathematical Monthly*, 100(5):442–455, 1993. http://hdl.handle.net/10427/015249.

[35] N. Richert. A canonical form for planar farey sets. *Proceedings of the American Mathematical Society*, 83(2):259–262, October 1981. https://doi.org/10.1090/S0002-9939-1981-0624910-3.

[36] A. M. Rockett and P. Szusz. *Continued fractions*. World Scientific Publishing Company, Singapore, first edition, 1992. `https://doi.org/10.1142/1725`.

[37] E. Sandifer. Who proved e is irrational? *MAA OnLine How Euler did it*, 12 2007.

[38] E. Scheinerman, T. J. Pickett, and A. Coleman. Another continued fraction for π. *The American Mathematical Monthly*, 115(10):930–933, 2008. `http://www.jstor.org/stable/27642639`.

[39] A. L. Schmidt. Farey triangles and farey quadrangles in the complex plane. *Mathematica Scandinavica*, 21:241–295, 1967. `https://doi.org/10.7146/math.scand.a-10863`.

[40] A. L. Schmidt. Diophantine approximation of complex numbers. *Acta Mathematica*, 134:1–85, 1975. `https://doi.org/10.1007/BF02392098`.

[41] C. Series. The geometry of markoff numbers. *The Mathematical Intelligencer*, 7(3):20–29, 1985. `https://doi.org/10.1007/BF03025802`.

[42] C. Series. The modular surface and continued fractions. *Journal of the London Mathematical Society*, 2(31):69–80, 1985. `https://doi.org/10.1112/jlms/s2-31.1.69`.

[43] I. Short. Ford circles, continued fractions, and rational approximation. *American Mathematical Monthly*, 118(2):130–135, 2011. `https://www.tandfonline.com/doi/abs/10.4169/amer.math.monthly.118.02.130`.

[44] I. Short and M. Walker. Even-integer continued fractions and the farey tree, 08 2015. `https://arxiv.org/pdf/1508.01373`.

[45] K. E. Stange. Visualising the arithmetic of imaginary quadratic fields. *International Mathematics Research notices*, 2018:3908–3938, 02 2017. `https://doi.org/10.1093/imrn/rnx006`.

[46] J. A. Stedall. Catching proteus: The collaborations of wallis and brouncker - 1. squaring the circle. *Notes and Records of the Royal Society of London*, 54(3):293–316, September 2000. https://doi.org/10.1098/rsnr.2000.0114.

[47] M. F. Wyman and B. F. Wyman. An essay on continued fractions - Leonhard Euler. *Mathematical Systems Theory*, 18:295–328, 01 1985. https://doi.org/10.1007/BF01699475.